A Pipeline of Methods for Evaluating Carbon Sequestration Potential of Forest using LiDAR Data and Abiotic Factors

Thesis submitted to the for the partial fulfilment of the requirements of the degree of

Doctor of Philosophy

by

Utla Chandra Sekhar

(Roll No. 176104018)

Thesis Supervisor

Dr. Ajay Dashora

Department of Civil Engineering

Indian Institute of Technology Guwahati

Guwahati–781039, Assam, India

December 2025

Dedicated to the almighty Kamakhya and my parents. I owe it all to you. Many thanks for the endless love, support and encouragement!

Department of Civil Engineering
Indian Institute of Technology Guwahati
Guwahati-781039, Assam, India

Declaration

I hereby declare that

- The work contained in this thesis is original and has been conducted by myself under the general supervision of my supervisor.
- The work reported herein has not been submitted to any other institute for any degree or diploma.
- Whenever I have used materials (concepts, ideas, texts, expressions, data, graphs, theoretical analysis, results, etc.) from other sources, I have given due credit to the authors/ researchers by citing them in the text of the thesis and providing their details in the references.
- Whenever I have quoted from the work of others, the source has always been given.

Date:

Place: Guwahati

(Utla Chandra Sekhar)
Research Scholar
Department of Civil Engineering
Indian Institute of Technology Guwahati
Guwahati-781039, Assam, India
Email: utla176104018@iitg.ac.in

chandra.sekhar.sekhar83@gmail.com

Department of Civil Engineering
Indian Institute of Technology Guwahati
Guwahati-781039, Assam, India

Certificate

This is to certify that this thesis entitled "***A pipeline of methods for evaluating carbon sequestration potential of forest using LiDAR data and abiotic factors***" submitted by **Utla Chandra Sekhar (Roll No. 176104018)**, to Indian Institute of Technology Guwahati for the award of the degree of Doctoral of Philosophy is a record of bonafide research work carried out by him under my supervision and guidance at the Department of Civil Engineering, Indian Institute of Technology Guwahati, Assam, India. In my opinion, the thesis has reached the requisite standard fulfilling the requirement for the degree of Doctor of Philosophy in Civil Engineering. To the best of my knowledge, no part of the work reported in this thesis has been presented for the award of any degree at any other institution.

Dr Ajay Dashora
Assistant Professor,
Department of Civil Engineering
Indian Institute of Technology
Guwahati

Acknowledgments

"**The PhD Journey**" is not only adapting to research environment and gaining academic excellence, it is a miniature version of life itself that we live in and learn, evolve and go through upgradations in this entire period. I remember a famous saying from my supervisor, "*In this fast growing world, biggest social problems always solved by simple mathematical equations and intelligence*". This work would not have been possible without the motivation and support I received from many people during this delightful journey of PhD. It goes without saying that this journey would not have been possible without constant support, profound encouragement and the unconditional love of my mother, my father, my brother and other family members. With their belief in me and my actions, decisions and interest, they never questioned my intentions and whole-heartedly supported me in all my endeavours.

No words can express my gratitude to them. I express my deepest sense of gratitude and veneration to my supervisor Dr. Ajay Dashora, Department of Civil Engineering, Indian Institute of Technology Guwahati (IITG) for his constructive suggestions, meticulous guidance, and sustained interest and patience through the present research. I am recipient of Mitacs Globalink Research Award - Shastri Indo Canadian Institute (SICI) program (Application Ref. IT34180). I will always be thankful to University of New Brunswick, Department of Natural Resources, NB, Fredericton, Canada. In addition, I would like to thank Compute Canada Server, which was provided by Dr. Rakesh Kumar Mishra and Prof. Yun Zhang. It is my sublime duty to express my deepest sense of indebtedness and reverence to the Chairman of my Doctoral Committee Prof. Arup Kumar Sarma, and other committee members especially, Dr. Archana M. Nair, for their eternal encouragement, valuable suggestions, and timely help provided at various stages of the investigation and compilation of thesis. Personally, I would like to thank my colleagues Dr. Atma Sharma, Dr. Sandeep Kumar Mondal,

Dr. Arnab Kumar Pal, Dr. Suresh Nama and Bonthu Satyanraayana for their encouragement. Finally yet importantly, I am grateful to Lohit hostel warden, Mr. Faitan Das, Surveying Lab in charge Mr. Madhav Rajbhongshi, Late Utla. Ammayamma, Late Utla. Chandrayya and Utla Ravana, Utla. Vineel Kumar, Utla. Prabhavathi, Utla. Ganapathi, Late Guttu Satyam, Guttu. Leelavathi, ammamma Lakshmi and almighty Maa Kamakhya.

Abstract

Forests serve as natural carbon sinks within the biosphere, absorbing CO_2, which is crucial for regulating climate-driven shifts. However, recent studies indicate that natural carbon pools are declining. For example, the current atmospheric CO_2 increase of approximately 2.5 ppm per year would have been around 1.9 ppm if natural sequestration had not started to fail. Specifically, forests in ecotone regions, which experience edge effects, often show disturbed biodiversity and decreased ecosystem productivity. Thus, accounting for carbon pools in forest ecosystems is necessary as a response to anthropogenic carbon emissions. Acadian Forest, situated in Canada, has been facing disturbances like fire; climate-induced dynamic patterns in temperature and precipitation are affecting ecosystem composition and carbon sequestration dynamics. To accurately account for carbon pools, a precise estimation of total biomass is essential. For extensive forest areas, remote sensing technologies, including satellite, airborne, and terrestrial platforms, are commonly employed to estimate aboveground biomass (AGB). LiDAR point cloud data enables more accurate retrieval of tree structural and geometric properties through derived metrics. Consequently, 3D point data enhances the allometric modeling of AGB dynamics in forests especially at the individual tree level. Major highlights are as follows:

- A modified method for crown structure modelling, branch collar detection and branch structure modelling from terrestrial LiDAR data has been presented. Angular and linear constraints has been presented to extract curvilinear branch and stem segments and shape model into small straight cylindrical segments. Errors in stem volumes are in range from 0.03 – 0.87 m^3 for estimated stem volumes in 1.1 – 17.68 m^3 against destructive estimates. Similarly, errors in crown volume are in range from 0.013 – 2.33 m^3 for estimated crown volumes in range of 0.105 – 25.95 m^3.

- An approximate method of biomass estimation from Airborne LiDAR Data has been given especially for Acadian forest that considers individual species canopy structure, and their growth characteristics (allometrics). Moreover, a parametric biomass model that integrates SRTM 30m DEM, and GEDI Level 4A data providing biomass estimates at 25m resolution has been given for boreal forests (Acadia Forest).
- A carbon sequestration model is given for Acadian forest where it considers varied biomass storage, soil organic storage. Moreover, it also takes in to account of abiotic factors that are essential for sustainable human survival. This research study models carbon sequestered with varying stored carbon (aboveground biomass (AGB), belowground biomass (BGB) and soil organic carbon (SOC)) of the Acadian Forest, carbon losses from wood harvesting and greenhouse gas emissions.
- For a 122.5-hectare area, Ecological Demography model, which models complex process of vegetation to simulate biomass carbon (AGB and BGB) revealed with a significant drop projected for year 2048, which are affected by changing structural soil carbon, leaf area index, evapotranspiration, temperature and precipitation patterns. SOC is modelled as a function of AGB and BGB. Carbon losses are estimated based on statistical data of New Brunswick. Results revealed that the rate of carbon sequestration change oscillates between negative and positive trends from 2029, as currently dominating species, i.e. Black Spruce and Balsam Fir, are more sensitive to climatic patterns. Aboveground biomass dynamics of Acadian forest revealed a decrease of forest carbon storage approximately 60,000 $Kg.C$ at year 2048 compared to 2021. This amount of carbon corresponds to approximately 1,00,000 m^2 area assuming a tree occupies 30 m crown width upon its maturity and a maximum carbon storage of 500 $Kg.C$. It also corresponds to a change in forest cover of approximately 1.2% by year 2048.

Contents

List of Figures

List of Tables

List of Abbreviations and Symbols

Abbreviation and Symbols	Description
LiDAR	Light Detection and Ranging
PPM	Parts Per Million
ALS	Airborne Laser Scanner
TLS	Terrestrial Laser Scanner
SRTM	Shuttle Radar Topography Mission
GEDI	Global Ecosystem Dynamics Investigation
CO_2	Carbon Dioxide Gas
3D	Three Dimensional
2D	Two Dimensional
AGB	Aboveground Biomass
BGB	Belowground Biomass
R^2	Correlation Coefficient
$RMSE_r$	Relative Root Mean Square Error
RMSE	Root Mean Square Error
SOC	Soil Organic Carbon
NCC	Nature Conservancy of Canada
FAO	Food and Agriculture Organisation
IPCC	Inter Governmental Panel on Climate Change
REDD	Reducing Emissions from Deforestation and Forest Degradation
PPM	Parts per Million
ABA	Area based Approach
CHM	Canopy Height Model
DEM	Digital Elevation Model
DSM	Digital Surface Model
DTM	Digital Terrain Model

MCH	Mean Canopy Height
QMCH	Quadratic Mean Canopy Height
CGV	Crown Generated Volume
CPA	Canopy Projection Area
HCD	Height Multiplied by Crown Diameter
DBH	Diameter at Breast Height
H	Tree Height
NRC	Natural Resource of Canada
BEF	Biomass Expansion Factor
DNR	Department of Natural Resources, New Brunswick
PC	Point Cloud
BS	Set of Crown Point Cloud
ST	Set of Stem Point Cloud
CBH	Crown Base Height
BCL	Branch Collar Level
RANSAC	Random Sample and Consensus
CNP	A set of Canopy Point Cloud
C_S	Carbon sequestered by the Forest
C_{AGB}	Carbon from Aboveground Biomass
C_{BGB}	Carbon from Belowground Biomass
C_{SOC}	Carbon form Soil Organic Carbon
C_h	Carbon Emissions from Wood Harvesting
C_{GHG}	Carbon Emissions from Greenhouse Gases
EDM	Ecological Demography Model
NB	New Brunswick
NS	Nova Scotia
PEI	Prince Edward Island

भारतीय प्रौद्योगिकी संस्थान गुवाहाटी
Indian Institute of Technology Guwahati

CHAPTER 1 INTRODUCTION

1.1 Background

Forest ecosystems serve as vital natural carbon sinks, actively sequestering atmospheric carbon in response to abrupt climate changes primarily driven by escalating carbon emissions from human activities (Beer et al., 2010; Bonan, 2008; Marchand et al., 2018; Pan et al., 2011; Pugh et al., 2019). These anthropogenic interventions lead to shifts in climate patterns by altering temperature and precipitation levels. Furthermore, human activities, particularly the emission of greenhouse gases from industrial processes reliant on fossil fuels and the widespread practice of deforestation, are significant contributors to global warming and climate change. Recent research indicates that carbon emissions from fossil fuel combustion in industries overshadow the impacts of deforestation, resulting in a temperature increase of approximately 1°C (Jayakrishnan et al., 2022). Conversely, the depletion of forests, especially secondary forests, due to human actions and resulting climate change can yield both positive and negative outcomes.

The expansion of industrial activities and the need to accommodate a growing population necessitate the conversion of new agricultural and open lands for food production, housing, and other living requirements (Culas, 2009). Additionally, the cumulative emissions resulting from fossil fuel consumption by humans are an inescapable reality. Consequently, both human interventions and industrial development disrupt the natural carbon cycle of the atmosphere, exacerbating global climate change (Li et al., 2022; Malhi et al., 2002; Sloan and Sayer, 2015).

Moreover, shallow water tables combined with environmental gradients, particularly in ecotone regions that encompass boreal and temperate forests, often display disturbed biodiversity and diminished ecosystem productivity (Bouman et al., 2020; Dimitrov et al., 2014; Frazier et al., 2015; Hufkens et al., 2009; Kark, 2012; Pearson and D'Orangeville, 2022). Moreover, growth of biomass and carbon storage in a forest also depends on many environments and ecological factors like precipitation (snow cover), temperature, albedo, evapotranspiration, soil nutrients, and abundance of sunlight (Bonan, 2008). In the Acadian ecotone regions of eastern Canada, located between northern hardwood temperate and boreal forests, empirical studies reveal that the Acadian Forest is experiencing significant transformations that alter its ecosystem composition and species trajectories due to rising temperatures (Bouchard et al., 2019; Boulanger et al., 2022; Brecka et al., 2020; D'Orangeville et al., 2018; Taylor et al., 2017, 2014). Simultaneously, an increase in disturbances, particularly

from clear-cutting practices within the Acadian Forest, has also been documented (Cox et al., 2023).

1.2 Motivation

Vegetation, including forests and grasslands, absorbs approximately 50% of the carbon dioxide present in the atmosphere (Bonan, 2008). However, deforestation significantly diminishes these vital carbon sinks. In temperate regions like Canada, the rate of increase in forest cover, particularly in secondary forests, has been declining since 2005 (Keenan et al., 2015).

The Acadian Forest, located in the ecotone regions of eastern Canada, lies between the northern hardwood temperate and boreal forests and is home to over 32 tree species. This forest is particularly significant due to its unique ecological characteristics. Recent empirical studies indicate that the Acadian Forest is experiencing substantial transformations, which are altering its ecosystem composition and species trajectories as a result of rising temperatures (Bouchard et al., 2019; Boulanger et al., 2022; Brecka et al., 2020; D'Orangeville et al., 2018; Taylor et al., 2017, 2014). At the same time, there has been an increase in disturbances, especially from clear-cutting practices, which are impacting the Acadian Forest (Cox et al., 2023). Moreover, Acadian Forest is also a vital habitat for diverse species, including moose, black bears, lynx, and the endangered Atlantic salmon, contributing to its rich biodiversity. Sustainable forestry initiatives and conservation efforts spearheaded by organizations such as the Nature Conservancy of Canada (NCC) aim to protect old-growth forests and restore biodiversity within this region. Furthermore, the Acadian Forest holds significant cultural and economic value, with Indigenous and Acadian communities historically depending on its resources for their livelihoods. While forestry remains a crucial industry in New Brunswick, there is a growing emphasis on eco-tourism, carbon sequestration, and sustainable wood harvesting practices to ensure the forest's long-term health and ecological functionality.

Despite its critical importance for human survival, the impacts of environmental variables on species composition within the Acadian Forest are not fully understood. Specifically, the effects of localized changes on individual species' biomass distribution and their subsequent influence on the overall carbon sequestration capacity of the forest remain unclear. Furthermore, the long-term effects of urbanization and clear-cutting on the carbon sequestration potential of the Acadian Forest have not been thoroughly investigated.

Research conducted by Schlamadinger and Marland, (1996) and Schlamadinger et al. (1997) proposed a methodology for accounting for carbon pools in forest ecosystems. This

methodology requires two primary components: forest carbon storage and carbon emissions into the atmosphere. Carbon storage includes the total biomass of the forest at a given time, as well as the soil organic carbon stored in the forest's ground surface. In contrast, carbon emissions data should encompass statistical information specific to the forest's location, particularly regarding wood harvesting and greenhouse gas emissions. This emissions data must also account for contributions from transportation, residential areas, agriculture, forestry, waste management, buildings, electricity, and commercial industries (Filonchyk et al., 2024). 2024).

To accurately account for carbon pools, a precise estimation of total biomass is essential. For extensive forest areas, remote sensing technologies, including satellite, airborne, and terrestrial platforms, are commonly employed to estimate aboveground biomass (AGB). However, visible and near-infrared (NIR) bands can experience signal saturation when estimating high-density AGB (Duncanson et al., 2010; Luo et al., 2017). Microwave radiation can penetrate dense cloud cover, aiding in the development of AGB models for optically shadowed regions, although radar signals struggle to penetrate deeply into vegetation. Conversely, point cloud data enables more accurate retrieval of tree structural and geometric properties through derived metrics (Staben et al., 2018). Consequently, 3D point data enhances the allometric modelling of AGB dynamics in forests (Dalponte et al., 2019; Næsset et al., 2013). However, this method requires significant computational time and advanced hardware resources (Duncanson et al., 2021; Rosenqvist et al., 2003). Despite these demands, 3D point data provides a precise method for estimating AGB at the individual tree level. In the case of the Acadian Forest, only destructive allometric methods are available, and it contains LiDAR data collected by Leading Edge Geomatics. Additionally, remote sensing data for soil organic carbon is also accessible. . The study of Aboveground Biomass (AGB) and its trends is essential for the health and sustainability of Acadian forests. AGB serves as a key indicator of forest biodiversity, supporting various plant and animal species while playing a crucial role in carbon sequestration, which helps mitigate climate change. Utilizing advanced technologies like LiDAR and satellite-based data allows for precise monitoring of AGB, enabling researchers to assess forest dynamics, growth rates, and the impacts of climate change over time. This high-resolution data collection is not only cost-effective but also provides long-term insights that are vital for effective forest management and conservation strategies.

Beyond ecological implications, understanding AGB trends has significant social and economic ramifications. Engaging local communities in monitoring efforts fosters stewardship

and awareness of natural resources, while informed AGB data can guide sustainable forestry practices that balance economic needs with environmental health. Additionally, this information supports policymakers in crafting evidence-based conservation initiatives, ensuring the preservation of Acadian forests for future generations. Ultimately, the integration of AGB monitoring into forest management is crucial for enhancing climate resilience and maintaining the cultural heritage tied to these vital ecosystems. Next chapter discusses the importance of forests and literature on biomass estimation methods and challenges in assessing carbon sequestration followed by objectives observed in the Literature review.

CHAPTER 2 LITERATURE REVIEW

2.1 Role of forests in carbon sequestration

In recent decades, particularly since 1967, the levels of carbon dioxide (CO_2), a greenhouse gas, have been rising in the atmosphere, currently reaching a rate of 2.8 parts per million per year (ppm/year) as of 2023 (NOAA). This increase is primarily driven by the consumption of fossil fuels for electricity generation, industrial activities, household and commercial practices, as well as the burning of biomass, all of which contribute to higher CO_2 levels in both the atmosphere and oceans (Abas and Khan, 2014). Additionally, land use changes, particularly the conversion of forests to agricultural land, significantly contribute to CO_2 emissions (Abas and Khan, 2014; Malhi et al., 2002; Wei et al., 2014).

Forests serve as natural carbon sinks within the biosphere, absorbing CO_2, which is crucial for regulating climate-driven shifts (Abas and Khan, 2014; Beer et al., 2010; Bonan, 2008; Kindermann et al., 2008; Rosillo-Calle and Hall, 1992). However, Curran and Curran (2025) indicate that natural carbon pools are declining, having peaked in 2008. For example, the current atmospheric CO_2 increase of approximately 2.5 ppm per year would have been around 1.9 ppm if natural sequestration had not started to fail. Specifically, forests in ecotone regions, which experience edge effects, often show disturbed biodiversity and decreased ecosystem productivity (Bouman et al., 2020; Dimitrov et al., 2014; Frazier et al., 2015; Hufkens et al., 2009; Kark, 2012; Pearson and D'Orangeville, 2022). Therefore, accounting for carbon biomass storage in forests in ecotone regions, is essential not only for human survival but also for climate policies set by organizations like the (IPCC) and (REDD), especially in the context of a growing population and the pursuit of a sustainable future.

Only destructive allometric methods are currently available for assessing forest carbon storage for Acadian Forest. LiDAR data owned by Leading Edge Geomatics, which provides detailed three-dimensional information about the forest canopy and terrain, is an invaluable high-resolution data for understanding forest dynamics and structure. In addition to LiDAR, access to remote sensing data related to soil organic carbon levels within the Acadian Forest is also useful. This combination of 3D data, image data, and thematic data is crucial for evaluating the carbon storage potential of the forest ecosystem, as soil organic carbon plays a significant role in overall carbon sequestration. These non-destructive methods and advanced remote sensing technologies enable researchers and conservationists to monitor and manage the

Acadian Forest effectively, ensuring its health and sustainability while minimizing ecological impact.

2.2 Biomass estimation methods

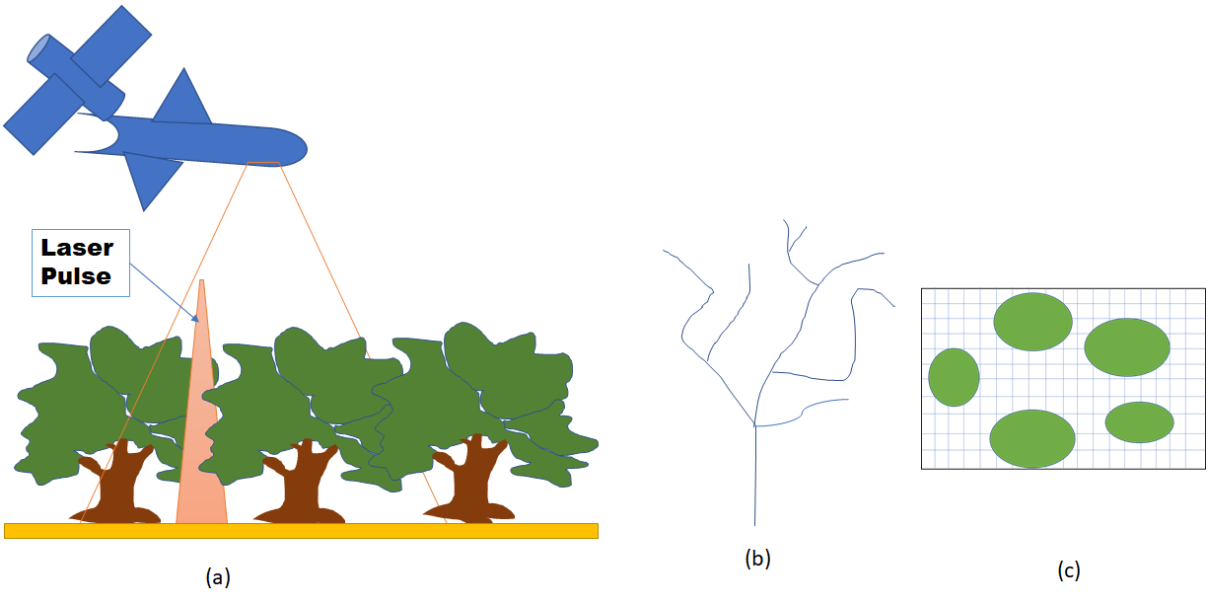

Figure 2.1 (a) Forest mapped by various sensors, (b) 3D skeleton of a tree, and (c) schematic optical image of a forest

2.2.1 AGB estimation from TLS

Terrestrial LiDAR is a popular technology for tree reconstruction and AGB estimation as it captures complete tree structure describing 3D skeleton and other semi-opaque components (Figure 2.2 (b) above) (Bremer et al., 2013; Calders et al., 2015; Holmgren et al., 2008; Raumonen et al., 2015, 2013; Rosenqvist et al., 2003). High-resolution LiDAR data not only characterises geometric variability in a tree but also records diversity of trees at the species level, which signifies its use for individual tree carbon storage (Jucker et al., 2022; Song and Dickinson, 2008; Vauhkonen et al., 2009, 2008; Verbeeck et al., 2019). For modelling tree components (crown, branches, and stem) and AGB estimation, two main approaches are geometric shape modelling and cluster-based approaches. Geometric methods derive a template of a tree by identifying the genus or geometric shapes. Geometric models approximate the outer surface of the crown by idealised shapes like cones, cylinders, or ellipsoids (Dong, 2010, 2009). However, the complex branch structure of the tree crown cannot be modelled. Recent studies like Hui et al., (2022) and Su et al. (2019) divided crown structure at multiple elevation levels to model crown variations. Irrespective of canopy shape, these studies sliced LiDAR data by parallel horizontal planes spaced at selected vertical interval. If the crown

structure of a tree hangs below the branch collar level, algorithms detect the stem as a canopy point. Moreover, if a large vertical interval (generally taken as 0.5 m) is selected, it may lead to incomplete canopy characterisation for dense canopies.

Clustering approaches, such as voxel-based, octree-based, distance cost function, graph-based based and cover set-based qualitative structure model (QSM) use high data density of LiDAR (Bailey and Ochoa, 2018; Bremer et al., 2013; Bucksch et al., 2009; Bucksch and Appel Van Wageningen, 2006; Fu et al., 2020; Raumonen et al., 2013; Su et al., 2019). Voxel-based methods primarily depict a 3D skeleton or a 1D descriptor for a tree. Cover set-based, and the Distance cost function focuses on the modelling of tree branches and the stem as small cylindrical segments. During modelling, every method first segments the point cloud in to small clusters of specific sizes of spheres and voxels. Thereafter, their eigenvalues are used to combine a cluster and its 8 or 26 neighbours. These eigenvalues are used to determine not only a cluster belonging to a segment of a branch or stem but also its direction. For this, tangent (ratio of first values is elongated) and normal space derived from eigenvalues are used. For a branch segment, the tangent space is elongated and vice versa for the stem. Secondly, the volume of all cylindrical and branch segments is calculated as the tree volume and the AGB of a tree is determined.

To date, the QSM method (Raumonen et al., 2013) is the most efficient, fast and approximate method of tree reconstruction. However, it requires the differentiation of the main trunk (dominant stem) a priori to model the remaining tree elements (branches). Furthermore, the QSM method demands relationships among neighbouring clusters to refine the process of tree structure extraction and AGB estimation. Also, the selection of voxel width and the diameter of a cluster influence the estimation of AGB (Menéndez-Miguélez et al., 2023; Raumonen et al., 2013). Although these methods achieve higher accuracies up to 92%, accuracy depends on tree structure and algorithm efficiency (Ai et al., 2020; Brede et al., 2019; Bucksch et al., 2010; Bucksch and Lindenbergh, 2008; Cárdenas et al., 2022; Raumonen et al., 2013). Moreover, acquiring terrestrial LiDAR data of a forest requires high-quality sensors, instrumentation and data storage. The above three factors cause difficulties in data registration from multiple scans, as forests do not often contain stable targets. Even with manmade stable targets, LiDAR data transfer requires high bandwidth connection, which is usually impossible in forests (Lindenbergh et al., 2025). Following section discusses AGB estimation using airborne LiDAR data. Below figure, 2.2 describes waveform and multiple return (discrete or pulsed) LiDAR return signals from a tree when mapped with Airborne LiDAR sensor.

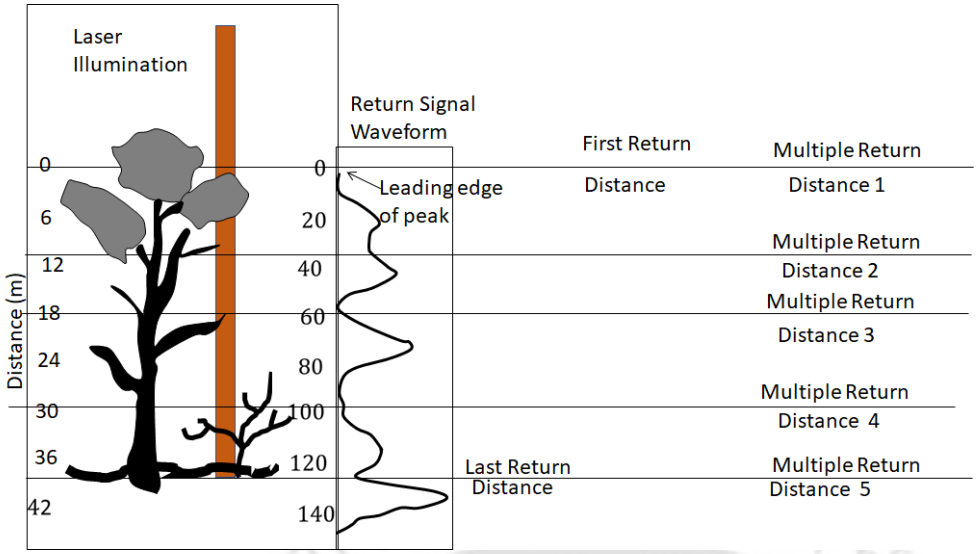

Figure 2.2 Signals from a tree mapped with waveform and discrete LiDAR

2.2.2 AGB estimation from Airborne LiDAR

Airborne point cloud data of a forest allows researchers to estimate the biomass of large and inaccessible forests with less data density of LiDAR data (typically less than 15 points/m²). Using airborne data, studies use two approaches, namely, area-based and individual tree-based approaches for estimating canopy volume and biomass distribution across a forest. Point and surface metrics are derived for biomass modelling in the two approaches at different plot scales (stand size). These metrics have been used to model biomass, forest types characterised by varying canopy density (mature, dense, open, over and under storey, degraded and non-degraded), and forest management techniques (planted, regrowth, or old).

2.2.2.1 Area-based approach

Area-based approach (ABA) uses canopy height model (CHM, also called canopy height profile) as a key variable for biomass modelling. CHM is a normalised digital surface model, constructed by subtracting a digital surface model (DSM) from a digital terrain model (DTM), which may be derived by waveform LiDAR, small-footprint LiDAR, or photogrammetry techniques for a study site. After creating CHM, the entire study area is divided into stands (horizontal or 2D grids) or voxels (3D or vertical grids) of pre-defined geometrical dimensions, which may be different from the CHM grid size. In addition, point and surface metrics are derived from CHM grids covering stands containing field inventory biomass data. Then, a mathematical allometric model is developed, and field inventory biomass data is modelled as a function of metrics. Thereafter, the developed mathematical model is assessed for its performance using R^2 and $RMSE_r$ using field inventory data.

The surface and point metrics reveal distinct patterns in the vertical structure of canopy layers, reflecting variations in vegetation types. Percentiles of the various metrics provide insights into the biomass distribution vertically, while summary statistics (standard deviation, kurtosis, skewness, and coefficient of variation of LiDAR Data points) offer an overview of the canopy's distribution in both vertical and horizontal directions. Further, measures like ‘differences in percentiles' highlight biomass distribution within the canopy, and 'proportion of canopy returns' measures forest height. Among the surface metrics, quadratic mean height (QMH or QMCH) and mean canopy height (MCH) are widely employed. QMCH is calculated as the square root of the sum of squared heights of all returns above the median height, representing the average height of the upper half of the canopy. Whereas, MCH is the mean of CHM values over a defined plot size, and the MCH indicates the average height of the canopy.

Nilsson, (1996)and Lefsky et al. (1999) are the earliest attempts using waveform LiDAR to model stand-wise biomass with LiDAR height and QMCH, respectively. However, in the early 2000s, researchers shifted from waveform LiDAR to small footprint LiDAR as latter capture more information on vegetation surface. Smaller footprint LiDAR provides detailed depth cross section profile of stands, which are used for stand-wise biomass modelling achieving higher accuracy for natural, planted, semi-natural, uneven-aged, extensively managed, and intensively managed forests. Moreover, using LiDAR data of available data density, studies focused on using existing or deriving new point or surface metrics for accurate biomass estimation and its dynamics for different types of forests and canopies at varying plot (stand) sizes.

Patenaude et al. (2004) explored the use of small-footprint LiDAR to model aboveground biomass (AGB) in trees and shrubs within temperate deciduous forests. They analysed 48 field plots (20m x 20m) with 2,272 trees and shrubs of varying maturity, achieving an R^2 of 0.74 by using the 80th height percentile for biomass modelling, which effectively distinguished between trees and shrubs. García et al. (2010) assessed biomass in Mediterranean forests in Spain, utilizing LiDAR densities ranging from 1.5 to 4.5 points/m² (hereafter $pts\ m^{-2}$). They introduced a density-weighted canopy reflection sum (DWCRS) metric, which indicated canopy closure. Their best AGB model at the species level, using DWCRS and the 90th height percentile, achieved an R^2 of 0.98, while the stand-level model using the 25th and 50th percentiles had an R^2 of 0.67. Thapa et al. (2015) developed biomass models for central Sumatran tropical forests over 8,072 hectares with a LiDAR density of 3.6 $pts\ m^{-2}$, finding

that a combination of the 75th height percentile, QMCH, and mean canopy height (MCH) explained over 73% of variance (R^2). Cao et al. (2019) studied biomass in managed bamboo forests and regrowth secondary forests, using 3.35 $pts\ m^{-2}$ LiDAR density across 31 circular plots (400 m² each). Their models, which included various height percentiles and canopy metrics, achieved a minimum R^2 of 0.78. They noted that low LiDAR density (less than 5 $pts\ m^{-2}$) was insufficient for capturing lower canopy structures. Following paragraph discusses vertical bin approaches that can distinguish lower canopy structures apart from tree height.

Vertical bins or voxels provide a detailed biomass distribution from ground to max imum height of stands in a forest. Asner et al. (2012) selected four tropical forest areas to develop a universal biomass model. Authors divided area into horizontal grids of 5 m × 5 m size and further divided each grid into vertical bins of 1 m height to calculate MCH. AGB is modelled with MCH, basal area (BA), and wood density by power rule. As collecting BA is intensive, authors replaced BA with a field-developed slope between BA and MCH. With replacement, authors achieved R^2 values between 0.68 and 0.85 for four regions. Adding another forest in Colombia, Asner and Mascaro, (2014) modified Asner et al. (2012) model. Instead of MCH, authors favoured top canopy height (TCH). The modified model achieved R^2 value of 0.923. In addition, authors found that uncertainties in AGB across plot sizes (0.01 to 100 ha) declined to minimum 10% at the one-ha plot size. Jucker et al. (2018) too attempted to understand uncertainty in AGB caused by both field and LiDAR metrics for varying plot sizes in Borneo tropical forests. Authors improvised AGB model of Asner and Mascaro (2014) by introducing canopy cover above 20 m from ground and obtained reduction in $RMSE_r$ from 32 to 19 Mg ha^{-1}. Similar results as of Asner and Mascaro (2014) for plot size are obtained.

2.2.2.2 ABA for biomass dynamics

Compared to static value of biomass for a forest at a specific time, temporal biomass models offer insights into forest dynamics influenced by climate conditions, human interventions, natural disturbances, and biological successions (Gao et al., 2013; Srivastava et al., 2017). Influences of these variables reflect in canopy surface characteristics, which is apparently reflected by CHM. Therefore, studies considered the CHM and derived metrics (canopy cover, and height percentiles and their summary statistics) to model forest dynamics at both stand and species levels. Studies determined biomass dynamics by defining vertical distribution of canopy layers using density metrics (percentiles or proportions point metrics in vertical direction) on temporal scale for all forests types (temperate, boreal, and tropical).

Cao et al. (2016) used regression based models with LiDAR data to predict forest biomass trends over two years for a mixed secondary subtropical forest having dense canopy. Authors derived percentiles of height differences and their L-moments, and canopy return density (the proportion of canopy hits exceeding a height threshold). Difference in mean height, and 75^{th} and 95^{th} percentiles of height differences were most responsive to biomass changes with R^2 value of 0.67 as these variables successfully capture shifts in vertical height distribution of growing canopy in the coniferous trees. Zhao et al. (2018) used LiDAR data and field inventories of multiple years to monitor tree growth, biomass dynamics, and carbon change in boreal forests of thin canopy in Scotland. For stands (size 25m × 25m), authors measured MCH and changes in canopy height density i.e. changes in proportion of number of LiDAR points in voxels of a stand over years to determine biomass change in for years 2008 and 2012. As changes in 3D canopy structure are vividly reflected by the CHM data on time scale, authors obtained R^2 value of 0.9 between change in canopy heigh density and field biomass. Dalponte et al. (2019) also investigated the carbon dynamics of Italian Alps at species level by canopy volume ratio (CVR) metric, which is ratio of sum of volumes under CHM pixels within a hexagonal stand to product of maximum height of the CHM pixels and area of the stand (707 m^2 area). If only top canopy layer is present, CVR metric is equal to 1 (otherwise less than 1 for multiple layers). Changes in CVR indicate temporal variations of biomass caused by variations of canopy heights. The study achieved low R^2 value of 0.53 for the biomass dynamic model at species level due to uneven aged mixed species forest. Some research studies like Hurtt et al. (2004), Stephens et al. (2007), and Thomas et al. (2008) coupled CHM metrics extracted from LiDAR data with ecological demographic models, and climate models for biomass forecasting. For such models, area-based methods illustrated superior accuracy than image-based methods with improvement in R^2 values from 0.53 to 0.98. These models, popularly known as 'ecological demographic models (or EDM)' use compels ecological processes, extensive climate, and other data for estimating biomass dynamics.

2.2.2.3 Tree based approach

For biomass modelling of individual trees, individual trees are extracted from CHM by segmentation using watershed algorithm (Alexander, 2009; Dalponte et al., 2019; Yang et al., 2020). The watershed algorithm considers LiDAR-derived CHM as topographic surface, where tree tops are peaks and gaps between trees are valleys. The algorithm simulates flooding of this surface with water filling up from the lowest points (valleys) and forming "watersheds" around each peak (tree top). By identifying watersheds around each tree peaks, the algorithm

effectively segments the CHM into distinct tree crowns and thereby extracts individual trees. For each of the extracted trees, point metrics (tree height, crown diameter, species density, canopy projection area or CPA), and crown generated volume (or CGV) are determined (Räsänen et al., 2013). Thereafter, field AGB values are modelled as function of point metrics.

With low LiDAR data density for large area forests, individual tree extraction based studies often focus to improvise tree segmentation methods, canopy surface based tree grouping, and integrating tree based and area based approaches. Kwak et al. (2010) studied individual tree biomass in stands of varying tree densities (high, medium and low tree densities) using small-footprint LiDAR for Korean temperate forests. For each tree in the forest, they modelled biomass using crown generated volume (CGV) and stem volume. With CGV metric as input variable, R^2 values of 0.5705, 0.6621, and 0.6832 were obtained for low, medium, and high-density stands, respectively. Lee et al. (2013) refined the watershed algorithm for tree segmentation for temperate forests by a cost function, which is a linear function giving equal weights to tree shape eccentricity and compactness of tree center with ellipsoid shape . Eccentricity is calculated by fitting ellipsoid shape to a segmented tree and compactness is the distance between the center of the fitted ellipsoid and coordinates of point of the maximum height for the segmented tree divided by half of sum of major and minor axis of the ellipsoid. Moreover, authors used overlapping ratio with cost function for accurate tree segmentation and achieved an accuracy of 93%. Subsequently, biomass is modelled as a polynomial function (up to 3rd order) of LiDAR height with an accuracy of 71%.

Though modifications improvised tree segmentation accuracies for temperate and boreal forests, yet existing tree segmentation methods often fail for tropical forests with complex and dense canopy surfaces. For the thick tropical forests, some studies calculate biomass as a direct function of crown volume. Coomes et al. (2017) devised a generalized tree-centric approach using crown radius and canopy height for four different tropical forests with data density of 7.3 $pts\, m^{-2}$. For a tree in each of the four forest types, authors used product of tree height and crown diameter (or HCD) to model individual tree biomass. An allometric equation was modelled for selected 91 trees in four forests and validated for 65. The model showed R^2 = 0.74 and $RMSE_r$ of 11.8%. Graves et al. (2018) investigated AGB models for individual trees with data density of 5.63 $pts\, m^{-2}$ for agricultural landscapes comprising different canopy covers. Depending on percentage of crown edge shared with the other neighbouring trees, authors grouped trees into three classes – isolated, intermediate, and complete edge-sharing trees – to identify different canopy covers. HCD was estimated for with equal numbers of trees

in each of three classes to formulate a linear AGB model. Due to inaccurate tree segmentation of trees, the method described low R^2 value of 43%. Goldbergs et al. (2018) modelled AGB for individual trees as a function of their heights for tropical savanna forests with data density of more than 15 $pts\ m^{-2}$ and achieved R^2 value of 0.754. Although tree segmentation methods improved the accuracy of biomass estimation, accuracy ($RMSE_r$ and R^2) remained limited to less than 75% with low data density (typically up to 15 $pts\ m^{-2}$). Table 2.1 indicates study area, type of data used, metrics used and model accuracy achieved with associated metrics.

Area-based methods and individual tree-based methods using 3D point cloud data are precise techniques for biomass estimation, as these methods are not dependent on environmental factors (temperature, precipitation, aerosol content etc) or vegetation stress (Rosenqvist et al., 2003). However, for large scale in diverse forests ABA frequently suffer for their reliance on expensive high-quality field inventory data, LiDAR point cloud data and low precision to capture individual tree properties within a CHM, and presumed homogeneity within plots. On the other hand, individual tree-based techniques demand high-resolution LiDAR data (more than 50 $pts\ m^{-2}$ is expected), propagate errors due to incorrect crown, and stem segregation.

2.2.3 Image-based AGB approaches

Image-based remote sensing techniques are widely used for mapping land cover and monitoring the environment of large-scale ecosystems (Xiao et al., 2006, 2005). Optical, NIR, and microwave data, which are readily accessible and precise for analysing tree structure, provide insights about spatial distribution, size, density (richness of vegetation), and canopy characteristics of individual trees, stands and forests. Research papers on image-based biomass models for forests can be classified into three categories: (I) assessing amount of biomass in a forest at stand or species level, (II) determining appropriate size of field plot (or stand) for a satellite image to model biomass, and (III) improvising accuracy of computational methods for biomass modelling. Table 2.2 below shows studies related to Image based methods.

After image data collection and corrections for topographic, radiometric, and atmospheric errors, the process of developing spectro-biophysical model (biomass) using 2D imagery for an area involves four key calculation steps. Steps are: (i) reflectance calculation; (ii) extraction of predictors such as brightness, backscatter, band ratios, and band transformations (e.g. PCA, TCA etc.), (iii) allometric modelling between AGB and the extracted parameters using regression or machine learning (ML) with a sample of minimum 20 field AGB data, and (iv) biomass prediction and building a wall-to-wall biomass map.

Table 2.1 LiDAR (Airborne Waveform or Discrete data type) based studies

Study Area	Remote Sensing Data	Metric or Dependent Variable for Biomass Model	R^2	$RMSE$ (Mg/ha) $RMSE_r(\%)$	Reference
Ålö Island, (Stockholm)	Airborne Waveform LiDAR data	LiDAR height	0.78		Nilsson, (1996)
Maryland, (USA)		Quadratic Mean Canopy Height	0.81		Lefsky et al., (1999)
Monks Wood National Nature Reserve	Airborne Discrete LiDAR data	Height percentile	0.74	26.21	Patenaude et al., (2004)
Alto Tajo, (Central Spain)		Height and its percentiles and summary statistics, Density Weighted Canopy Reflection Sum	0.67		García et al., (2010)
Riau Province, (Indonesia)		Height, Quadratic Mean Canopy Height, and its percentiles and summary statistics, Volume metric	0.73		Thapa et al., (2015)
Yushan Forest, (China)		Height and its percentiles and summary statistics, Canopy cover	0.78		Cao et al., (2019)
Hawaii Island, Madagascar, Amazonian Peru, and Central Panama		Mean canopy height	0.68-0.85		Asner et al. (2012)

Hawaii Island, Madagascar, Amazonian Peru, Colombia and Central Panama		Top of canopy height	0.923		Asner and Mascaro, (2014)
Borneo, (Malaysia)		Top of canopy height, Canopy cover		19	Jucker et al. (2018)
Yushan Forest, (China)		Height and its percentiles and summary statistics, Canopy return density	0.67		Cao et al., (2016)
Aberfoyle Village, (Scotland)		Mean canopy height, Canopy density	0.9		Zhao et al., (2018)
Lavarone (Trento), Italian Alps		Canopy volume ratio	0.53		Dalponte et al., (2019)
Gwangneung experimental forest		Canopy generated volume	0.57		Kwak et al., (2010)
National Arboretum, South korea		Tree height		71%	Lee et al., (2013)
Sepilok Forest Reserve, (Malaysia)		Top of Canopy height, Tree height, Crown diameter	0.74		Coomes et al., (2017)
Azeuro Peninsula, (Panama)		Tree height, Crown diameter, Crown overlap ratio with neighbouring trees	0.43		Graves et al., (2018)
Litchfield National Park, (Australia)		Tree height	0.754		Goldbergs et al., (2018)

Table 2.2 Satellite or Airborne (Visible, RADAR data type) based studies

Study Area	Remote Sensing Data	Metric or Dependent Variable for Biomass Model	R^2	$RMSE\ (Mg/ha)$ $RMSE_r(\%)$	Reference
Eglime and Zouzouvou, (Republic of Berlin)	IKONOS	Reflectance	0.72	74.5%	Thenkabail et al., (2004)
Finnish Forestry Centre (Southern Finland)	ASTER		0.56	44.7	Muukkonen and Heiskanen (2005)
Finnish Forestry Centre (Southern Finland)	ASTER & MODIS			10.1	Muukkonen and Heiskanen (2007)
Lake Tahoe Basin (California)	IKONOS	Shadow Fraction			Greenberg, Dobrowski, and Ustin (2005)
Chibougamau and Radisson (Quebec); Wabush (Labrado)	Quick Bird (PAN)		0.87		Leboeuf et al. (2007)
Minas Gerais (Brazil)	Geo Eye-1	Vegetation Indices	0.81		Coltri et al. (2013)
Mongolian Grasslands (China)	MODIS & LANDSAT-8		0.75		Li et al. (2016)

Xieertala Farm, Hulunber and Inner Mongolia (China)	SENTINEL-2 & LANDSAT-8		0.71		Qin et al. 2021
Helan Mountains National Nature Reserve (Ningxia Province)	SENTINEL-2		0.91		Ma et al. (2023)
Washburn Ranger District, (Northern Wisconsin, USA)	LANDSAT-7 ETM+		0.95		Zheng et al. (2004)
Karimunjawa and Kemujan islands (Indonesia)	ALOS AVNIR-2		0.62		Wicaksono et al. (2016)
Zagros Forests (Iran)	LANDSAT-8 OLI		0.681		Safari et al. (2017)
Greenbelt Farm of Agriculture and Agri-Food (Canada)	CASI hyperspectral data		0.78		Liu et al. (2004)
Majella National Park, (Italy)	Airborne Hyperspectral data	Red Edge Position Index	0.58		Cho and Skidmore (2009)
Majella National Park, (Italy)	Airborne Hyperspectral data		0.7		Cho et al. (2007)

Savannah River Site, (South Carolina)	AISA Hyperspectral data		0.926		Gong et al. (2012)
Bhitarkanika Forest Reserve, (India)	EO-1 Hyperion data	Vegetation Indices	0.81		Pandey, Anand, and Srivastava (2019)
Manaus (Brazil), Danum Valley Field Centre (Malaysia) and Khun Khong catchment (Thailand)	LANDSAT TM		0.71		Foody et al. (2003)
Georgia State (USA)	LANDSAT ETM+		0.58		Meng et al. (2007)
Madagascar (Analanjirofo Region)	WORLD VIEW-2	Vegetation Indices. Textures		6.82%	Eckert, (2012)

2.2.3.1 *Brightness-based approach*

Brightness value (DN) of a stand or a species, particularly in Red and NIR bands, is influenced by crown surface and composition. Moreover, these parameters vary with age of trees in a forest (Rosenqvist et al., 2003). Some research studies like Du et al. (2012) prefer to ignore age of trees to model biomass. However, most studies consider age of trees and use direct and indirect methods for estimating biomass of stands for forest inventory, agriculture crops, and large-scale forests.

Direct method divides stands according to age and model biomass as a function of brightness. Thenkabail et al. (2004) developed biomass models using age wise field data for oil palm trees (1 to 5 years) with IKONOS images (4m x 4m) in West African agroforests amid agricultural land conversion. As younger palm trees have less dense structures (Descals et al., 2024), study achieved R^2 value of 0.72. Muukkonen and Heiskanen (2005) developed biomass models to study the effects of stand size (1 to 3 hectares) on updating boreal forests inventory. Using ASTER, authors created a linear and neural network (NN) model for stand sizes from 0.06 to 30 hectares and observed an optimal size of 2.5 hectares. Furthermore, they found that both models overestimated biomass for stands less than 60 years age and underestimated biomass for stands over 80 years. For a large area forest (1,000 hectares), authors repeated same study in 2007. Muukkonen and Heiskanen (2007) used MODIS data (resolution 250 m), which covers stands of size 1-3 hectares. As average brightness value reduced the mixed pixel effect, all image pixels of ASTER data occupying a MODIS pixel were assigned DN value of MODIS. Due to large forest area, having diverse species of different ages, authors obtained $RMSE_r$ of 7.6%. Du et al. (2012) focused on non-linear partial least square (NLPLS) regression technique for biomass modelling of Maso bamboo forest of 6,700-hectare area using LANDSAT (30 m). NLPLS reduced multiple correlations between bands and achieved R^2 value of 0.949.

Indirect methods model biomass as a function of derived variables like shadow fraction from greyscale images. Greenberg, Dobrowski, and Ustin (2005) first introduced the indirect method that extracts shadow fractions of vegetation cover. Biomass is linearly modelled as a function of shadow fraction. Leboeuf et al. (2007) modified the shadow fraction method using azimuth and zenith angles. Authors also compared performance of modified method against original by R^2 value, which increased from 0.85 to 0.87. Brightness-based methods are affected by factors like vegetation stress.

2.2.3.2 *Vegetation indices-based approaches*

Vegetation indices (VIs) and band ratios (BRs) effectively identify characteristics of a stand or tree by minimising soil reflectance and atmospheric effects (Lillesand et al., 2015; Silleos et al., 2006). Distance-based and slope-based VIs indicate density of vegetation, and health of trees in a stand. Moreover, indices distinguish different age groups in a stand (Foody et al., 2003; Hu et al., 2020; Meng et al., 2007; Pandey et al., 2019; Powell et al., 2010; Rahman et al., 2008; Safari et al., 2017; Wicaksono et al., 2016; Zheng et al., 2004).

Conventionally, regression models link VIs and BRs to the AGB of stands. Coltri et al. (2013) developed models for coffee crops, an agricultural product in Brazil, using Geoeye-1 images (1.65 m resolution). Authors found that biomass is correlated with plant height and RVI, with 0.71 and 0.81 values, respectively. Li et al. (2016), Ma et al. (2023) and Qin et al. 2021 developed models for grasslands, which account for 41% of the land surface in China. Li et al. (2016) developed models for different ecological zones of grasslands using MODIS and LANDSAT-8 (30m resolution) data. Authors modelled biomass as function of four VIs. As RVI quantifies greenness of grasslands better than other indices and thus, models involving RVI achieved a minimum R^2 value of 0.75. Qi et al. (2021) compared biomass models of Sentinel-2 (10 m) and LANDSAT (30 m) for grasslands with different grazing intensities. Models with normalised difference phenology index, insensitive to soil reflectance, showed R^2 values of 0.763 and 0.721 with Sentinel and LANDSAT images, respectively. Ma et al. (2023) developed normalised pure vegetation index focusing on grasslands using intensities on red bands with Sentinel-2 images and obtained R^2 value 0.91.

VIs cannot quantify variations in biomass concentration between genus and species in a stand. Thus, several studies have proposed dividing stands according to age, disturbance, and species before modelling biomass collectively. Zheng et al. (2004) categorised pine and hardwood stands into specific age groups using inventory data (95 plots of 0.05 hectares) for an undisturbed boreal forest and R^2 value improved from 0.82 to 0.95. Wicaksono et al. (2016) and Safari et al. (2017) employed NDVI and LAI with LANDSAT images and limited field data to stratify disturbed forests of Mangrove Forest and Zagros Forest land (5 million hectares), respectively. By stratification, authors achieved model R^2 values of 0.62 and 0.681, respectively.

Unlike multispectral data, hyperspectral data captures subtle variations in reflectance of different species. Liu et al. (2004) used hyperspectral data to estimate biomass of wheat, soybean and corn. Authors achieved R^2 values of 0.78, 0.99 and 0.95 for biomass models for

wheat, soybean and corn, respectively. Along with VIs, Cho et al. (2007), Cho and Skidmore (2009), and Gong et al. (2012) used red edge position for biomass modelling of forest crops. Pandey, Anand, and Srivastava (2019) employed Hyperion hyperspectral data to classify mangrove forests into species and modelled biomass. Elevated reflectance levels in red and NIR spectral bands provided higher accuracies in both biomass and species classification (R^2 = 0.861 and 84%).

VI-based methods are focused on modelling biomass for a study site. Contrarily, Foody et al. (2003) and Meng et al. (2007) addressed applicability of VI models for regions showing fewer variations in elevation, temperature, precipitation, and soil type. Foody et al. (2003) produced R^2 value greater than 0.71 with Neural Network. Meng et al. (2007) studied effect of intra-site characteristics on biomass modelling for various counties in the USA and obtained R^2 value of 0.58. Image textures complement VIs as they discriminate mixed pixels into pure pixels, and enhance the detection of small-scale features. Co-occurrence matrices, known as global co-occurrence matrices (GLCM), are widely used. Eckert (2012) quantified carbon stock for naturally disturbed humid rainforests by stratifying forests into degraded and non-degraded areas and developed models using VIs, reflectance, and GLCM measures. Authors obtained $RMSE_r$ of 6.82% for degraded forests with GLCM.

Image-based methods are limited in capturing the crown's underlying structural details and has signal saturation issue, where sensors lose sensitivity to capture vegetation traits beyond a certain biomass threshold (250-275 Mg/ha) (Pham et al., 2023). Furthermore, high-resolution sensors like Sentinel-2 still face challenges in penetrating dense forests (Duncanson et al., 2010; Ma et al., 2023; Mutanga et al., 2023). Together, these limitations highlight the need for advanced techniques that characterize vertical data and improve biomass estimation.

2.2.4 Carbon pool monitoring of a forest

In a forest, carbon stored in different sinks which can be seen in figure 2.3. below which are formed during the tree growth stages and also by naturally.

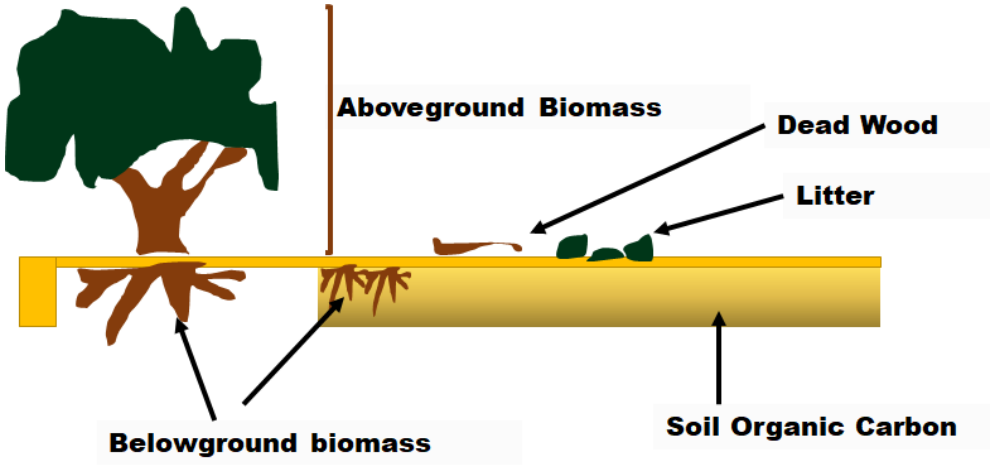

Figure 2.3 Different carbon pools in a forest

For carbon monitoring in any forest ecosystem, popularly used simulation models are, namely 'Forest Vegetation Simulator' (or FVA) and 'Integrated Valuation of Ecosystem Services and Tradeoff' or (IVEST) (Ismaili Alaoui et al., 2023). These two models measure changes in land usage and land cover of the forest using moderate resolution satellite images such as LANDSAT, MODIS etc. However according to Haseeb et al., (2024), above simulation models cannot adequately capture unique growth-mortality characteristics and species diversity of boreal and temperate forests. In addition to above, according to Schlamadinger and Marland (1996) and Schlamadinger et al. (1997) for accounting for carbon pools in forest ecosystems two primary components – forest carbon storage and carbon emissions into the atmosphere – are required. Carbon storage includes the total biomass of the forest at a given time, as well as the soil organic carbon stored in the forest's ground. In addition, carbon emissions data should encompass statistical information specific to the forest's location, particularly regarding wood harvesting and greenhouse gas emissions. This emissions data must also account for contributions from transportation, residential areas, agriculture, forestry, waste management, buildings, electricity, and commercial industries aligning with the state, province or country policies (Filonchyk et al. 2024).

2.2.4.1 Carbon pool monitoring of a Acadian forest

Allometric models are considered state-of-the-art models for studying carbon sequestration for the Acadian Forest. Albert et al. (2023), Bashir et al. (2019) and Bill et al. (2023) are very few studies addressing biomass dynamics due to disturbances like fire, climate induced dynamic patterns in temperature and precipitation, and spruce webworm diseases in the Acadian Forest, respectively. These studies critically assessed resilience of the Acadian Forest by estimating forest biomass patterns at the species level using geometric variables

(allometric equations), environmental factors, and soil carbon. Study by Bashir et al. (2019), predicting forest biomass dynamics by carbon sequestration at stand level in the Acadian Forest, found that hardwood-dominated stands in these forests exhibited increased carbon levels with age. In contrast, Balsam-fir dominated stands experienced a decline in carbon after reaching 80 years of age. Albert et al. (2023), which included environmental variables to model biomass, highlighted need of re-evaluation of existing forest biomass storage in the Acadian Forest. The study predicted biomass changes against possible environmental shifts, specifically 4–6°C increase in mean annual temperature between years 2071 and 2100, which would result in a 39%–77% increase in growing degree days and a 48 -79 mm decrease in summer atmospheric water balance throughout New Brunswick state. These environmental changes will also affect water and heat balance cycles. Bill et al. (2023) observed that carbon storage in soil is essential for biomass production, plant growth, and mortality. However, each of these studies considered impacts of mentioned variables in isolation, thereby missing potential interactions and cumulative effects of the involved variables. In addition, the Acadian Forest has unique species composition and respective growth-mortality attributes that affect carbon sequestration and its dynamics, especially for old stands in New Brunswick province. The species composition not only influences biomass accumulation (carbon storage) and growth rates of individual species but also affects forest structure and functions. Further, competitive interactions can affect resource allocation for species growth by influencing light availability, and soil nutrient uptake, which affect carbon sequestration capabilities (Neilson et al., 2007). Apart from that, allometric models for the Acadian Forest frequently fall short of forest structure details needed for estimating biomass dynamics.

2.3 Conclusion from literature review

Although highly dense LiDAR data depicts tree structure efficiently though, its full potential to estimate wood volume is not yet fully realized. State-of-the-art methods are prone to assumptions like regular geometric shapes, uniform distribution of crown, and vertical orientation of stem structure. Also, the recently proposed methods suffer from subjectivity in deciding geometric parameter values, i.e. vertical interval, voxel width, cover diameter, etc. High-resolution remote sensing and high-quality ground-truth data are also essential for AGB model calibration and validation. Significant challenges for the AGB estimation are field data collection and data processing. Despite its significance, accurate biomass mapping of boreal forests using satellite images faces significant challenges as harsh climatic conditions, difficult terrain, limited accessibility, larger spatial expanse, and remote locations of the forests restrict

comprehensive and precise ground truth data collection for traditional biomass measurement methods (Bruening et al., 2023). Moreover, integrating multiple attributes of these datasets in computationally efficient manner for biomass estimation of boreal forests also poses additional challenges. First, the integration of two data sets, such as GEDI and Sentinel-2 is inherently complex due to different spatial resolutions, temporal frequencies, and data formats. Moreover, these datasets require pre-processing steps such as atmospheric correction, mosaicking, and resampling to ensure compatibility and consistency. The process is further complicated when incorporating topographic data from DEM, necessitating additional adjustments to account for terrain effects on biomass distribution. Secondly, while indices from Sentinel-2 are valuable for capturing vegetation characteristics, combining them with GEDI's vertical structure metrics and DEM-derived slope and aspect information involves careful consideration (Nguyen and Kappas, 2020). Therefore, which combinations of variables provide the most reliable predictors for aboveground biomass (AGB) without introducing redundant or noisy data is also difficult.

In the case of the Acadian Forest, despite LiDAR data are available, the first challenge is that only non-destructive allometric methods for aboveground biomass estimation are available,. Further, species-wise field measurements (DBH, H) on stands of 400 m^2 are available allover New Brunswick state though, very few plots overlap the LiDAR data. Thus, it remains challenging to model biomass distribution all over the Acadian Forest, coupling field measurements and Airborne LiDAR data. Moreover, for areas where LiDAR data is not available or accessible, we want to develop a generic biomass model leveraging advantages of high resolutions spectral bands and vegetation indices derived from Sentinal-2, topographic data (slope and aspect) from SRTM 30m DEM, and GEDI Level 4A data providing biomass estimates at 25m resolution. Secondly, even though statistical data of carbon emissions are available, to date, no comprehensive method for accounting of carbon pools in forests, especially Acadian forests, is available. Thirdly, soil organic data for the entire New Brunswick is available for 2021, yet no model exists that includes effect of soil data for biomass estimation. Because of the above, this thesis is focused on developing an accurate biomass estimation method for trees and forest addressing the challenges faced during the application of the technique to terrestrial LiDAR data, airborne LiDAR data, and dynamically changing geospatial thematic data like temperature, precipitation, soil distribution, biodiversity, plant species distribution, hydrological cycle, carbon cycle etc. Finally, the thesis develops a carbon sequestration model that integrates biotic (such as tree growth) and abiotic (such as greenhouse gas emissions) components of the Acadian Forest and provides a comprehensive method for

estimating carbon sequestration within the forest ecosystem using ecological demographic model. Objectives of the thesis are as follows:

I. To develop a biomass estimation method using high resolution terrestrial LiDAR data for individual tree. This requires extraction of various interweaved features of a tree (canopy, stem, branch etc) for multi-branch structure for biomass estimation.

II. To adapt and refine the biomass estimation methos for TLS for the for the airborne LiDAR data (ALS) to address the challenges of lower data density in Acadian forests. It includes automated tree extraction for a large forest data and developing allometric equations.

III. To develop a generic biomass model leveraging advantages of high resolutions satellite data facilitating derivations of spectral bands and vegetation indices and topographic data (slope and aspect) from DEM, and GEDI Level 4A data providing biomass estimates at 25m resolution. This work allows examining performance of two algorithms for regression based modelling,

IV. To model carbon sequestration in Acadian forests using real-time airborne LiDAR data considering various factors like temperature precipitation, terrain elevation, landscape, albedo, soil nutrients and soil types, and location of the forests and combined them to monitor carbon storage and its dynamics. This work includes information derived from forest structure information using 3D data, environmental variables, terrestrial biosphere models. Further, carbon sequestration is modelled using soil carbon, species composition, and abiotic factors.

Next chapter presents methods for the biomass estimation for individual tree and forest from terrestrial and airborne LiDAR data. Moreover, it also provides the configuration of Ecological Demography model and its outputs for accounting carbon pools in the Acadian Forest.

CHAPTER 3 METHODOLOGY

3.1 Study Area

Acadian Forest study site, centred at 65.1667° W longitude and 46° N latitude, emerged after wildfires from years 1880 to 1905. Located between north-eastern North America's boreal and temperate northern hardwood forests, the site covers approximately 90 km^2 area around Fredericton city in New Brunswick province (Canada). The Acadian Forest climate is characterized by prevailing continental westerly winds influenced by the nearby Atlantic Ocean and varying weather patterns with high humidity and mild winters. Also, higher elevation of the region (around 820 meters) and the neighbouring northern Appalachian Mountain range contribute to high precipitation and cool and humid summers.

Recent data confirm that average monthly precipitation is approximately 93 mm with 20% snowfall. In addition, average annual temperature has increased from years 1981 to 2010. A mean value of 5.24°C and around 100 frost-free days per year are reported. Moreover, the January and December months of a year typically experience minimum and maximum daily temperatures of −15.7°C and 11.7°C, respectively. As a result, the Acadian Forest are undergoing transformations including shifts in ecosystem composition and unexpected disturbances such as fire and clear-cutting. Moreover, the urban population for their survival harvesting softwood and hardwood (Bennemann et al., 2023) often uses Acadian Forest.

The Acadian's ecotone region, consists of boreal and temperate forests, containing both deciduous and coniferous trees and hosting approximately 32 tree species. The forest is primarily dominated by eight tree species, namely, Black spruce (*Picea mariana*), Balsam fir (*Abies balsamea*), Yellow birch (*Betula alleghaniensis*), White spruce (*Picea glauca*), Sugar maple (*Acer saccharum*), Red maple (*Acer rubrum*), and White birch (*Betula papyrifera*). Among these, Black spruce, Balsam fir, and White spruce are associated with cooler boreal forest types (Albert et al. 2023). Randomly distributed field data, which were collected over circular field plots each of 400 m^2 area, is available for the whole New Brunswick. Next sub-section presents details of LiDAR remote sensing data. Figure 3.1 below shows location map of the study site.

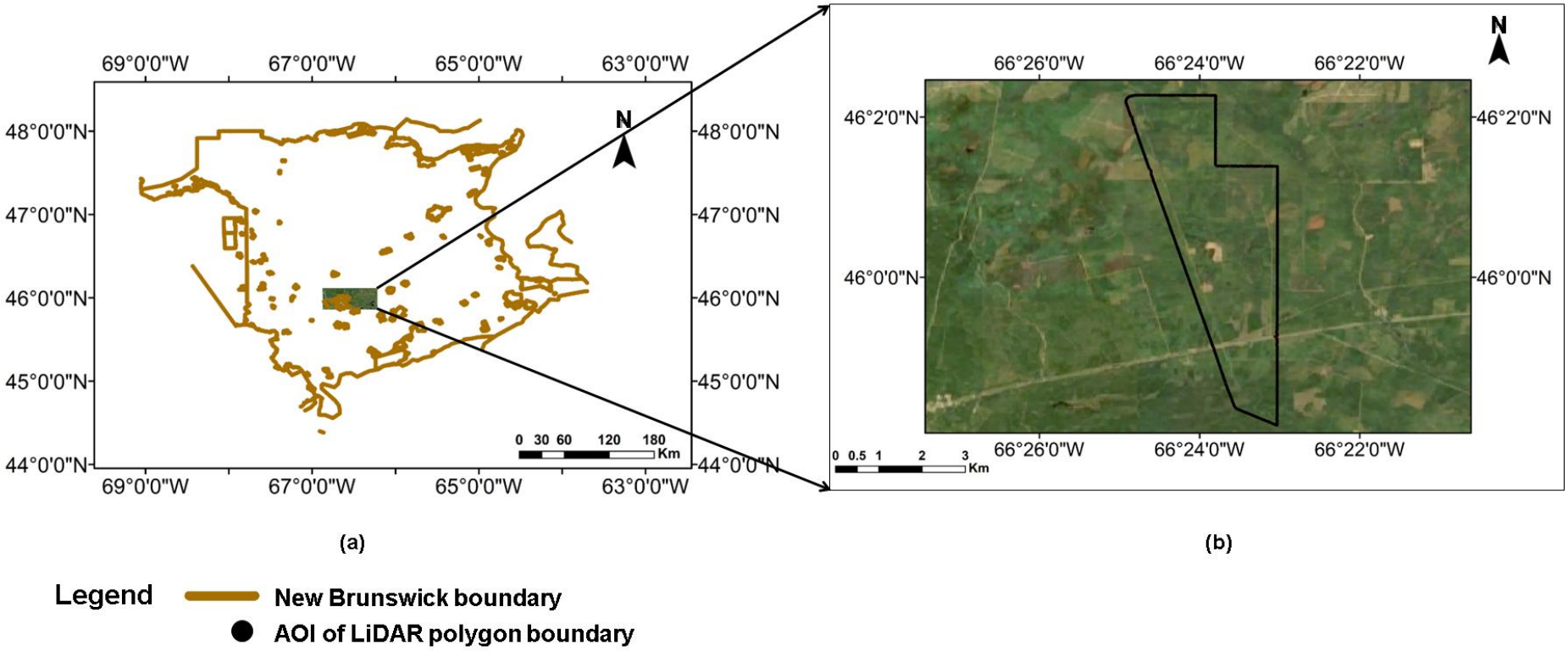

Figure 3.1 (a) Administrative boundaries of New Brunswick and (b) Google image of the AOI of Acadian Forest area

3.2 Data Sources

3.2.1 Terrestrial LiDAR Data

Terrestrial LiDAR data sets were obtained from a repository created by Gonzalez de Tanago et al. (2018) to create a tree reconstruction method for accurate biomass estimation as terrestrial data is not available for the study site. In this repository, LiDAR data of 29 individual trees were acquired by terrestrial LiDAR scanner with a beam divergence of 0.35 mrad and scanning resolution of 0.06°. Co-registered data show an accuracy of 1cm and data density of more than 1000 points/m^2 for each tree. Moreover, the repository also contains harvested biomass volume, density, and biomass expansion factor (BEF) for all trees.

The repository contains trees of three locations, Peruvian, Indonesian and Guyanese, located in Peru, Indonesia, and Guyana respectively. The repository contains fourteen tree species: Wallaba Ituri, Huruasa, Korokororo, and Wallaba soft, etc (identified at the flora level). The spatial locations of the acquired data sets are Peruvian dataset −12.27 Latitude (lat), −69.10 Longitude (long); Indonesian dataset −2.41 lat, 113.13 long; and Guyana dataset 6.04 lat −58.70 long. In addition, the trees' height in the Peruvian region ranges from 29.4 to 36.2 m. In the same way, the height of trees in the Guyanese and Indonesian regions varies from 28.74 to 48.64 m and 24.34 to 38.45 m, respectively. The volume of the trees determined by the field destructive method is also included in the repository. From visual examination of the LiDAR data from Peruvian site that the crown depth and diameter cover greater volume than the stem. However, for the other two sites (Indonesian and Guyanese), volume of stem is more than that of crown. Additionally, the tree canopy in each of the three locales ranges from sparse to dense. Next section discuss the methodology to estimate carbon from above ground biomass using terrestrial LiDAR data, airborne LiDAR data.

3.2.2 Airborne LiDAR Data

Scenesharp Technologies Incorporation (Canada) provided the LiDAR data, which was originally collected by Leading Edge Geomatics. The data was acquired with data density of 6 points/m^2 in year 2021 in five separate tiles encompassing a total of 9.955 km^2 area. A black-coloured line in Figure 1 above shows the extent of the LiDAR polygon, which lies between latitudes of 45.97° N to 46.04° N and longitudes of 66.52° W to 66.34° W.

Each of the five tiles is geo-registered in NAD83 reference frame, with heights referred to Canadian geodetic vertical datum (year 2014). Point clouds were registered within the spatial reference system of the New Brunswick Double Stereographic Projection and transverse

Mercator projection with vertical accuracies (Root Mean Square Error, $RMSE$), respectively, of 0.0509 m and 0.0998 meters at 95% confidence interval.

3.2.3 Sentinel-2 data

For estimating biomass of the large forest area, we used Sentinel-2 Level 2A (L2A) data. Sentinel-2 offers high-resolution multi-spectral imagery with 13 spectral bands, covering visible to shortwave infrared wavelengths (Mohite et al., 2024). The L1C data were processed to L2A using the ATCOR algorithm through the Sen2Cor plugin, correcting for atmospheric effects (Askar et al., 2018). Figure 3.2 shows the Sentinal-2 imagery of the study site.

Figure 3.2 Sentinel-2 L2A Imagery Acadia Forest (Source: www.copernicus.eu, accessed on May 26, 2024)

Specific bands and variables from the Sentinel-2 data including vegetation indices are selected to serve as input features for biomass estimation. Table 3.1 shows the selected variables, band information, and significance of band for biomass estimation.

Table 3.1 Raw bands and vegetation indices used in the study

Categories	Variables	Bands & Resolution	Significance	Ref.
Raw spectral features	Coastal aerosol	Band-1(B1)-60m	Atmospheric correction, especially for aerosol detection and water vapor correction	(Nuthammachot et al., 2022)
	Blue	Band-2(B2)-10m	Crucial for assessing vegetation health, density, and biomass	(Nguyen and Kappas, 2020)
	Green	Band-3(B3)-10m	Sensitive to vegetation greenness	(Nguyen and Kappas, 2020)
	Red	Band-4(B4)-10m	Sensitive to changes in chlorophyll content and leaf structure and capture subtle variations in vegetation density and structure	(Nguyen and Kappas, 2020)
	Vegetation red edge	Band-5(B5)-20m	Indicate the amount and health of vegetation	(Nuthammachot et al., 2022)
	Vegetation red edge	Band-6(B6)-20m	Can penetrate through the canopy to some extent, providing information about the vegetation structure beneath the canopy	(Nuthammachot et al., 2022)
	Vegetation red edge	Band-7(B7)-20m	Sensitive to vegetation characteristics such as leaf structure and water content	(Nuthammachot et al., 2022)
	NIR	Band-8(B8)-10m	Sensitive to the structural properties of vegetation, such as leaf area and canopy structure	(Nguyen and Kappas, 2020)

	Vegetation red edge	Band-8A(B8A)-20m	Sensitive to changes in vegetation health, biomass, and structure	(Nuthammachot et al., 2022)
	Water vapor	Band-9(B9)-60m	Sensitive to vegetation water content	(Nuthammachot et al., 2022)
	SWIR	Band-11(B11)-20m	Sensitive to vegetation properties such as water content and biomass density	(Nuthammachot et al., 2022)
	SWIR	Band-12(B12)-20m	Sensitive to vegetation water content and canopy structure	(Nuthammachot et al., 2022)
	TCI	10m	Determine stress on vegetation by temperatures and excessive wetness	(Nuthammachot et al., 2022)
Vegetation indices	VARI	10m	Reduces the influence of soil background and non-photosynthetic vegetation.	(Croci et al., 2022)
	EVI	10m	Sensitive to vegetation health and density and more responsive to variations in canopy structure.	(Croci et al., 2022; Nguyen and Kappas, 2020)
	MTVI2	10m	Capturing information about chlorophyll content, canopy structure and leaf area.	(Croci et al., 2022)
	NDVI	10m	provides a measure of the health and density of vegetation	(Croci et al., 2022)
	SAVI	10m	Reduction of Soil Influence and Improved Vegetation Estimation.	(Croci et al., 2022; Nguyen and Kappas, 2020)
	MSAVI	10m	minimize the influence of soil brightness	(Croci et al., 2022)

	DVI	10m	used to assess vegetation health, vigor, and biomass density	(Croci et al., 2022)

3.2.4 Digital Elevation Model (DEM)

The Shuttle Radar Topography Mission (SRTM) datasets are global digital elevatiom model (DEM) products prepared by collaborative efforts involving National Aeronautics and Space Administration (NASA), National Geospatial-Intelligence Agency (NGA), and contributions from the German and Italian space agencies (Nguyen and Kappas, 2020). These datasets provide DEM with a spatial resolution of 1 arc-second, equivalent to approximately 30 meters at the equator. Figure 3.3 exhibits DEM data of the study site.

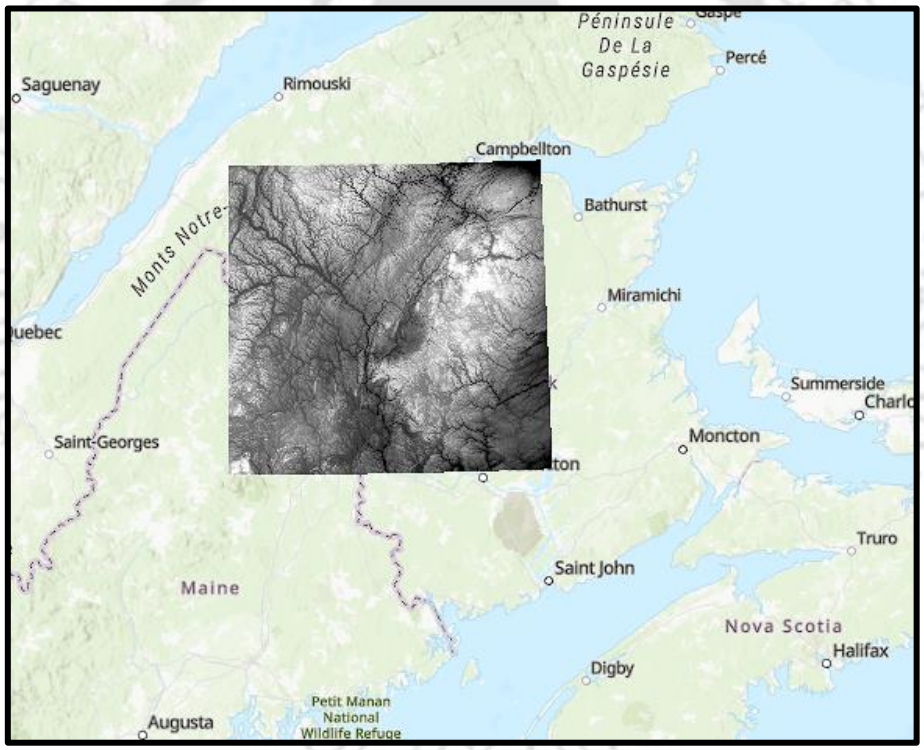

Figure 3.3 DEM data for Acadia Forest (Canada)

The DEM attributes (elevation, slope, and aspect each at 30m cell size), which characterize terrain and environmental conditions, are selected as topographical features for the biomass model for the two study sites. These attributes directly influence light and water availability, soil condition, and other factors essential for biomass estimation studies. Consequently, DEM data enhances the accuracy and reliability of above-ground biomass density (AGBD) estimation models.

3.2.5 Global Ecosystem Dynamics Investigation (GEDI)

The study used monthly GEDI Level 4A (L4A) (version 2) predictions of above-ground biomass density (AGBD) as target or dependent variables. GEDI, equipped with full-waveform Lidar at 1064nm, illuminates Earth's surface with footprints of approximately 25 meters and collects detailed three-dimensional data about Earth's forests and topography. Specifically, GEDI gathers canopy height, canopy structure, biomass estimates, ground elevation, and vegetation cover data from the International Space Station (ISS), providing insights into carbon stocks in forests (Mohite et al., 2024). The L4A product, derived through parametric linear models, correlates GEDI L2A waveform metrics with AGBD, encompassing broad forest vegetation coverage (Morin et al., 2022). Figure 3.4 shows satellite trajectory and wide coverage of GEDI biomass data over the study site.

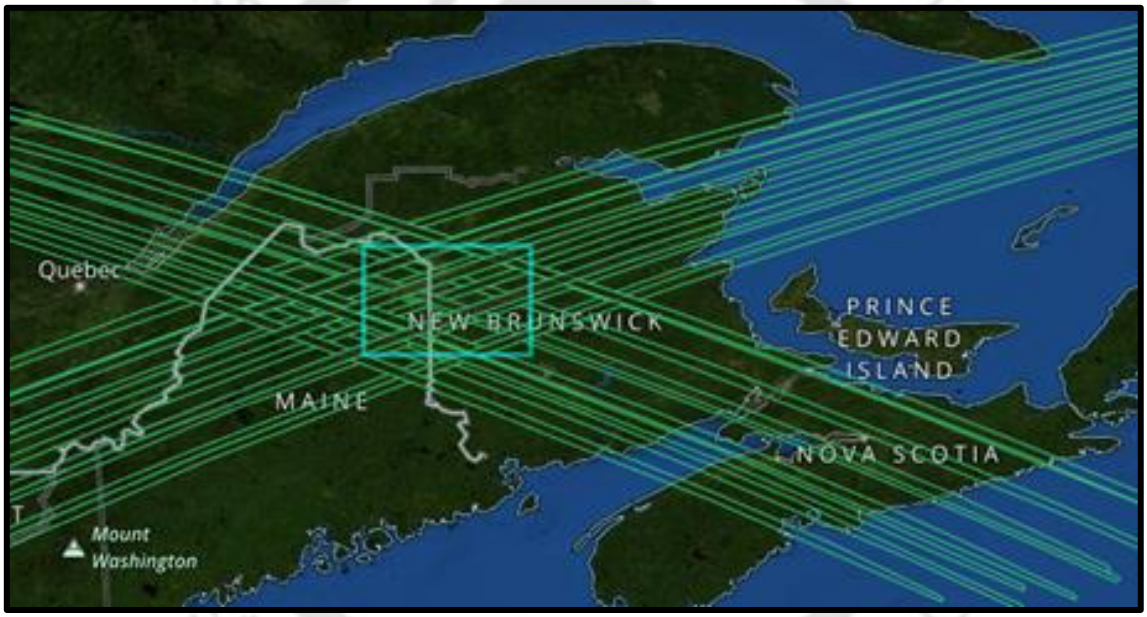

Figure 3.4 GEDI L4A trajectory for Acadia Forest

Figure 3.4 trajectories of footprints of about 25 m every 60 m along the track of GEDI instrument (in yellow colour). These beam transects are roughly 600 m apart, covering an across-track width of approximately 4.2 km. Aboveground biomass density (AGBD) estimates are derived from parametric models linking simulated GEDI Level 2A (L2A) waveform height metrics to field plot AGBD estimates. A calibration dataset was created by compiling height metrics from simulated waveforms and field estimates across various regions and plant functional types (PFTs), such as deciduous and evergreen trees, grasslands, and shrubs. For each of the eight beams (yellow), AGBD estimates come with accompanying uncertainty metrics, quality flags, model inputs, and additional details about the GEDI L2A waveform for

selected algorithm settings. Model inputs consist of scaled GEDI L2A height metrics, geolocation variables, and land cover data, including PFTs and region identifiers. Outputs also include AGBD predictions in both natural and transformed units, along with prediction uncertainties.

3.2.6 Allometric data

Table 3.2 below shows summary of field inventory data for 10,000 samples of 7 numbers of species for New Brunswick provided by Natural Resources and Energy Development – New Brunswick (DNR) (hereafter DNR).

Table 3.2 Summary of field inventory data (DBH, H) of seven species across New Brunswick (Min, Mean, Max and Sd indicate minimum, average, maximum and standard deviation, respectively)

Variables	**No. of Samples**	***DBH* (cm)**				***H* (m)**			
		Min	**Mean**	**Max**	**Sd**	**Min**	**Mean**	**Max**	**Sd**
White birch	817	7.1	18.18	64.5	8.08	1.9	13.21	30	4.65
Black spruce	2080	7.1	18.39	72.5	7.68	1.3	12.76	29.6	4.16
Red spruce	1453	7.1	24.86	62.5	11.32	1.3	14.98	30.7	4.97
White spruce	574	7.8	25.19	59.1	10.7	2.2	15.36	29.3	5.65
Balsam Fir	4179	5.8	17.73	85.1	7.05	1.3	12.47	30.1	4.32
Red maple	1274	7.1	21.48	79.7	10.5	1.6	14.51	29.6	4.22
Norway spruce	25	9	19.47	30.9	6.64	4.9	9.8	13.7	1.912

Table 3.2 above shows that for seven species, DBH and H vary nonlinearly. Table 3.3 below shows species wise samples of DBH and H along with their range.

Table 3.3 Summary of samples of DBH and H of seven species across New Brunswick province

Variables	DBH range (cm)	Number of samples	H range (m)	Number of samples
White birch	7.1 - 21.45	588	1.89 - 11.26	263
	21.45 - 35.8	206	11.26 - 20.63	511
	25.8 - 64.5	23	20.63 - 30	43
Black spruce	7.1 - 28.9	1903	1.3 - 10.73	657
	28.9 - 50.7	167	10.73 - 20.16	1325
	50.7 - 72.5	10	20.16 - 29.60	98
Red spruce	7.1 - 25.6	832	1.3 - 11.10	345
	25.6 - 44	525	11.1 - 20.9	935
	44 - 62.5	95	20.9 - 30.7	172
White spruce	7.8 - 25.27	312	2.2 - 11.23	161
	25.27 - 42.73	235	11.23 - 2027	297
	42.73 - 60.2	38	2027 - 29.29	127
Balsam fir	5.8 - 32.23	4042	1.3 - 10.9	1571
	32.23 - 58.67	136	10.9 - 20.5	2445
	58.67 - 85.1	1	20.5 - 30.1	163
Red maple	7.1 - 31.3	1070	1.6 - 10.93	231
	31.3 - 55.5	190	10.93 - 20.26	939
	55.5 - 79.7	14	20.26 - 29.6	104
Norway spruce	9 - 17.1	11	4.9 - 7.83	4
	17.1 - 252	8	7.83 - 10.76	12
	25.2 - 33.3	5	10.76 - 13.69	8

As evident from Table 3.2 and Table 3.3, variation of DBH (reported by standard deviation) is greater than tree height for each species.

3.3 Data Processing and Analysis

For terrestrial LiDAR data, no-de noising has been applied as the data provided is accurate according to Gonzalez de Tanago et al. (2018). However, for airborne LiDAR data two steps has been applied. In the first step, point cloud that contain electric transmission lines

are manually removed from each of the five tiles. Thereafter, for each tile MATLAB default denoising method is used, where the method removes the noise from data based on nearest neighbours of a point (Rusu et al., 2008).

3.4 AGB estimation of individual tree from TLS data

A tree stem (or trunk) diverges into branches from the branch collar level (Hackenberg et al., 2014). From this level upwards, branches and leaves combine to form crown and canopy of tree. In the proposed three-step method for trees which have crown surface above or at the branch collar level, stem data and crown data are separated automatically and provided as inputs. The first step divides stem data by adaptive vertical slicing followed by geometric modelling. Second and third steps model crown structure of tree. In second step, a 3D plane having maximum crown projection area and centred at the tree's center of gravity is defined as canopy plane. Thereafter, crown points are sliced vertically, projected on the canopy plane, and divided into canopy and non-canopy points. In third step, with canopy points serving as seed points, non-canopy points are classified into various branches using a sphere clustering process.

The clustering process classifies crown data for both straight and curvilinear branches. For a straight branch, data points are fitted to cylindrical shape. For a curved branch, data points are further grouped in collinear and connected segments for cylinder fitting. Branch volume is calculated as sum of all straight and collinear segments. Finally, Wood volume is estimated as sum of volumes of stem and all branches. Figure 3.5 below shows detailed steps of methodology.

Let ***PC*** be the point cloud of an individual tree, which consists of *N* number of points. Each point is identified by its coordinates (X, Y, Z). Points below branch collar level and above branch collar level are referred as sets ***ST*** and ***BS***, respectively. Height of first branch of a tree from ground level is referred as crown base height (CBH). Sections 3.4.1 to 3.4.5 describe details of the three-step method.

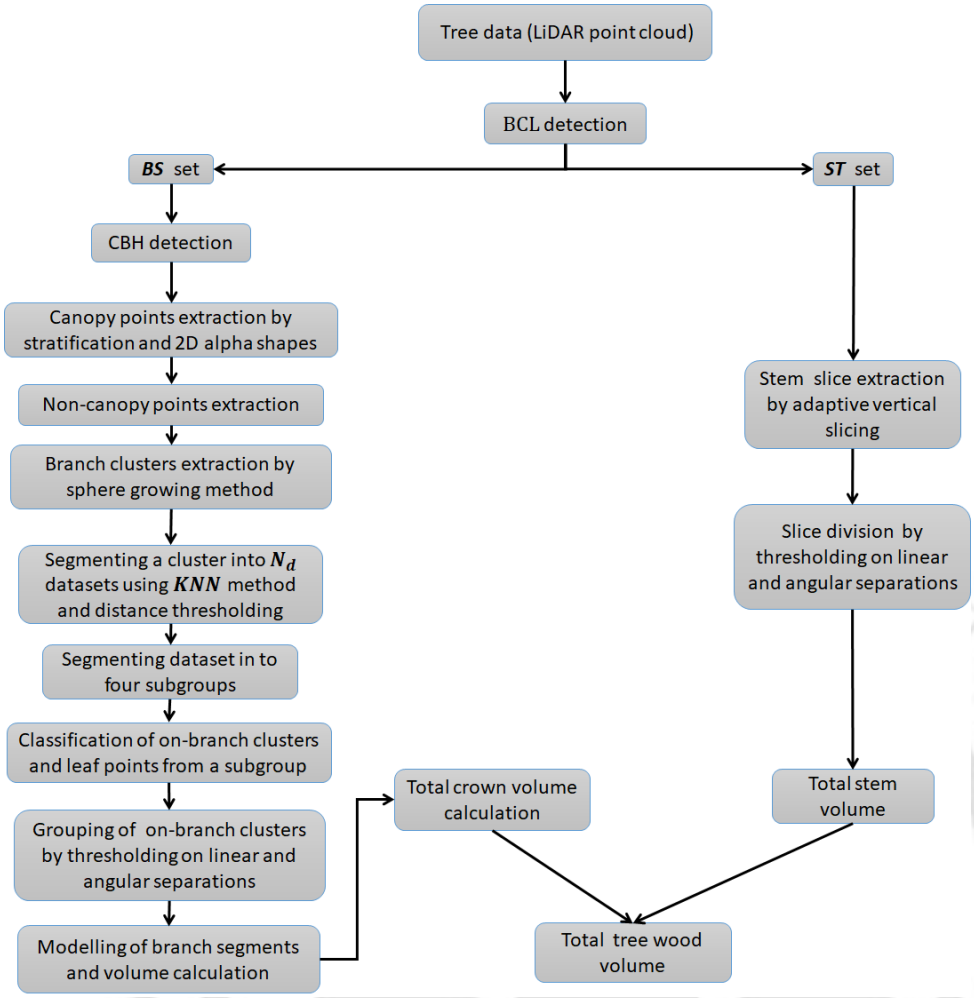

Figure 3.5 Flow chart of proposed method

3.4.1 Branch collar level detection

BCL is typically characterized by a swollen horizontal cross-sectional area, where minimum two branches emerge from stem. Thus, stem and crown data can be separated at the BCL. To detect the BCL in point cloud of a tree at the BCL, the point cloud data is sliced in vertical direction from minimum to highest elevations with 5 cm interval, which is defined as stem interval. This value of the stem interval for dense LiDAR data of trees is adopted from Eto et al. (2020). Next, a slice of point cloud is vertically projected onto a horizontal plane ($Z = 0$). For the projected points, a circle is fitted. This process is repeated for each of the slices. For two consecutive point cloud slices, difference of radius values of their respective circles is calculated. If the difference is less than or equal to 1.7 cm, which is equal to one-third of stem interval (5 cm), both point cloud slices belong to stem. However, if the difference exceeds 1.7 cm, which is equivalent to 1° deviation of line joining centres of the two fitted circles from vertical, the two point cloud slices are segregated into stem and crown. Lower and upper slices

are assigned to stem and crown, respectively. The lower elevation of upper slice (or upper elevation of lower slice) is calculated as the BCL.

3.4.2 Stem shape modelling

A tree stem is usually of cylindrical shape. However, in some cases, cylinder radius and thus stem curvature changes. Also, stem shape is irregular at bottom of tree, where stem connects to ground surface. For modelling stem of tree, we start with conventional approach of forestry for slicing ***ST*** set into vertical bins (of 1 m height) (Eto et el., 2020). After creating bins, RANSAC method (Fischler and Bolles, 1981) is used for cylindrical shape fitting for data of each bin. For a bin, angular deviation of axis of fitted cylinder from vertical (θ_s) and linear deviation of data points from the cylindrical surface (d_s) are calculated by dot products of involved vectors – dot product of vertical axis and centroid of bin provides angular deviation, and dot product of cylindrical surface equation and a data point in a bin determines linear deviation of the data point. Figure 3.6 schematically shows the two variables (θ_s and d_s) for a bin or slice of the stem.

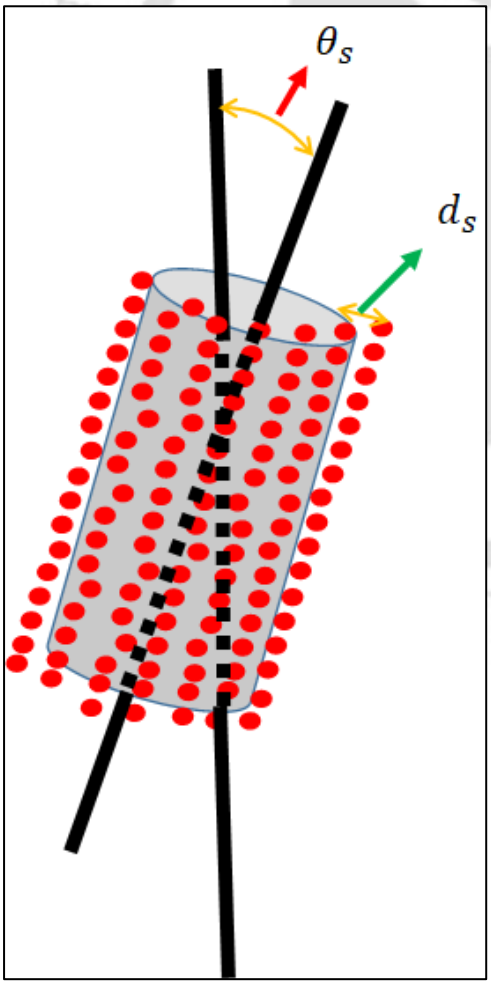

Figure 3.6 Angular deviation (θ_s) and linear deviation (d_s) for a stem slice.

If axis of a fitted cylinder for a bin deviates by 2° from the vertical direction, the bin is sliced into two bins of equal vertical heights. On the other hand, minimum vertical height of a bin is restricted to 15 cm, allowing a maximum deviation of 1.5 cm from axis of the fitted cylinder in horizontal plane. Cylinder height (h_s) and radius (r_s) are estimated for all bins. Multiplying cylinder height and its cross-section area (πr_s^2) determined volume of a bin. As mentioned before, stem area located around buttress of a tree may show irregular shapes. For this area, a bin is considered as irregular shape and 3D alpha shape is used to generate mesh to find volume.

3.4.3 Crown structure modelling

3.4.3.1 Canopy points extraction

LiDAR data points of crown surface or outer surface represent canopy points and shape of tree. Crown data contains $|\boldsymbol{BS}|$ data points. Canopy point extraction process consists of following four steps:

Step-(i): A 3D plane passing through tree's centre of gravity and having maximum crown projection area is determined by maximum Eigen vector of canopy data points. Plane containing maximum Eigen vector not only passes through centre of gravity but also contains maximum area of crown. This plane is referred as canopy plane.

Step-(ii): After determining canopy plane in step (i), crown data ($\boldsymbol{BS}$) is divided into different strata with statistically determined vertical interval as mentioned in Su et al. (2019). For this, canopy point cloud is sorted in ascending order of height data (Z-coordinate). Height difference between a point and its immediately following point of the sorted data is determined. The largest of these differences is selected as canopy interval (c). $\boldsymbol{BS}$ data is divided into n_S number of strata, which is calculated as:

$$n_S = \frac{Z_{max} - Z_{CBH}}{c} \quad (3.1)$$

where c = canopy interval

Z_{max} = maximum value of Z coordinates for tree canopy

Z_{CBH} = elevation of lowest crown point (or elevation of crown base height)

State of the art studies assume the lowest point of crown as branch collar level (BCL) and divide the crown in to vertical slices. However, in certain cases, the lowest point of crown is at an elevation higher than the BCL. In these instances, points located on the branch are erroneously categorized as canopy points. Hence, in order to determine the lower crown level accurately, a three-dimensional convex hull is produced for the $\boldsymbol{BS}$ set. Subsequently, the sorted Z values of surface points of the convex hull are plotted. The plotted curve shows the Z

value associated with discontinuity or vertical offset. The elevation value of upper end of the vertical offset is considered as Z_{CBH}. Figure 3 .7 shows plotted values of the Z values of points on convex hull surface for a tree. In figure 3.4 (c), Z levels are shown by vertical offset starting from 18.5 m to 23.714 m. Discontinuity in Z levels at 23.714 m is the crown base height (CBH). However, for simulation we lower this value by 5% i.e. value of variable $\boldsymbol{Z_{Crown}}$ is taken as the 22.5283m in this example.

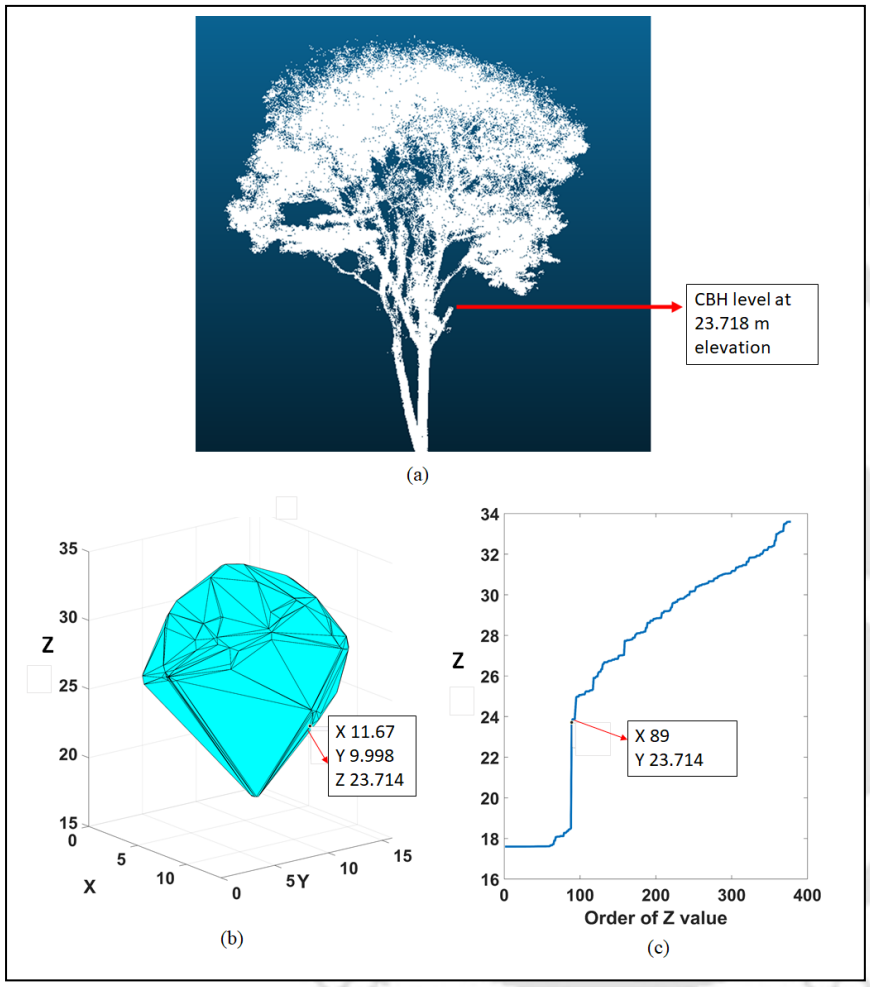

Figure 3.7 (a) Actual CBH level of tree, (b) and (c) Convex hull of BS set and Z values of BS set varying with number of Z values of the convex hull.

Step-(iii): After dividing crown data into strata in step-(ii), data points in a stratum are projected onto the canopy plane. Out of these projected points in canopy plane, outermost points show irregular shape of boundary of stratum. To detect the boundary points, Lindberg et al. (2014) and Liu and Wu, (2019) fit ellipse and triangular irregular network (TIN), respectively. However, regular shapes like ellipse fail to model irregular shape. On the other

hand, the quality of TIN models is highly dependent on the sampling density. In regions where data points are sparse, TIN might fail to accurately represent boundary, resulting to omit boundary points. To alleviate this problem, we first increased number of boundary points to avoid error of omission by projecting points in canopy plane onto a horizontal plane. Figure 3.8 schematically explains the process of canopy point detection for a stratum.

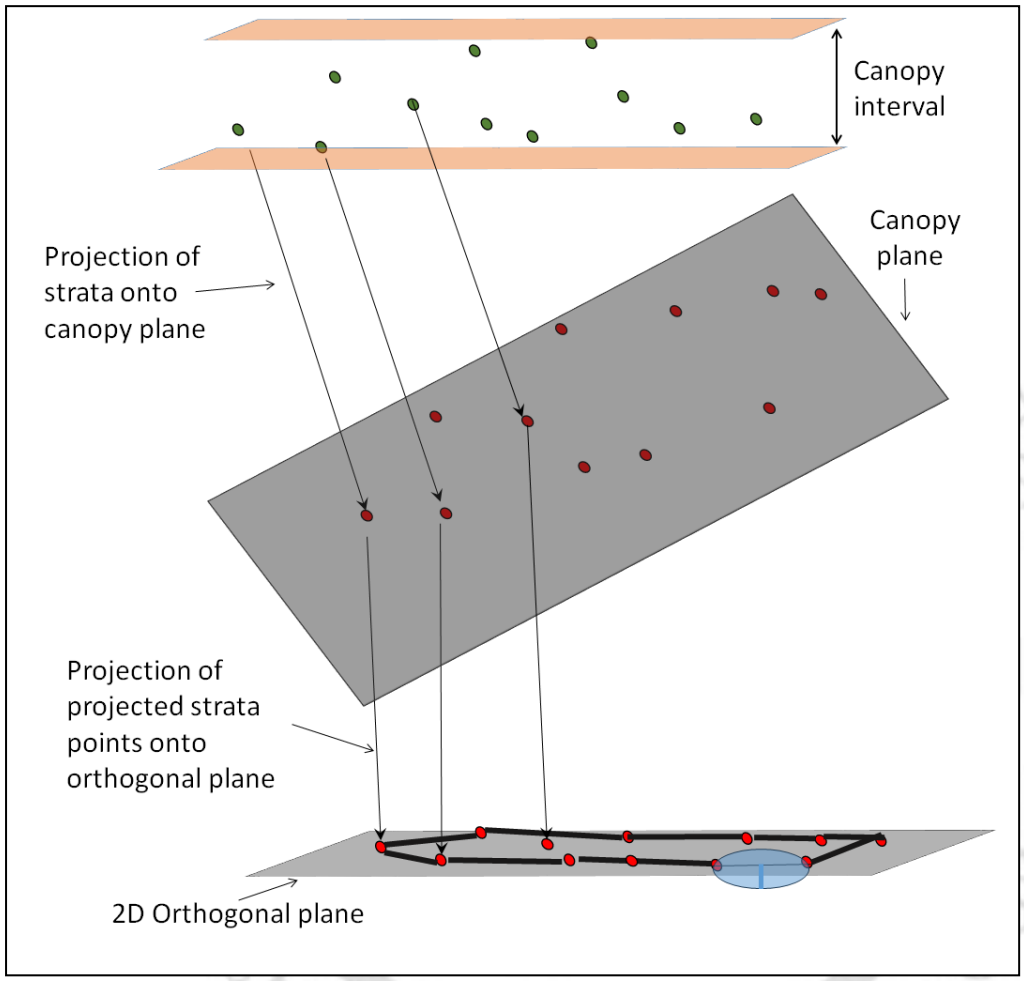

Figure 3.8 Schematic view of canopy points extraction for a strata.

After densification of the boundary points, we use 2D Alpha shapes for accurate delineation of boundary points. 2D alpha shape constructs a polygonal representation of points in a plane by Delaunay triangulation. A triangle is removed, if the radius of circumcircle for the triangle is larger than the specified alpha value. Remaining triangles form alpha complex. The boundary of this complex is the alpha shape (Guo et al., 1997; Hadas et al., 2017). Boundary points, obtained by alpha shape correspond to canopy points in a stratum. Above procedure, i.e. from steps (ii) to (iii), is repeated for n_S numbers of strata and canopy points are obtained for each

of the strata. Combining all canopy points for all strata derives canopy points of a tree. Using the derived canopy points, next sub-section extracts branch structure from a tree crown.

3.4.4 Branch data clustering

Canopy points show the outer surface of crown structure terminating with leaves and branch ends. Within crown structure of tree, branches merge and meet at a joint. Joints successively become ends of preceding branches. Following this, branches and joint structure develop spatial hierarchy of crown structure in 3D space and finally merges into stem.

Clustering process uses the canopy points as endpoints of branches, and traces course of a branch through non-canopy data points till the branch meets with another branch and form a joint. This classifies crown data points into different branches.

Canopy points extracted from $\boldsymbol{BS}$ is named as $\boldsymbol{CNP}$. Remaining points in $\boldsymbol{BS}$ data set are non-canopy points. As the distance between two branches is always greater than or equal to the canopy interval (c), we select one of the canopy points and its q nearest neighbours as seed points in canopy points ($\boldsymbol{CNP}$). Search radius for nearest neighbours is equal to canopy interval (c). These $(q + 1)$ seed points represent ends of branches or surface points of leaves. For each of the candidate points, a sphere is defined to classify non-canopy points into different branches. Radius of sphere (r_{sphere}) is set to 0.3 m.

Non-canopy points lying within the sphere of radius (r_{sphere}) are classified to a branch, which terminates at one of the canopy points. From this cluster of points formed in first iteration, the farthest point from the seed point (or centre of sphere) is selected as the centre point of sphere for second iteration. After the second iteration, cluster is updated with new data points and centre of recent cluster is used as centre of sphere for subsequent iterations. Also, after the first iteration, radius of sphere is incremented by 0.5 cm for each of the subsequent iterations. This clustering process, which recursively assigns points to a branch with moving sphere, continuously traces points for straight or curvilinear branch with minimum deviation of the points from centre axis of the branch. If two or more spheres, belonging to $(q + 1)$ candidate points, intersect at a non-canopy point, the non-canopy point indicates a joint.

Schematic figure of branch extraction from canopy points is shown by figure 3.9 below. In the figure 3.9, the seed point in canopy is represented by C. Points C1, C2, and C3 are three nearest neighbours of the candidate point C. The spheres centred at these points are highlighted in yellow, red, blue, and green colours, respectively. Blue arrows show the movement of spheres along the branches. As shown in the figure, the spheres from C and C1 merge at point p1,

consequently the point p1 is chosen as the centre point of sphere for next iteration. Similarly, for the spheres starting at points C2 and C3, the starting point for next iteration is p2.

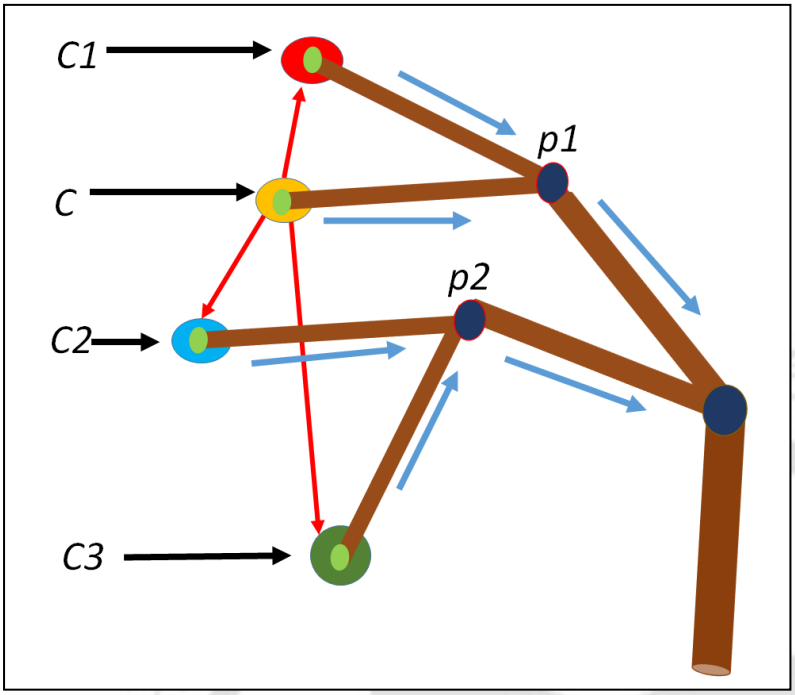

Figure 3.9 Spheres starting with canopy points C, C1, C2, C3 and its movement denoted by blue arrows.

As the clustering process progresses to assign data points in different branches from non-canopy data, special case of data discontinuity may appear.

3.4.4.1 Data discontinuity

Due to a discontinuity of data points on a branch, centre of sphere is not updated for specific number of iterations. In this case, the clustering process is terminated after limiting number of iterations. As length of a branch cannot be longer than diameter of crown, the limiting number of iterations (M) is determined by equations 2, 3, and 4 for a candidate point as:

$$M = \frac{\sqrt{(C_W \times 0.5)^2 + C_H^2}}{r_{sphere}} \qquad (3.2)$$

where $C_H = Z_{max} - Z_{CBH}$ (3.3)

$$C_W = \sqrt{(X_{max} - X_{min})^2 + (Y_{max} - Y_{min})^2} \qquad (3.4)$$

Where X_{max} and X_{min} are the minimum and maximum values of X coordinates in set $\boldsymbol{BS}$. Similarly, Y_{max} and Y_{min} are maximum and minimum of Y coordinate values, respectively. The method uses a single sphere for a seed point if no neighbour exists (or $q = 0$).

3.4.5 Cluster to branch segregation

A data cluster obtained in section 3.4.4 may contain multiple branches. To assign data points to a branch, we used nearest neighbour and line fitting processes, which are explain below:

3.4.5.1 Sub-grouping process

For clusters belonging to dense canopy, distance between points should be less compared to that of a sparse canopy. Thus, if a dense cluster is divided into smaller data sets, each divided dataset will contain more points compared to a sparse canopy cluster. We assume that if a cluster consists of more than 7 points, it is a dense cluster and may contain multiple branches. We divided such clusters into N_d datasets, each of which contain K points. Number of K nearest points in each of the N_d dataset are determined by equation (3.5):

$$K = round\left(\frac{100}{d_a}\right) \qquad (3.5)$$

Number of datasets (N_d) in a cluster can be calculated as:

$$N_d = \left(\frac{N_c}{K}\right) \qquad (3.6)$$

In equation (3.5) and (3.6), 100 is scaling factor and

d_a = average distance between data points of cluster (m)

N_c = number of data points in a cluster

A dataset (containing K points) derived from a cluster may contain mixture of branches and leaves points. We assume a maximum of four straight branches in a dataset. Therefore, to assigning data points in a dataset to different branches and subsequently to remove leaf points from each branch of the dataset, we further divided a dataset into four sub-groups in two stages by fitting 3D lines. This process of dividing a dataset into maximum four sub-groups consists of fitting a 3D line through all points of the dataset. Subsequently, for each point within the dataset, perpendicular distance from the point to the 3D line is calculated. Based on the positive or negative sign of the calculated distance, points are divided into two groups: positive group and negative group. This process of the line fitting and identifying two groups is repeated for the positive group and the negative group to create total four sub-groups. After this de-grouping process, each of the four sub-group defines a straight cylindrical branch.

3.4.5.2 Leaf points removal process

Though first step in above section, explained above, divides each of the four sub-groups may indicate individual branches, yet the leafy points in a sub-group behave as noise for a cylindrical shape of the branch (sub-group). For points belonging to surface of a branch, axis of cylinder (branch) is normal to both the individual points as well as to a plane created by any of the three neighbouring surface points of the branch. Thus, to remove leafy points, we construct a plane passing through three neighbouring in a sub-group. In other words, for a point on the branch surface, normal of the fitted plane is at right angle to the 3D axis of the branch. Whereas, if the plane consists of a leafy point, the plane cannot maintain right angle with the axis. Mathematically, for each point in a sub-group, dot product between normal vector of the fitted plane through three neighbouring points and the 3D axis of the branch should be equal to zero. However, as slight deviations are expected, authors have chosen threshold (t_d) calculated by equation 3.7.

$$t_d = 0.08\ (1\ + 0.5 \times\ d_g) \qquad (3.7)$$

Where $d_g =$ average distance between points in a sub-group (m)

If the dot product value exceeds threshold, t_d, the point is declared as leafy point and removed from the branch data (or the sub-group data). Data points obtained after this process are referred as on-branch points for a sub-group.

Figure 3.10 schematically shows a case of a KNN set, which contain two data points of branches represented by yellow and red colour (cylinders of pink and blue colours show two straight branches). Figure 3.10(a) shows dividing a dataset by a 3D line into two sub-groups: positive and negative. The two sub-groups are shown above and below black line, respectively. It should be noted that upper sub-group is denoted by two cylinders, yet they represent a sub-group. As a results, one sub-group is above the fitted line and one-sub-group is below the fitted line are shown in the figure 3.10(b). Each of the positive and negative sub-groups are further divided into positive and negative sub-group in second iteration. This provided maximum two more sub-groups in the second iteration. Figure 3.10(c) shows one of the four sub-groups with its 3D axis. Third step removes leafy points from a sub-group points as shown in figure 3.10(d).

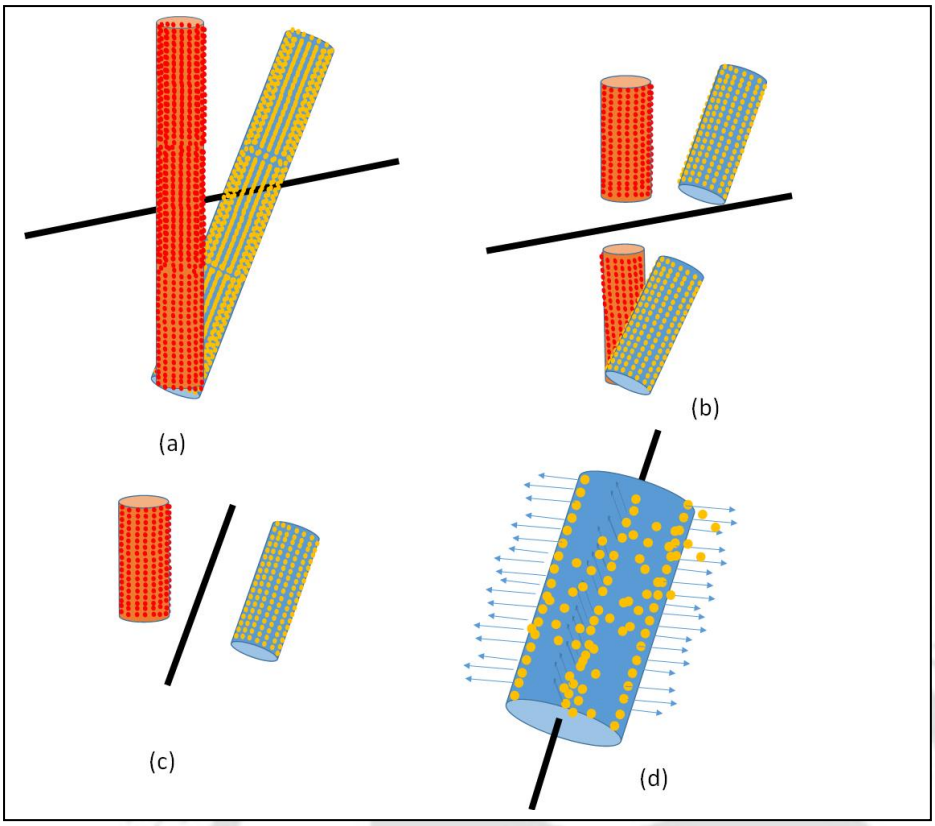

Figure 3.10 De-grouping of a dataset : (a) data points of a dataset of K points, (b) dividing a dataset into two sub-groups, (c) dividing two sub-groups into maximum four sub-groups (or four straight branches), and (d) normal to branch surface through points in a subgroup

3.4.5.3 Re-grouping of on-branch datasets and sub-groups

After de-grouping process, we obtain four sub-groups for a dataset. Two processes consisting of 'sub-grouping process' and 'leaf point removal process' are applied to all clusters and on-branch dataset are obtained. The four numbers on-branch datasets, belonging to a sub-group, may be parts of a branch. Therefore, for combining on-branch datasets of a sub-group, following two conditions are adopted: (i) angular deviation of 3D axis of any two on-branch datasets is less than 2.5°, and (ii) distance between the centroids of any two on-branch datasets is less than 4 cm. This process resulted in maximum four datasets and minimum one dataset for a subgroup (of K points). This process of de-grouping, characterized by two conditions above, is applied on adjacent sub-groups to combine multiple sub-groups, belonging to a cluster, of one branch. In case, if two sub-groups have multiple on-branch datasets, the two on-branch datasets are randomly selected and combined till no further combinations are possible. After this treatment, the resulted data sets are straight branch segments. Shape modelling of the straight branch segments are explained in next sub-section below.

3.4.5.4 Shape modelling of branch data

The above retrieved branch segments are assumed as straight branch segments. A straight branch segment is modelled as right circular cylinder. Length (l_b) and radius (r_b) of cylindrical branch segment are calculated for each of the segments by least trimmed squares, and hyper circle method, respectively (as explained by Nurunnabi et al. (2017)**).**

3.4.6 Volume estimation

Steps explained in sections 3.4.1 to 3.4.5 divide LiDAR point data in different branches and stem into straight segments, and identify branch joints. For each of the straight segments, a cylinder is fitted and volume of the cylinder is calculated. Similarly, for bottom part of a stem, which is not in cylindrical shape, volume is calculated by mesh generated by alpha shape. Sum of volumes of all straight segments and curvilinear segment at bottom of stem provide total volume of a tree. Volume multiplied by wood density and carbon conversion provides the carbon from above ground biomass of an individual tree.

For Acadian forest, terrestrial LiDAR data and field biomass data are not available. Furthermore, we applied the proposed method to individual trees but observed that airborne data contains only outer tree structure or crown data mostly. And no complete point cloud data on branches, which results in complete 3D cylinder construction and over estimation of branch volume and also without stem full complete tree reconstruction is impossible. The above factors will lead to under estimation of biomass by the above proposed tree reconstruction method. Next section describes how we addressed these challenges and proposed an approximate biomass estimation method that uses Airborne LiDAR and accurate allometric data provided by DNR.

3.5 AGB estimation of forest from ALS data

The biomass calculation method is motivated from the method proposed by Greenberg et al. (2005). For the Acadian forest site although airborne data is available, but due to no field data authors developed a method using DBH and LiDAR tree height. The methodology is given in the below figure.

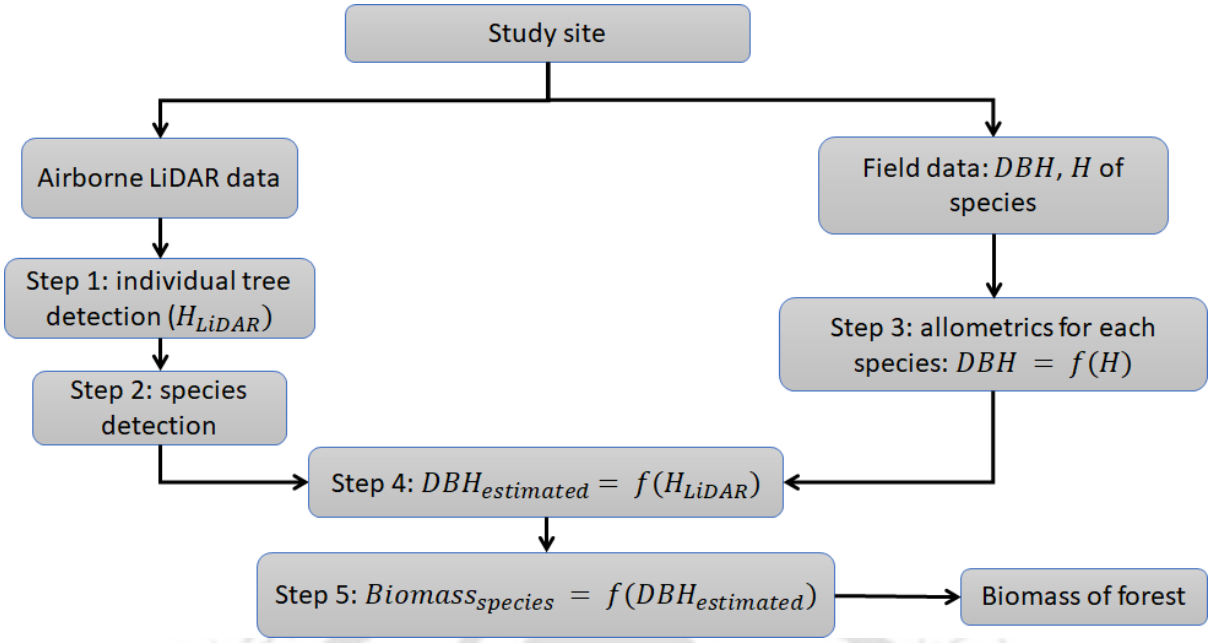

Figure 3.11 Methodology for biomass estimation of a forest

3.5.1 Individual Tree Identification

For the five LiDAR data tiles covering the Acadian Forest region MATLAB is used to implement the watershed algorithm. Digital terrain and digital surface models are first generated by local binning algorithm at a resolution of 0.5 meters to identify individual trees. Canopy height model (CHM) of 1m resolution was then produced by subtracting the digital surface model from the digital terrain model. The generated CHM represents tree heights for each cell (i.e. vertical distance between ground level and the highest points within each 1-meter grid cell). Duplicate points and those with negative values are removed. Gaussian low-pass filter of 5 × 5 window size was applied to smooth the CHM. A variable window radius, which is calculated by crown radius and height of the CHM grid is used to identify tree tops for each grid in the CHM. Based on gradient of the CHM, potential tree tops are detected, and individual trees are segmented. Coomes et al. (2017) can be referred for the detailed procedure.

3.5.2 Tree Species Classification

To classify identified trees into different species, a two-step process was applied. Accordingly, trees point clouds were tested to refine tree class. Using crown height information, trees were classified into Group A and Group B and further classified into species based on crown width. Following steps describe the classification of individual trees to four major species (black spruce, balsam fir, maple and birch):

Step (i): To remove falsely detected trees, we computed the lowest crown surface elevation for a point cloud of each tree and standard deviation of all elevations (as derived in section 3.5.1). For a tree point cloud, if elevation of a 3D data point is less by the value of standard deviation below the lowest crown point, the point cloud is excluded or rejected as false tree.

Step (ii): After refining tree point clouds for individual trees in step (i), remaining point clouds are classified into two categories: Group A and Group B. Group A typically exhibits a lower canopy (lower crown height) near to ground level of forest landscape and includes species namely Black spruce and Balsam fir. Whereas Group B, which includes maple and birch species, tends to show higher canopy. Next, in each group, crown spread (crown width) was further used for species classification. For example, Balsam fir has a narrower crown spread than Black spruce, while maple has a broader crown than birch (Côté et al., 2010)

3.5.3 Biomass Estimation

Ter-Mikaelian and Korzukhin, (1997) published biomass equations for the Acadian Forest, for which diameter at breast height (DBH) is a prerequisite. Also, for the Alberta Forest site in Canada, 20 allometric equations between H and DBH are published by (Shongming Huang et al., 2011). First, we applied Shongming Huang et al. (2011) equations to the field inventory data provided by DNR (Table 3.2 and 3.3), assuming the growth characteristics (DBH, H) of species in Canada was the same, but could not achieve better fits to the data. On the other hand, the Acadian Forest (LiDAR polygon) contain fewer circular inventory plots created by Natural Resources and Energy Development and less samples, making it impossible to fit allometric between DBH and H values. Nevertheless, field inventory (Table 3.2 and 3.3) consists of more than 10,000 tree sample data for the New Brunswick. Though (although authors have more than 20,000 samples however only 10,000 samples are shown), (Shongming Huang et al., 2011) published allometric equation for the Alberta Forest, these equations are modified for achieving best fit model for all species in New Brunswick. Non-linear equations (Eqn. 3.8 to 3.10 below), which contain exponential, logarithmic, and third order polynomial expressions, established relationship between DBH and H for each of the species (Table 3.2 and 3.3) of the study site.

$$DBH = aH^3 + bH^2 + cH + d \tag{3.8}$$

$$DBH = a + b\,(\log H)^c \tag{3.9}$$

$$DBH = a\ (\log H)^2\ + b\ (\log H) + c \qquad (3.10)$$

Among these equations, the most suitable allometric model (DBH as a function of H) was determined by maximizing correlation coefficient (R^2) and minimizing $RMSE$ value. These equations are used for estimating DBH using LiDAR-derived tree heights (H) for individual tree belonging to a species. Next, we have opted biomass equations provided by Ter-Mikaelian and Korzukhin, (1997) which has R^2 value greater than 0.9 for estimating biomass variables, namely dead above ground biomass (branch and stem) and leaf biomass. These equations express biomass as a polynomial function of DBH for each tree species. The calculated biomass of each tree is summed up for all the species to calculate biomass of forest. Next section discusses proposed method for AGB estimation from satellite data, where ALS data is not available or in accessible for the Acadian Forest.

3.6 AGB estimation from satellite data

In this study, , we integrated NASA's GEDI Level 4A product, Sentinel-2 multi-spectral images, and SRTM DEM data for the months from May to September for the year 2021-2022 due to visible vegetation and no snow cover. Spectral indices were computed from pre-processed Sentinel-2 data to capture essential vegetation characteristics. Subsequently, GEDI data points served as the target variable, while Sentinel-2 bands and spectral vegetation indices, along with DEM derived slope and aspect were used as feature variables. Figure 3.12 demonstrates the methodology and work flow.

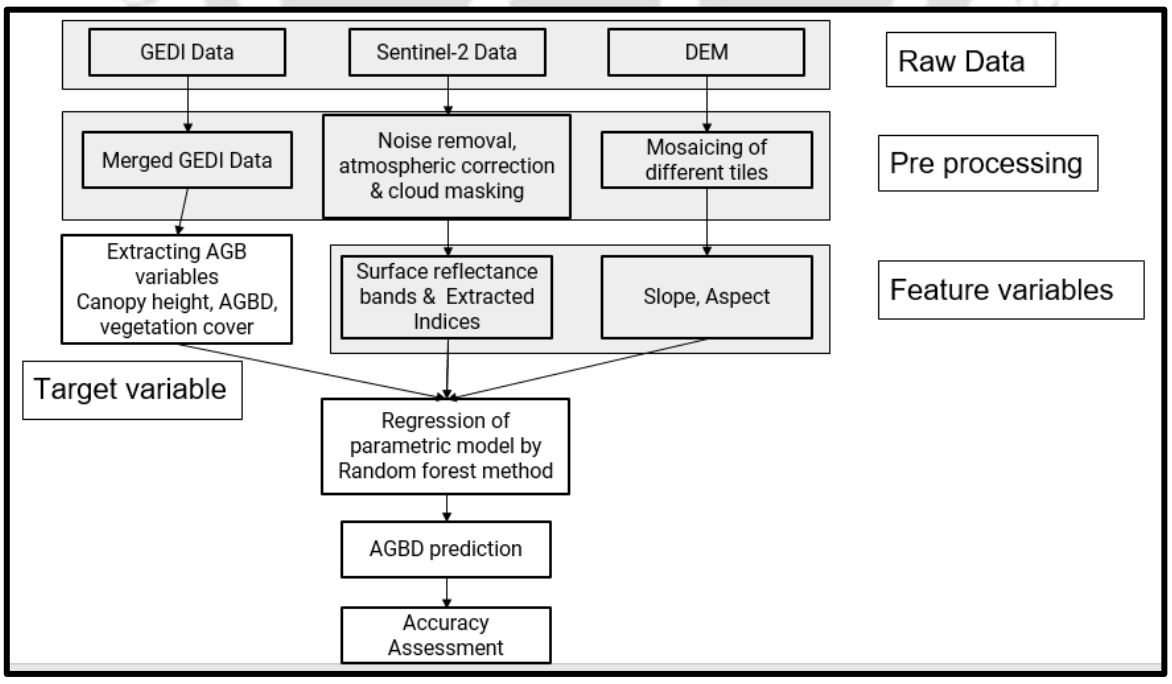

Figure 3.12 Methodology and work flow

Noise removal applied for noise reduction techniques to eliminate any sensor-specific noise artefacts that could affect the accuracy of the spectral data. Atmospheric correction was performed to adjust for atmospheric distortions ensured that the surface reflectance values were accurate, accounting for the effects of atmospheric particles and gases. Similarly, cloud masking was implemented to identify and exclude cloud-covered pixels from the dataset. This pre-processing step was critical to prevent clouds from skewing the vegetation indices and biomass estimation. Post correction and masking, we computed various vegetation indices known for their correlation with biomass. These indices provide valuable insights into the vegetation characteristics and health. In addition, the GEDI Level 4A data required specific pre-processing steps to integrate and align with the study. Individual GEDI trajectory files were merged to create a comprehensive dataset that covered the entire study site. This merging ensured a continuous and complete set of biomass measurements across the Acadia Forest of Canada. We derived slope and aspect information from the DEM data to capture the terrain characteristics. These variables are essential as they influence biomass distribution and forest structure. The slope and aspect information was integrated with the Sentinel-2 and GEDI datasets for the biomass estimation model.

Following above steps, Random Forest model was utilized to train and test the datasets, predicting the aboveground biomass density (AGBD). The integration of multisource data allowed the model to leverage a diverse set of features, enhancing its predictive capability. The model was rigorously trained using an 80:20 training-testing split, ensuring robust validation and testing. The Random Forest algorithm, known for its high accuracy and ability to handle complex interactions between field data variables, provided reliable biomass predictions and efficiency of the proposed model for biomass estimation.

3.6.1 Implementation

The methodology is implemented systematically in a series of steps. Before deriving various variables from the data sets, pre-processing steps were undertaken for Sentinel-2 and GEDI data to ensure data quality and compatibility. Initially, Sentinel-2 images were compiled to create a comprehensive image composite covering the study area, with a cloud cover threshold of less than 1% to minimize atmospheric interference. Processing Sentinel-2 Level 1-C to Level-2A using the ATCOR algorithm corrected for atmospheric effects, yielding bottom of atmosphere-corrected reflectance imagery. Mosaicking images thus prepared provided seamless coverage, enhancing uniform analysis. Subsequently, the process included selecting raw bands, vegetation indices (VIs), and textures as input variables. Seven vegetation indices

were chosen based on comparative analysis and relevant studies for biomass estimation (Amuyou et al., 2022; Askar et al., 2018; Croci et al., 2022; Kanmegne Tamga et al., 2023; Li et al., 2021; Nguyen and Kappas, 2020; Potapov et al., 2021; Sothe et al., 2022b; Wang et al., 2024; Zhang et al., 2024). Table 3.4 shows calculations of spectral indices, namely EVI, SAVI, VARI, MTVI2, NDVI, DVI and MSAVI.

Table 3.4 Algorithms used for calculating vegetation indices

Variables	Algorithms	References
SAVI	$\frac{(1+0.5)(B8-B4)}{(B8+B4+0.5)}$	(Croci et al., 2022; Nguyen and Kappas, 2020)
VARI	$\frac{B3-B4}{B3+B4-B2}$	(Croci et al., 2022)
EVI	$\frac{2.5*(B8-B4)}{(B8+6*B4-7.5*B2+1)}$	(Amuyou et al., 2022; Croci et al., 2022; Nguyen and Kappas, 2020)
MTVI2	$1.5*(1.2*(B8-B3)-2.5*(B4-B3))\sqrt{((2*B8+1)^2-\left(6*B8-5\sqrt{(B4)}\right)-0.5)}$	(Croci et al., 2022)
NDVI	$\frac{(B8-B4)}{(B8+B4)}$	(Croci et al., 2022)
DVI	$B8-B4$	(Croci et al., 2022)
MSAVI	$0.5*(2*B8+1-\sqrt{(2*B8+1)^2-8*(B8-B4)})$	(Croci et al., 2022)

On the other hand, GEDI data points were consolidated into a cohesive dataset, while DEM data from SRTM were processed to derive slope and aspect information. Employing a Random Forest regression algorithm and K-nearest neighbour (KNN) algorithm, we developed two biomass estimation models for each of the two sites. The datasets of each site were split into 80% and 20% ratios for training and testing sets to train and evaluate the model performance, respectively. This methodology was applied to the Acadia Forest, and the accuracy of the model was assessed by calculating RMSE and R^2 values.

In addition to developing the biomass estimation model, we calculated the variable importance as weights using the Random Forest algorithm to determine the contribution of each feature to the model accuracy. Variable importance scores were computed for all input variables, including the Sentinel-2 spectral bands (red, green, blue, near-infrared, SWIR and red-edge bands RE1, RE2, RE3), vegetation indices (EVI, SAVI, VARI, MTVI2), and terrain variables (slope and aspect). Importance of each variable was assessed based on the decrease in the model accuracy when that variable was removed, providing insights into which features were most influential in predicting AGBD. This analysis helped

to identify the key factors driving biomass distribution and informed the selection of the most relevant predictors for the parametric model. By understanding the variable importance (weights), we ensured that the model was not only accurate but also interpretable, allowing us to highlighting the critical environmental and spectral characteristics that contribute to biomass estimation.

3.7 Carbon Sequestration Model

Although above ground biomass for the study area can be calculated using LiDAR data for a year, however in order to understand the carbon sequestration dynamics a terrestrial biosphere model is used. Biosphere model simulates dynamically growing biomass under soil data, meteorological data, and plant functional types. Further, carbon sequestration model estimates resilience potential of a forest under anthropogenic interventions and natural factors. Methodology is shown in Figure 3.9 below and explained in below sections.

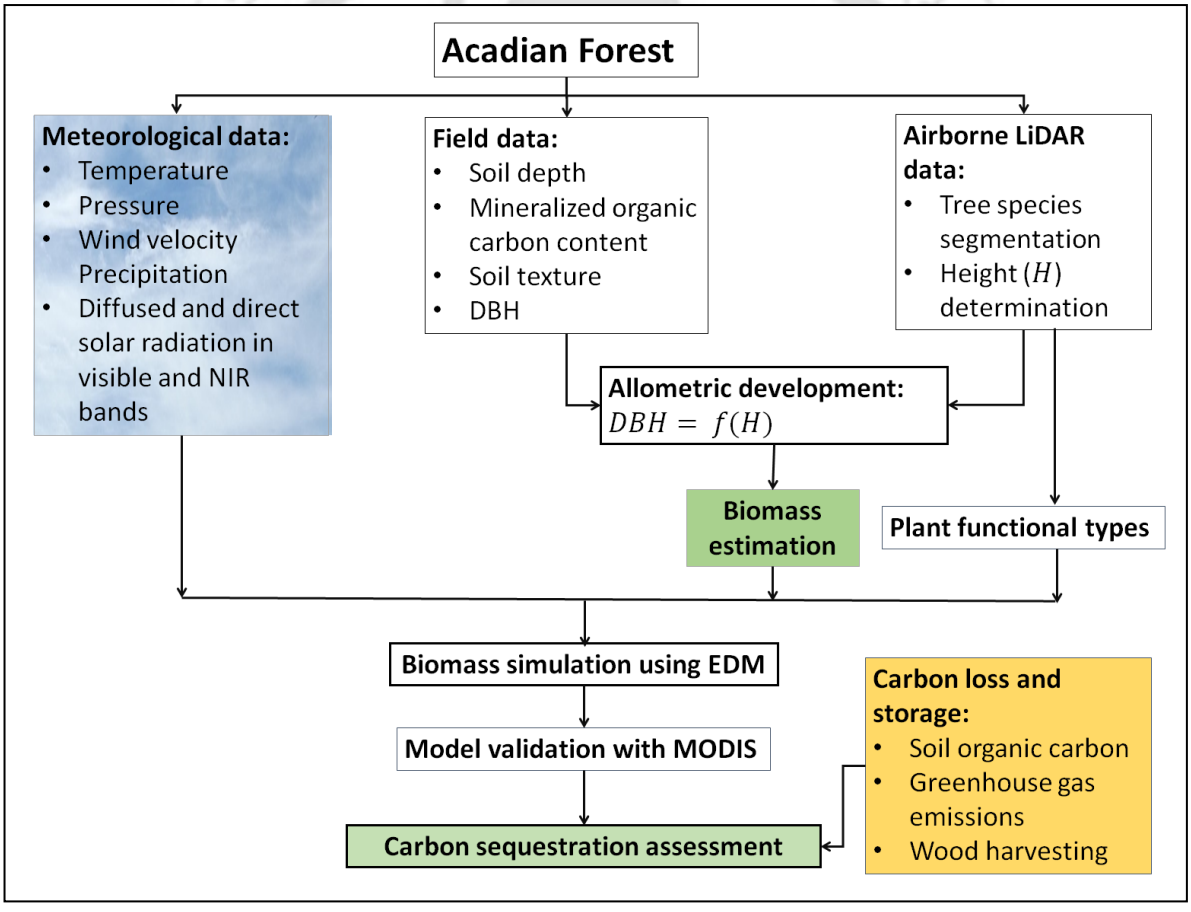

Figure 3.13 Methodology of carbon sequestration model

To examine future trends in forest biomass, we employ ecological demography model or EDM (version 2.2), which was developed by Princeton University (USA) and has been used since year 2001 by many studies successfully as a valuable tool for prediction of future biomass trends, species divergence, and biodiversity assessment. To estimate carbon sequestration

potential of any forest, studies of Schlamadinger and Marland, (1996) and Schlamadinger et al. (1997) suggested an approach for carbon sequestration of forests. Accordingly, authors proposes a linear model that calculates Acadian forest carbon storage for a year by accounting forest biomass growth and soil organic carbon from the atmosphere, and carbon loss resulting from wood harvesting and greenhouse gas emissions into the atmosphere. The model is an algebraic sum of five carbon components over a reference year: (a) above ground biomass, (b) below ground biomass, (c) soil organic carbon, (d) wood harvesting, and (e) carbon emitted by greenhouse gas emissions (Filonchyk et al., 2024) The carbon sequestration model is written as:

$$C_{s_t} = \quad C_{AGB_t} + C_{BGB_t} + C_{SOC_t} - (C_{h_t} + C_{GHG_t}) \tag{3.11}$$

where:

C_{s_t} = Carbon sequestered by the forest site in a reference year

C_{AGB_t} = Above ground biomass carbon in a reference year

C_{BGB_t} = Below ground biomass carbon in a reference year

C_{SOC_t} = Soil organic carbon in a reference year

C_{h_t} = Carbon from wood harvesting in a reference year

C_{GHG_t} = Carbon from greenhouse gas emissions over study site in a reference year

Equation 3.11 calculates the carbon sequestered (C_{s_t}) by a forest site in the current year. C_{AGB_t} and C_{BGB_t} can be calculated by sum of carbon of all trees in a sample area and extrapolating this value over area of the forest study site. Moreover, C_{SOC_t} for a current year can be determined from proportion of above and below ground biomass converted to soil organic carbon along with its decomposition in to the forest soil. For this, authors modelled soil organic carbon by a linear model consisting of the three components stated earlier can be depicted in equation 3.12 below. Furthermore, C_{h_t} can be calculated using volume of woodcut (in m^3) multiplied by wood density and wood to carbon conversion factor. In addition, C_{GHG_t} can be calculated using the greenhouse gas emissions in metric tonnes of the forest study site.

$$C_{SOC_t} = C_{SOC_{t-1}} + \lambda_1 \times C_{AGB_t} + \lambda_2 \times C_{BGB_t} - d \times C_{SOC_{t-1}} \quad (3.12)$$

where

$\lambda_1 =$ Proportion of above ground biomass converted to soil organic carbon

$\lambda_2 =$ Proportion of below ground biomass converted to soil organic carbon

$d =$ Soil organic carbon decomposition rate

Rate of carbon sequestration between two years i.e., change between reference and year of question can be calculated using equation 3.13.

$$r_{C_{s_t}} = \frac{C_{s_t} - C_{s_{t-1}}}{t - (t-1)} \quad (3.13)$$

where

$r_{C_{s_t}} =$ rate of carbon sequestration for t^{th} year from $t-1^{th}$ year

$C_{s_t} =$ Carbon sequestered in year t

$C_{s_{t-1}} =$ Carbon sequestered in year $t-1$

3.7.1 EDM Implementation

Ecological demography models forecast changes in species distribution due to climate conditions, assess biodiversity impacts, simulate effects on hydrological cycles and water quality, and evaluate the long-term consequences of human activities on forest biomass. These models incorporate various ecological, demographic, and biophysical processes to simulate forest growth in response to environmental factors (Oddou-Muratorio et al., 2020). They utilize data from sources like satellite imagery, forest inventories, and climate records to reflect current forest dynamics, considering factors such as sunlight, water availability, and nutrient levels to estimate tree and vegetation growth. Additionally, these models predict patterns in species distribution, forest structure, and biodiversity based on ecological interactions and environmental conditions, which can inform assessments of forests' roles in ecosystem services like carbon sequestration (Blanco and Lo, 2023). One such model, the Ecological Demographic Model (EDM version 2.2), simulates the eco-physical and bio-geochemical dynamics of forests, integrating energy balance, water budget, and carbon cycle to comprehensively estimate biomass across various spatial scales (Longo et al., 2019).

EDM is a terrestrial biosphere model designed to simulate vegetation dynamics across various ecosystems, ranging from boreal to tropical forests (Longo et al., 2019). It operates as

a cohort-based, geographically implicit model, employing a size and age-structured system of partial differential equations to simulate the behaviour of spatially distributed vegetation (Moorcroft et al., 2001). EDM integrates multiple modules to forecast various components of the simulated ecosystem, including soil biogeochemistry, plant growth, mortality, phenology, disturbance, and hydrology. It utilizes a range of plant functional types (PFTs) to account for intra- and inter-specific variability, with these PFTs exhibiting differences in leaf physiology, phenology, growth and allocation strategies, mortality, and sensitivity to environmental conditions (Medvigy et al., 2009).

EDM calculates and updates the carbon biomass in forests by modelling ecological processes of forest carbon. These processes include photosynthesis, respiration, and soil interactions. EDM tracks carbon movement from photosynthesis to biomass growth and plants to soil due to plant death (mortality) and disturbances. It also monitors carbon decomposition in various areas (metabolic litter, structural litter, soil slow, soil passive, wood product, harvested crop, etc.) and carbon release from events like fires. The model updates the carbon at the tree level and then expands to the whole forest (Ma et al., 2022).

3.7.1.1.1 Static levels

To simulate biomass, the EDM model requires site conditions of the study area as environmental variables in the model calculations, including meteorological data (temperature, pressure, wind velocity, precipitation, diffused and direct solar radiation in visible and NIR bands) and soil conditions. For meteorological data of the Acadian Forest site, we obtained hourly data from years 2017 to 2020 from the National Renewable Energy Laboratory database. Additionally, the geo-potential height of the study site is 70 m, as per the NRC. Moreover, CO_2 value of 399.6 ppm has been given as per the NRC.

The study site contains sandy clay loam texture, with clay and sand measuring 0.368% and 0.111%, respectively (Mansuy et al., 2014). While Mansuy et al. (2014) specified a maximum soil depth of 0.69 m for the Acadian Forests, observations by Milburn et al. (1989) suggest that plants in New Brunswick may penetrate to depths exceeding 1 m. Consequently, we assumed a maximum soil depth of 2 m for the Acadian Forests for simulation purposes. This depth is partitioned into five layers, each with maximum ranges of 2.0m, 1.0m, 0.55m, 0.30m, and 0.12m from the ground surface of the forest. The ED model incorporates soil depth information to estimate plant growth, mortality, and carbon sequestration. The depth of the roots of various plant species affects how easily they can get water and nutrients. Larger root systems may be

supported by deeper soils, which would enhance biomass and carbon storage. The health of plants and the productivity of ecosystems are impacted by shallow soils because they restrict root access to water. The depth of the soil also influences the water availability, particularly in times of drought or high water content, which influences the growth of trees and consequently biomass.

3.7.1.1.2 Plant Functional Type Parameters

PFT parameters govern how plants and trees interact with their environment, affecting population dynamics and shaping ecosystem functions. Moreover, incorporating specific characteristics, such as leaf area, wood density, and seed size, provide precise predictions of demographic outcomes. In addition, PFT parameters dictate accuracy of EDM output variables, namely, gross primary production (GPP), net primary production (NPP), net ecosystem production (NEP), and above ground biomass (AGB).

Based on species data from the research area (as explained in section 3.5.2), two distinct PFTs were identified: (i) Northern Pine (comprising black spruce and balsam fir), and (ii) Early Hardwood, (consisting of red maple and birch). We adjusted or refined PFT parameters, as recommended by Dashti et al. (2021) and Meunier et al. (2022), because uncertainty of PFT parameters contributes to model output variability. Additionally, we modified additional parameters with guidance from the Chave et al. (2007) and OSLON database. Apart from that, according to Chu et al. (2023), Northern pines respond to seasonal cues primarily driven by temperature fluctuations, with their leaf phenology adapting to changing conditions, thereby influencing ecosystem structure and function. Therefore, adjustments were applied solely to Northern pine PFTs (Group A species) for biomass growth simulations. Table 3.5 below presents the comprehensive list of updated PFT parameters with references.

Table 3.5 PFT Parameters of the Northern pines (Balsam fir and Black Spruce)

Parameter name (unit)	**Abbreviation in EDM**	**Value set**	**Reference**
Specific leaf area (m^2/kg)	SLA	5	(Dumais et al., 2014)
Maximum carboxylation rate ($\mu mol\ CO_2/m^2/\ sec$)	Vm0	33.59	(Matthew E. Akalusi, 2021)
Maximum electron transport rate ($\mu mol\ CO_2/m^2/\ sec$)	Jm0	52.78	(Matthew E. Akalusi, 2021)

Clumping (dimensionless)	clumping_factor	0.735	(OLSON, 2024)
Leaf turnover rate $(1/yr)$	leaf_turnover_rate	0.33	(OLSON, 2024)
Quantum efficiency $(mol\ CO_2/mol\ photons)$	quantum_efficiency	0.036	(OLSON, 2024)

3.7.1.1.3 EDM Configurations

In addition to the PFT parameters, EDM requires information, namely, plant canopy structure of cohorts (closed or thin-shaped information for individual tree), canopy radiative transfer models (e.g. two-way or multiple scattering), and trait plasticity, which collectively contribute to the uncertainty of model outcomes. Meunier et al. (2022) indicate that these factors typically contribute to less than 5% of the EDM outcomes variance, thus we opted default values of these parameters for simulation.

3.7.1.1.4 EDM Initialization

In this study, the EDM model was initialized by individual tree (cohort) size distribution (DBH, H). For initialization, the study site was partitioned into square patches (horizontal grids), each of 35m × 35m size. Within each patch or grid, cohorts representing individual trees were allocated to their respective PFTs and biomass (AGB) was computed for the grid (as outlined in section 2.2.3). Moreover, mineralized soil nitrogen and fast soil nitrogen were calculated for each patch using equations proposed by Mahendrappa et al. (1986). Additionally, a leaf area index value of 3.99 was assigned to each cohort (as suggested by Chen et al. (2002)). Default values were employed for the remaining patch and cohort parameters as adopted from Longo et al. (2019). These cohorts and patches parameters serve as inputs for vegetation dynamics for EDM. Above mentioned data inputs, environmental variables, and other parameters were submitted to EDM on Compute Canada server, an online facility provided by Digital Research Alliance of Canada for academic purposes. The server allows running the simulation for 10 days.

3.7.1.1.5 AGB Simulation

EDM uses static and dynamic levels of forest surface to simulate biomass of a forest site. For dynamic levels, initial forest ecosystem structure in the form of cohorts and patches derived from airborne LiDAR data are provided. Ideal forest conditions and no anthropogenic disturbances are assumed to assess carbon potential of the forest. The ideal conditions include pasturing (only affected by animal grazing, if any) and influence of natural tree fall or growth processes. To account for natural tree fall, it is assumed that forest vegetation dynamics occur

during the seventh month of the year in North America. Monthly simulation models of Acadian woodland biomass are conducted from the sixth month of year 2021 for durations of next 75 years (from year 2021-2095).

3.8 Summary

Sections 3.1 to 3.7 discusses methodology for estimating biomass and carbon sequestration assessment. However, to implement equation 3.11 for assessing carbon sequestration, three other components viz., wood harvesting, SOC and GHG emissions require insitu or statistical data of the three components for the study site. Based on the statistical data, a linear growth or de-growth model can be established which can be used as inputs to equation 3.11. Next chapter describes results of methods proposed for biomass estimation method for individual tree and forest from terrestrial and airborne LiDAR data. Moreover, it also provides the results of Ecological Demography model, soil organic carbon and its outputs for accounting carbon pools in the Acadian Forest.

CHAPTER 4 RESULTS

4.1 AGB estimation from Terrestrial LiDAR data

The proposed method for wood volume estimation by tree reconstruction was implemented in MATLAB and applied on LiDAR data of 23 individual tree data sets were obtained from a repository provided by Gonzalez de Tanago et al. (2018).

4.1.1 Branch collar detection

The method for branch collar detection is applied to 23 trees by first horizontal slicing the data above DBH (or 1.3m) of a ***PC***, and secondly the radius of the fitted circle for each data slice is calculated. Height of the BCL obtained using the proposed method underestimate the wood volume. As a result, while we decide the BCL value, we added 5 cm to the originally determined height (elevation) of the BCL by the proposed method. The following sections discuss processes of stem extraction, canopy points extraction, branch modelling, and volume estimation.

4.1.2 Stem extraction

For each of 23 trees, ***ST*** set is divided into vertical bins and RANSAC method is used for cylinder fitting for each bin. Furthermore, a maximum deviation of 5° from vertical was permitted by the specifications of 1.5 cm between the cylinder surface and points in a bin having minimum size of 15 cm. Additionally, a maximum variation of a distance of 0.5 cm between the cylinder surface and points in a bin was obtained by restricting 2° deviation of 15cm cylindrical axis of the bin. For the bottom most bin for a stem, mesh is generated by alpha shape with radius less than or equal to two times of the stem diameter. This value is preferable for accurate mesh generation by alphas shapes. For example, if main stem diameter is 0.23 m, alpha shape with a radius of 0.45 works better to generate mesh. From the repository of trees, buttress volumes and stem volumes are collected and used the sum of the two values as total stem volume. Figure 4.1 shows adaptive vertical slicing for a ***ST*** set of a tree and modelled cylinders and mesh.

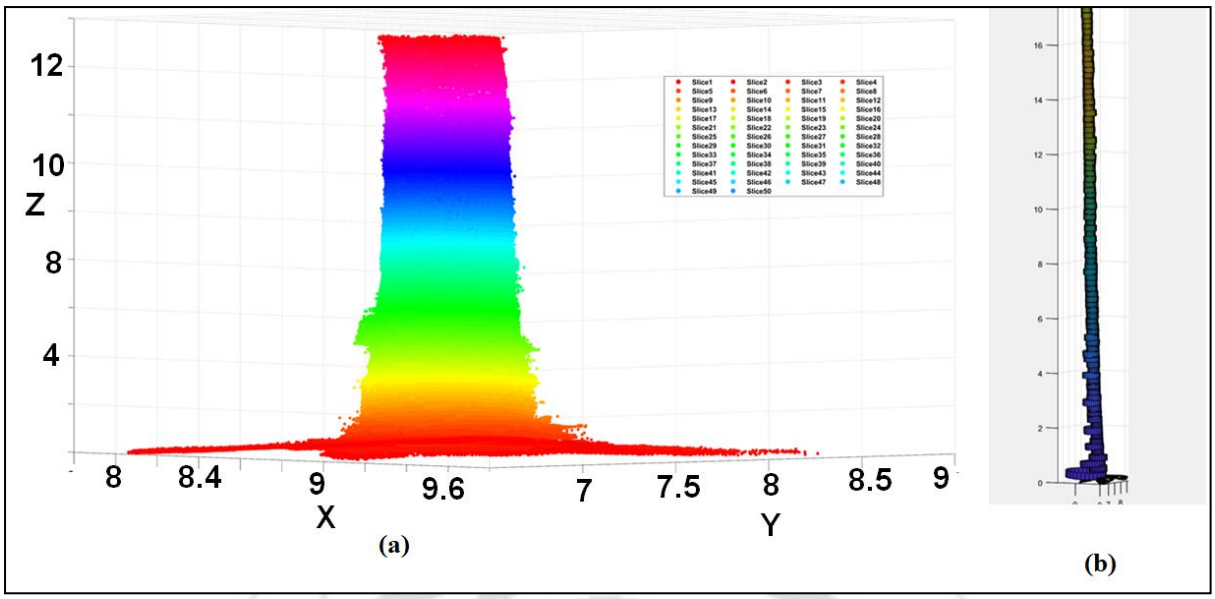

Figure 4.1 Slices of a stem shown in different colours and (b) fitted cylinders to the stem slices and mesh generated by alpha shapes to the bottom slice (Slice1).

4.1.3 Canopy surface points

For canopy points extraction, we used boundary tool of MATLAB, which computes boundary of a set of points based on the Delaunay triangulation of the points. Shrink factor controls areas of triangles to be included as part of the boundary. When a shrink factor of 0.75 is specified, the function retains triangles, which have smaller circumradii than the 0.75 times maximum circumradius of the Delaunay triangles. A value of 0.75 achieved balance by removing small gaps or abnormalities from the projected strata points of a slice and capturing the overall canopy form of a tree avoiding tiny spaces in the canopy points. Shrink value one, on the other hand, introduces concave or jagged edges and produces an extremely sensitive border. Boundary extraction or canopy points for a slice obtained by 0.75 shrink factor is shown in figures 4.2(a), 4.2(b), and 4.2(c) below.

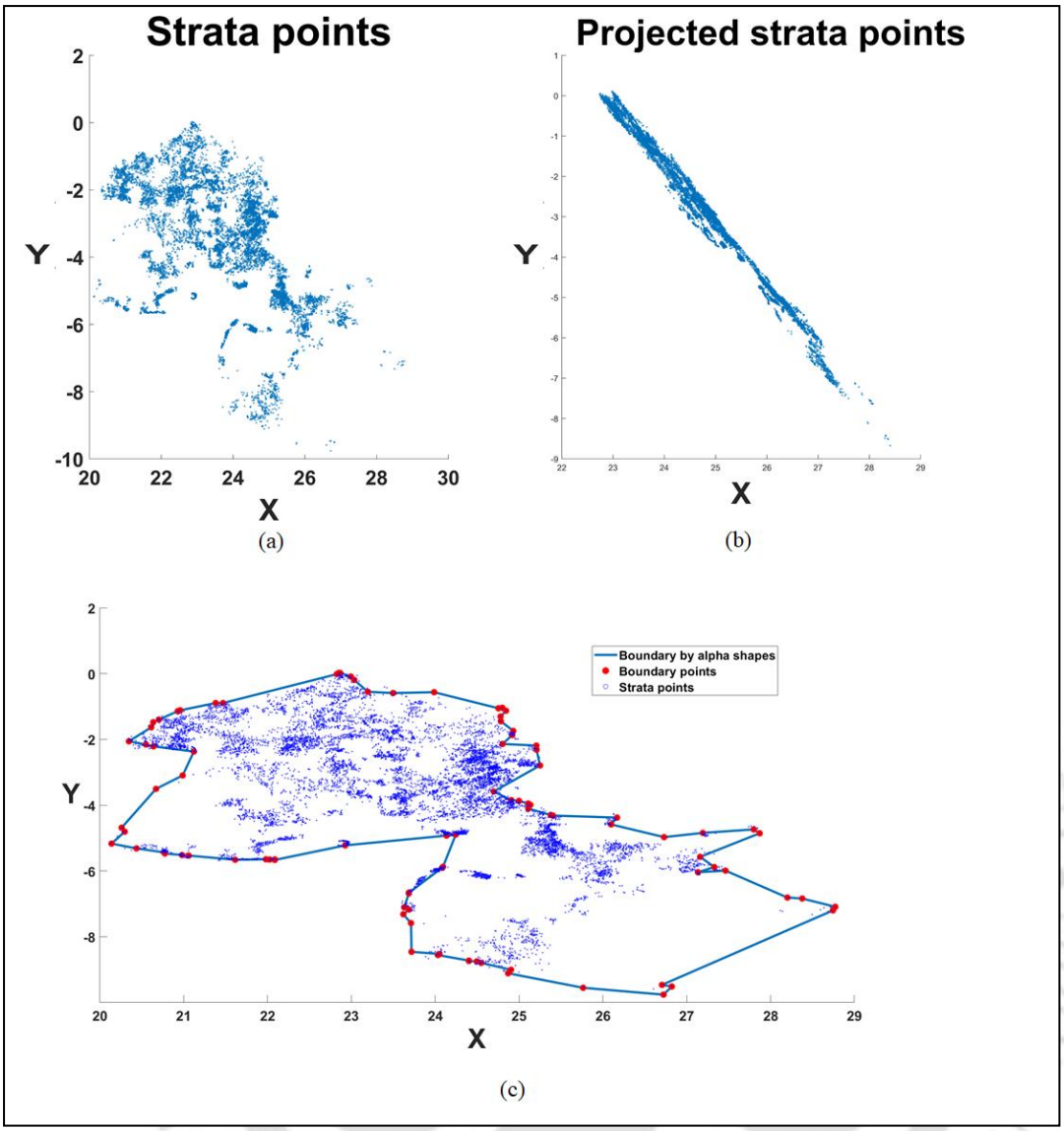

Figure 4.2 (a) strata points for a point cloud of a tree, (b) projected strata points, and (c) boundary points derived by alpha shapes with a shrink factor of 0.75

From the figure 4.2 (a) and 4.2(b), it is evident that strata points (fig. 4.2 (a)) for a tree are densified after projecting on to the canopy plane. For these projected strata points boundary points by 2D alpha shapes is retrieved and plotted in figure 4.2 (c). Figure 4.2 (c) highlights canopy points extracted by the proposed method along with the strata points set of a tree. This process applied to LiDAR point data of all 23 trees. Canopy interval (c) depends on LiDAR data density of a crown and canopy voids. For the 23 trees, canopy interval vary from 2 cm to 55 cm, and the number of points vary from 1083 to 38070, which conforms to the minimum number of points required for reliable crown signatures, as suggested in Dong, (2010).

4.1.4 Branch clustering and reconstruction

4.1.4.1 On-branch cluster

Branch clusters are extracted for all strata starting from highest point of a crown. Thereafter, method presented in sections 3.4.4 and 3.4.5 are applied to determine the branch segments (on-branch clusters) of $\boldsymbol{BS}$ set of a $\boldsymbol{PC}$. Figure 4.3 below shows branch segments obtained after re-grouping of on-branch clusters.

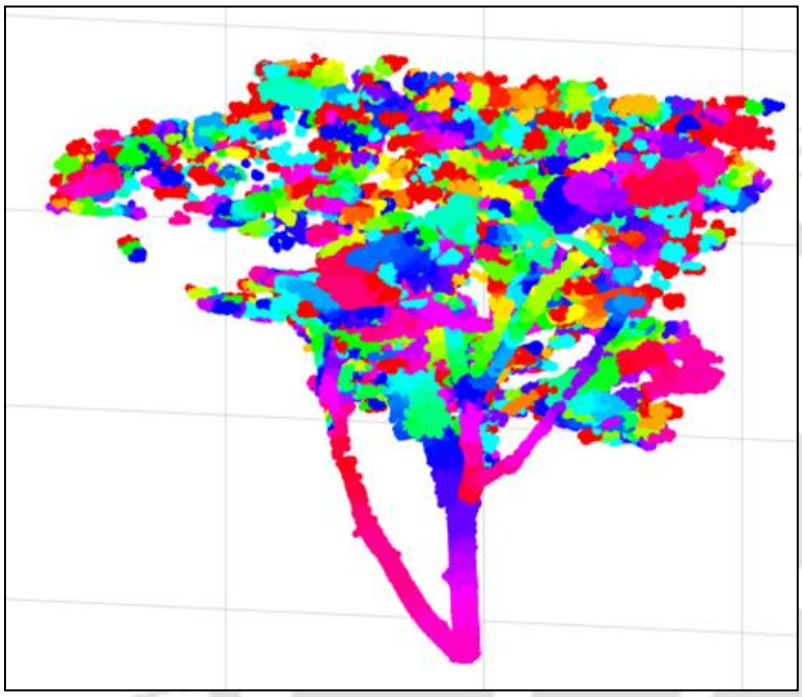

Figure 4.3 Branch segments after re-grouping of on-branch clusters.

4.1.4.2 Crown volume

A branch is modelled as a right circular cylinder as explained in section 3.4.5. Although dot product threshold removes most of the leaf points, still small leaf points which are near to branches are remained and incorrectly classified as branch segments. Leafy points are considered as outliers. Majority of the outliers in leafy part, which contains more data points than the woody portion of tree. To remove outliers, we calculated mean absolute distance between cylindrical surface and data points. If mean absolute distance value is more or equal to 0.01 m, a point is removed as outlier.

4.1.5 Accuracy assessment and discussion

Tree volume is estimated as sum of crown volume (C_e) and stem volume (S_e). The crown volume is sum of volumes of all branch segments, whereas the stem volume is sum of volumes of all vertical bins of the stem. Estimated values of total volume of trees are compared with the

harvested or reference volumes (V_R) provided in the repository. Accuracy analysis is performed for each of three components of tree volume: stem volume, crown volume, and total volume. Accuracy for each of the three components is calculated as differences of estimated volume and reference volume divided by reference volume. Following formulas calculate error and accuracy figure in percentage for three variables (stem volume, crown volume, tree volume):

$$e = V_E - V_R \qquad (4.1)$$

$$\eta = 100 - \frac{|V_E - V_R|}{V_R} \times 100 \qquad (4.2)$$

Where V_E = estimated volume, V_R = harvested or reference volume, η = percentage accuracy of the method for a tree and e = error in estimated volume.

Volume, error, and accuracy figures are denoted for stem volume, crown volume and total volume as V_{SE}, e_S, η_S, V_{CE}, e_C, η_C, V_{TE}, e_T, and η_T, respectively. Similarly, for accuracy analysis, reference volumes for stem, crown, and total volume can be indicated by V_{SR}, V_{CR}, and V_{TR} in equation 8. Table 4.1 shows results of estimated volume, error in estimated volume, and accuracy of the estimated volume for the 23 trees. Tree identification number, species name, crown height, and stem height are also mentioned. Table 4.2 shows species wise results and their statistics. Due to only 23 number of trees and 14 species, we prefer maximum, minimum and median values for analysis of results for the stem volume, the crown volume, and the total volume.

Table 4.1 Estimate, error, and accuracy of wood volumes for 23 trees (G, I, and M indicate trees in Guyana, Indonesia, and Peruvian regions

Site	**Tree (Stem height (m), Crown height (m))**	**Species name**	***Stem* Volume**			**Crown volume**			**Total volume**		
			V_{SE} (m^3)	e_S (m^3)	η_S (%)	V_{CE} (m^3)	e_C (m^3)	η_C (%)	$V_{TE} = V_{SE} + V_{CE}$ (m^3)	e_T (m^3)	η_T(%)
Guyana	G01 (15.88, 9.52)	*Wallabaituri*	*5.140*	0.23	95.71	11.492	1.396	89.17	16.632	1.626	91.09
	G03 (18.8, 14.45)		*2.856*	0.25	91.95	5.670	0.668	89.32	8.525	0.605	90.28
	G04 (16.98, 5.23)		*3.450*	0.42	89.15	6.441	0.608	89.46	9.891	0.918	90.59
	G05 (19.52, 10.08)		*3.641*	0.32	91.92	6.606	0.784	91.38	10.247	1.028	90.27
	G06 (19.87, 8.93)		*5.115*	0.03	99.39	7.886	1.039	89.39	13.001	1.104	92.39
	G07 (22.83, 6.37)		*7.184*	0.12	98.37	11.939	1.161	88.36	19.123	1.070	93.73
	G08 (14.02, 12.98)		*4.283*	0.47	90.04	7.641	0.649	91.14	11.923	1.280	91.39
	G02 (17.65, 9.95)	*Huruasa*	*2.231*	0.20	91.59	3.238	0.401	92.17	5.581	1.123	90.21
	G09 (24.24, 5.56)	*Korokororo*	*12.343*	0.87	93.41	14.260	0.873	94.23	26.603	1.744	93.85
Indonesia	I01 (14.83, 6.5)	*Tetramerista glabra*	*1.118*	0.14	89.03	0.422	0.040	91.42	1.540	0.177	89.67
	I02 (14.7, 6.5)		*2.058*	0.24	89.65	0.338	0.020	94.35	2.396	0.258	90.28
	I03 (14.15, 11.55)		*4.632*	0.25	94.95	0.789	0.063	92.65	5.422	0.309	94.61

	I04 (11.99, 14.41)	*Parastemon-urophyllus*	*1.450*	0.08	94.51	0.105	0.013	88.74	1.555	0.097	94.10
	I07 (20.95, 15.55)	*Shorea-teysmanniana*	*1.550*	0.13	92.22	0.935	0.123	88.37	2.485	0.254	90.73
	I08 (11.6, 15.72)	*Aglaia-rubiginosa*	*3.107*	0.17	94.81	1.597	0.154	91.23	4.705	0.324	93.56
Peruvian	M01 (15.75, 28.25)	*Buchenavia macrophylla*	*14.868*	0.75	95.23	25.948	2.333	91.75	40.816	3.078	92.99
	M02 (14.46, 17.54)	*Dacryodes peruviana*	*4.837*	0.49	90.81	5.648	0.674	89.34	10.485	1.164	90.01
	M03 (19.25, 15.75)	*Couratari macrocarpa*	*5.858*	0.39	93.81	6.853	0.587	92.11	12.711	0.974	92.89
	M05 (24.19, 17.81)	*Sloanea eichleri*	*15.920*	0.67	95.96	10.689	1.016	91.32	26.609	1.686	94.04
	M06 (28.81, 21.69)	*Pterygota amazonica*	*17.683*	0.230	98.72	12.686	1.499	89.43	30.369	1.729	94.61
	M07 (29.19, 19.41)		*14.384*	0.410	97.22	7.103	0.958	88.12	21.487	1.369	94.01

	M08 (17.08, 28.82)	*Pseudopiptadenia suaveolens*	*7.744*	0.520	93.66	11.434	1.061	91.51	19.178	1.585	92.37
	M09 (22.3, 16.9)	*Nectandra longifolia*	*5.345*	0.290	94.79	2.102	0.256	89.16	7.447	0.549	93.13
		Minimum	1.118	0.03	89.03	0.105	0.013	88.12	1.540	0.097	89.67
		Maximum	17.683	0.87	99.39	25.948	2.333	94.35	40.816	3.078	94.61
		Mean	6.382	0.333	93.78	7.041	0.719	90.61	13.423	1.046	92.24
		Standard deviation	4.924	0.212	3.025	5.913	0.558	1.807	10.324	0.699	1.70

Table 4.2 Site wise and species wise statistics of algorithm performance for stem, branch and total volume.

		η_S (%)			η_C (%)			η_T (%)		
Site	**Species (Number of trees)**	**Max**	**Min**	**Median**	**Max**	**Min**	**Median**	**Max**	**Min**	**Median**
Guyana	*Wallaba ituri (7)*	99.38	89.14	91.95	92.17	90.15	89.46	93.73	90.27	91.01
	Huruasa (1)			91.59			89.23			90.21
	Korokororo (1)			93.41			94.23			93.85
Indonesia	*Tetramerista glabra (3)*	94.95	89.03	89.65	94.35	91.42	92.65	94.61	89.67	90.28
	Parastemon urophyllus (1)			94.51			88.74			94.10

	Shorea teysmanniana (1)			92.22			88.37			90.73
	Aglaia rubiginosa (1)			94.81			91.23			93.56
Peruvian	*Buchenavia macrophylla (1)*			95.23			91.75			92.99
	Dacryodes peruviana (1)			90.81			89.34			90.01
	Couratari macrocarpa (1)			93.81			92.11			92.89
	Sloanea eichleri (1)			95.96			91.32			94.04
	Pterygota amazonica (2)	98.72	97.22	97.97	88.12	89.43	88.78	94.61	94.01	94.31
	Pseudopiptadenia Suaveolens (1)			93.66			91.51			92.37
	Nectandra longifolia (1)			94.79			89.16			93.13

4.2 AGB estimation from Airborne LiDAR data

4.2.1 Tree composition

The CHM model generated assist detecting potential tree tops by identifying significant peaks. Grids having heights above 0.5 m in the canopy height distribution were extracted as trees. Consequently, 270902 numbers of trees were originally detected. These trees were refined and the number reduced to 268648 trees. Out of these many trees, 91114 were spruce, and 177534 were balsam fir. However, maple or birch species were not detected in the five LiDAR tiles. Additionally, balsam fir exhibits a preference for shaded regions, where it can thrive even with limited sunlight availability. These factors likely contribute to their abundance in the selected area and throughout the Acadian forest.

4.2.2 Allometric equation results

For modelling allometric equations using field inventory data, we applied equations 1 to 3 and $RMSE$ was calculated for each model equation. To identify the best fit allometric model, values (DBH, H) that fell within 75% of the maximum $RMSE$ of a fitted equation were used. For Balsam fir and black spruce, equation 3 provided the best fit. Figures 4.4(a) and 4.4 (b) depict the fitted curve and the corresponding inventory data for Balsam fir and Black spruce, respectively.

On the other hand, for Maple and Birch, the best fits were exhibited by equations 1 and 2, respectively. Table 4.3 shows best-fit allometric equations, their parameters, and performance ($RMSE$) for 4 major species. Best model equations corresponding to each species (mentioned in Table 4.3) were subsequently employed to estimate dead above ground biomass (branches and stem) and leaf biomass for patches and cohorts establishment.

Table 4.3 Allometric equation parameters of species

Species	**Parameters**				R^2	$RMSE$ (cm)	**Type of best fitted Allometric equation**
	a	***b***	***c***	***d***			
Balsam fir	11.24	- 40.83	48.33		0.81	2.45	Equation 3
Black spruce	12.10	- 42.76	48.15		0.83	2.28	Equation 3

Red maple	0.01	0.54	-8.4304	57.77	0.65	5.95	Equation 1
Birch	12.53	0.01	6.93		0.60	3.6	Equation 2

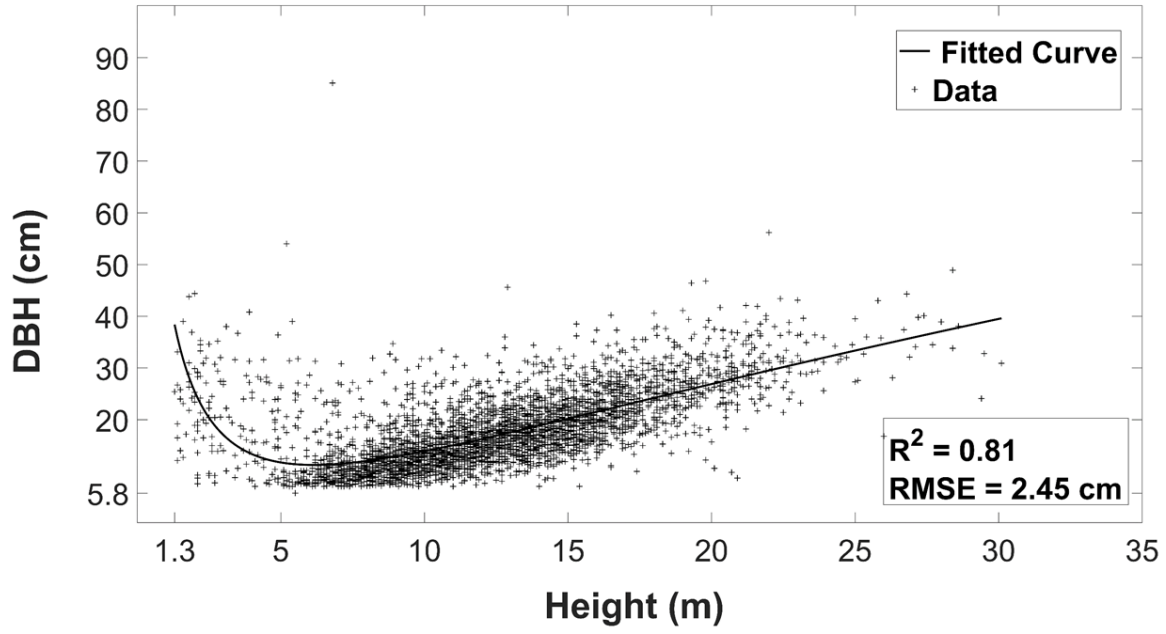

(a)

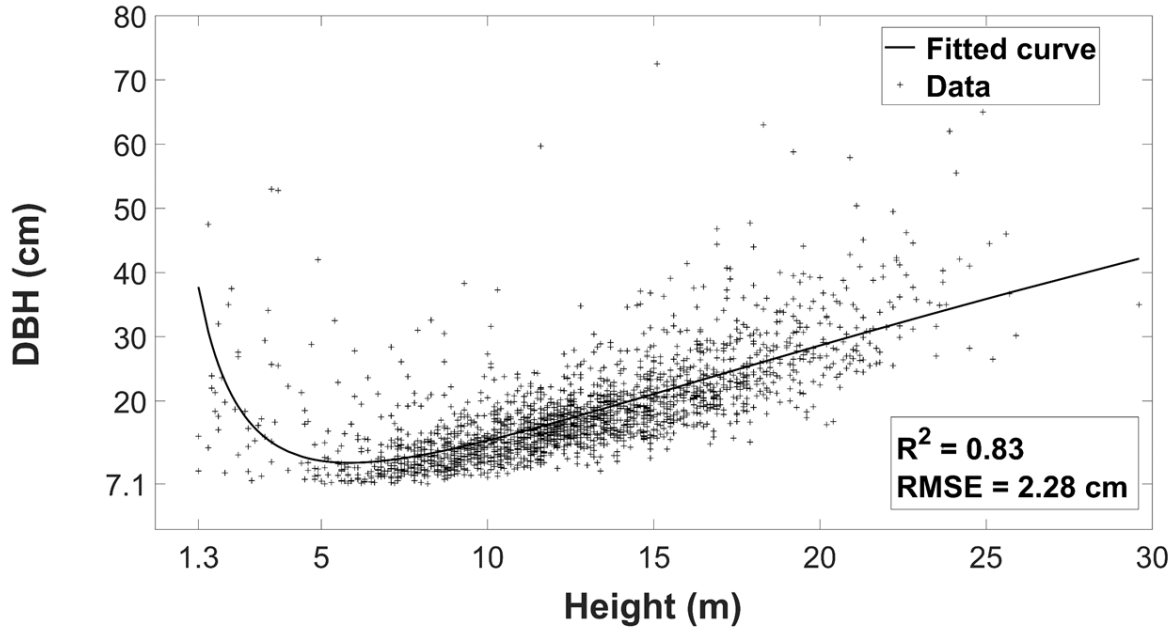

(b)

Figure 4.4 DBH vs H data and fitted curves: (a) for Balsam fir, (b) for Black spruce

.

4.2.3 Biomass distribution

As explained in section 3.5.3 and from table 4.3 and figure 4.4, for 268648 trees encompassing extracted from five LiDAR tiles equations provided by Ter-Mikaelian and Korzukhin, (1997) is used for biomass estimation. Out of these many trees, these equations were used for 91114 black spruce, and 177534 balsam fir species which has R^2 value greater than 0.9. Figure 4.5 below shows the aboveground biomass distribution for the Acadian forest encompassing an area of 9.955 km^2.

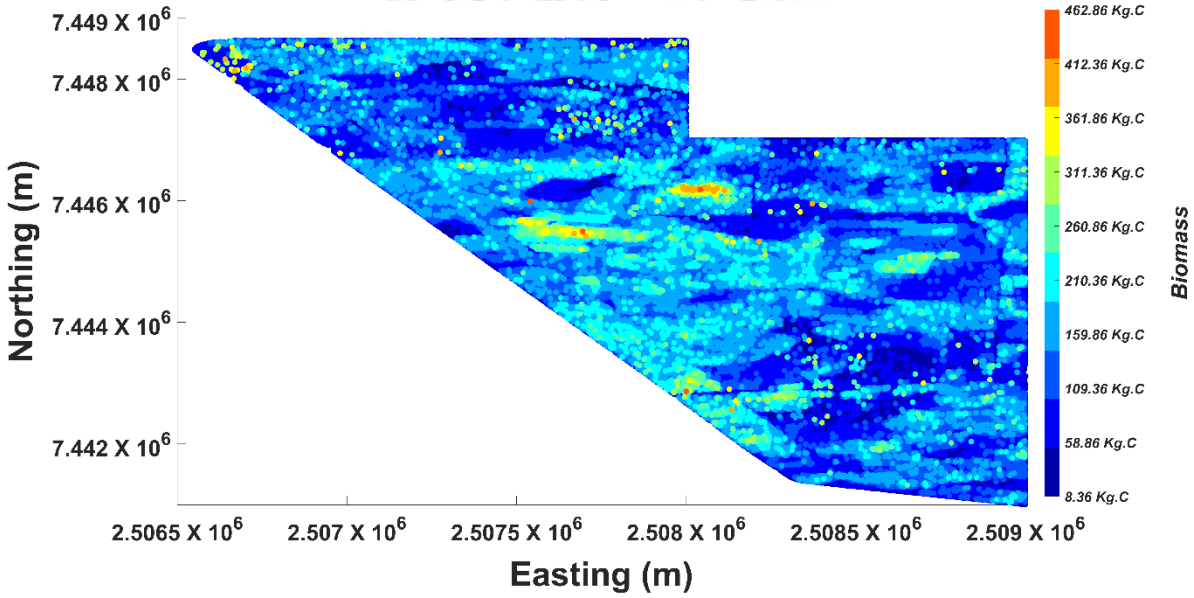

Figure 4.5 Biomass distribution for the whole LiDAR polygon area

From the above figure, one can observe more than 90% of trees or majority of trees has AGB values in the range from 8.36 to 260.86 $Kg.C$. This also indicates that that the LiDAR data has trees aging from young to mature.

4.3 AGB estimation from Satellite data

The proposed parametric model is implemented for the two study sites. For the Acadia Forest site, $RMSE$ of 9.29 Mg/ha and an R^2 of 0.94 for the training set, and $RMSE$ of 23.52 Mg/ha and R^2 of 0.60 for the test set were obtained. Figure 4.6 shows the biomass modelling by input and output variables with 80:20% ratios. Table 4.4 compiles performance results.

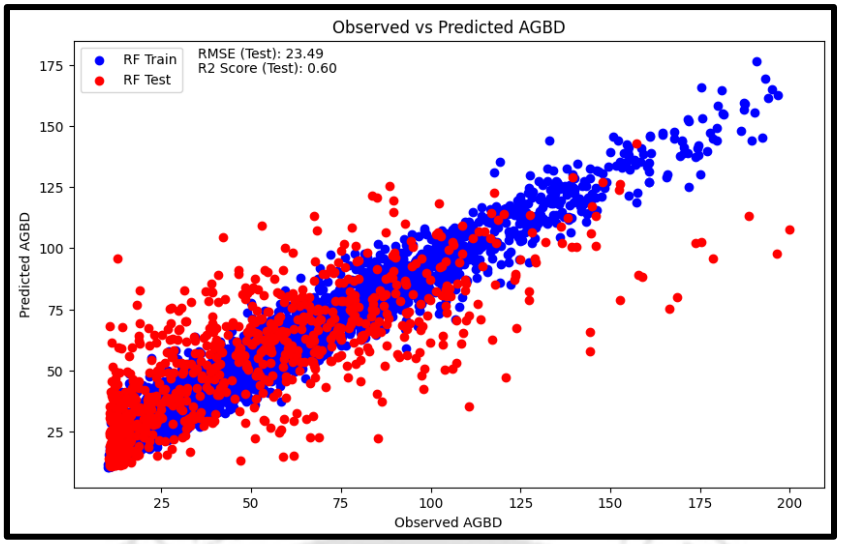

Figure 4.6 Observed and predicted values of AGBD for Acadia forest

Table 4.4 RMSE and R^2 values for different model

Location	**Model**	**Train : Test**	**RMSE (Mg/ha)(Train)**	**RMSE (Mg/ha)(Test)**	**R^2 (Train)**	**R^2 (Test)**
Acadia Forest	RF	80:20	9.29	23.52	0.94	0.60
	KNN	80:20	23.81	27.31	0.61	0.45

The Random Forest algorithm derives importance (or weights) for input variables for achieving minimum error in biomass estimation. Table 4.5 mentions the derived weights for each variable in four categories according to range of weights: high importance, moderate importance, low importance and negligible importance.

Table 4.5 Variable importance (weights) derived by Random Forest algorithm

Acadia Forest Canada	
High importance	
Feature	**Importance**
Band-4	0.209180
DEM	0.085483
EVI	0.071259
MTVI2	0.071213
SLOPE	0.068535
Band-12	0.060139

Moderate importance	
Band-8	0.058010
Band-9	0.051307
Band -5	0.049157
Band-1	0.044430
Band-11	0.036633
VARI	0.034561
ASPECT	0.032957
Band-2	0.032806
Low importance	
Band-3	0.027908
Band-6	0.023478
Band-7	0.021673
Band-8A	0.021272
Negligible importance	
NDVI	0.016174
SAVI	0.015614
DVI	0.014231
MSAVI	0.012135

Among the four categories of variables mentioned in the table above, the first category of variables, namely Band-4, Band-12, DEM, EVI, MTVI2, and SLOPE, is regarded as highly important for estimating AGBD. Band-4 (red) and Band-12 (shortwave infrared), derived from Sentinel-2 LA data, are known to provide critical information regarding vegetation health and moisture content, which are essential for the assessment of biomass. Topographic data is offered by DEM, encompassing elevation and terrain features that are influenced by vegetation growth patterns and biomass distribution. It has been established that EVI and MTVI2, as vegetation indices, enhance sensitivity to canopy characteristics and reduce atmospheric effects, thereby improving the accuracy of biomass estimations (Amuyou et al., 2022; Croci et al., 2022; Nguyen and Kappas, 2020). Slope, which is derived from DEM, is noted to affect water runoff and soil properties, subsequently influencing vegetation structure and density (Nguyen and Kappas, 2020).

In the second category, the variables Band-1, Band-2, Band-5, Band-8, Band-9, Band-11, VARI, and ASPECT are found to be moderately important for estimating AGBD. These variables primarily correct atmospheric effects and enhance the accuracy of surface reflectance measurements that detect chlorophyll absorption and assess vegetation health. Band-5 (red edge) and Band-8 (NIR) have been identified as particularly valuable for the monitoring of plant biomass and stress due to their sensitivity to chlorophyll content and overall vegetation structure. Assistance in atmospheric correction is provided by Band-9 (water vapour), while Band-11 (SWIR) is utilized for detecting moisture content in vegetation and soil. The design of VARI is intended to minimize atmospheric interference, thereby providing a more accurate measure of vegetation health (Nuthammachot et al., 2022). Aspect, derived from DEM data, influences microclimatic conditions and vegetation growth patterns by affecting sunlight exposure and moisture retention (Nguyen and Kappas, 2020).

The importance of third category variable i.e. Band-3 (green), Band-6 (red edge 1), Band-7 (red edge 2), and Band-8A (red edge 3) for estimating AGBD is Band-3, situated in the green spectrum, is sensitive to chlorophyll concentration and provides insights into plant vigour. Band-6, Band-7, and Band-8A, located in the red-edge spectrum, are crucial for detecting subtle variations in vegetation structure and stress (Nuthammachot et al., 2022). These bands are particularly effective for monitoring canopy density and biomass because the red-edge region is highly responsive to changes in leaf area index and biomass. Lastly the fourth category variable having negligible importance in prediction due to almost negligible effect in the accuracy of the estimation if they are removed. Next section discusses about implementation of Ecological Demography Model (EDM) and its results to estimate carbon sequestration potential of Acadian Forest.

4.4 Carbon Sequestration Model

4.4.1 EDM Initialization

Initialization of EDM requires tree heights, DBH with locations, PFTs, mineralized soil nitrogen, fast soil nitrogen, leaf area index, and individual tree above ground and leaf biomass, tree density in a patch as inputs. The area of forest site containing the five LiDAR tiles large for simulation and more than 9.955 km^2. Thus, authors focused on an area of 1.225 km^2 (122.5 hectare) for biomass simulation, which consists of young to mature species (figure 4.7, 4.8 and 4.9 below). This area consists of approximately 1000 patches (grids) housing 27,119 individual trees (cohorts). Among these, 8,775 (32.3%) cohorts belong to Black spruce, while 18,344 (67.7%) are Balsam fir. Furthermore, from the figure 4.7, each patch consists of both balsam

fir and black spruce, indicated by yellow and green colours, respectively. Within this selected 122.5-hectare area, trees exceeding 5 m in height to avoid shrubs were considered for above ground biomass simulation by EDM (Wang and Gao, 2019).

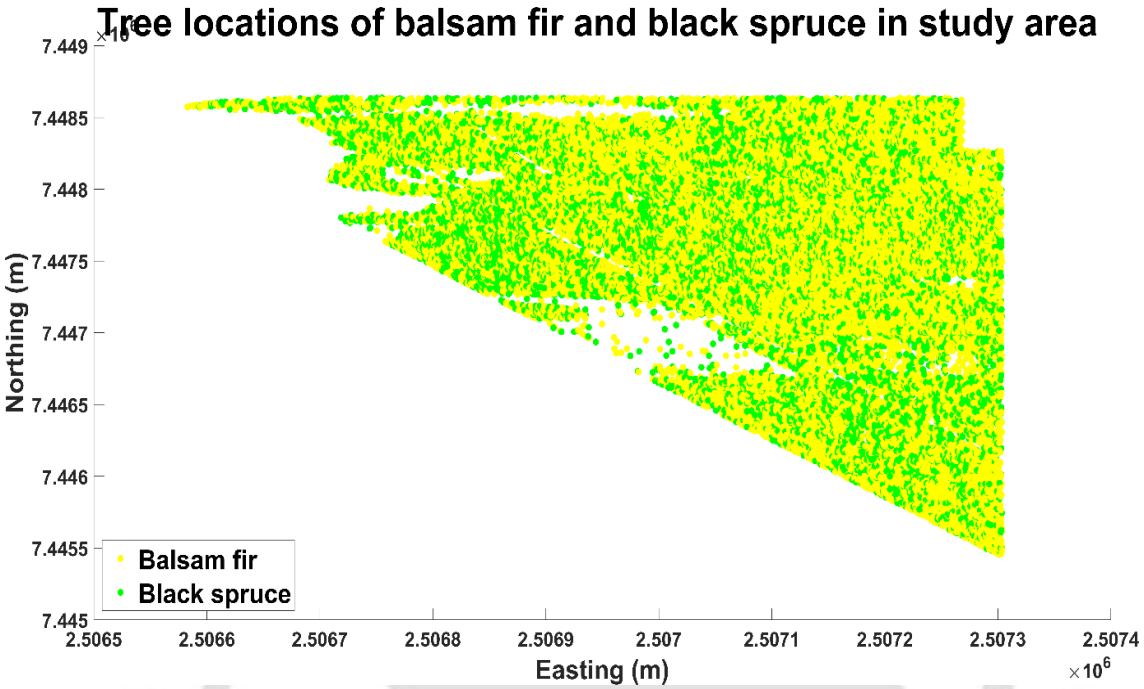

Figure 4.7 Spatial distribution of Balsam fir and Black spruce extracted from airborne LiDAR data

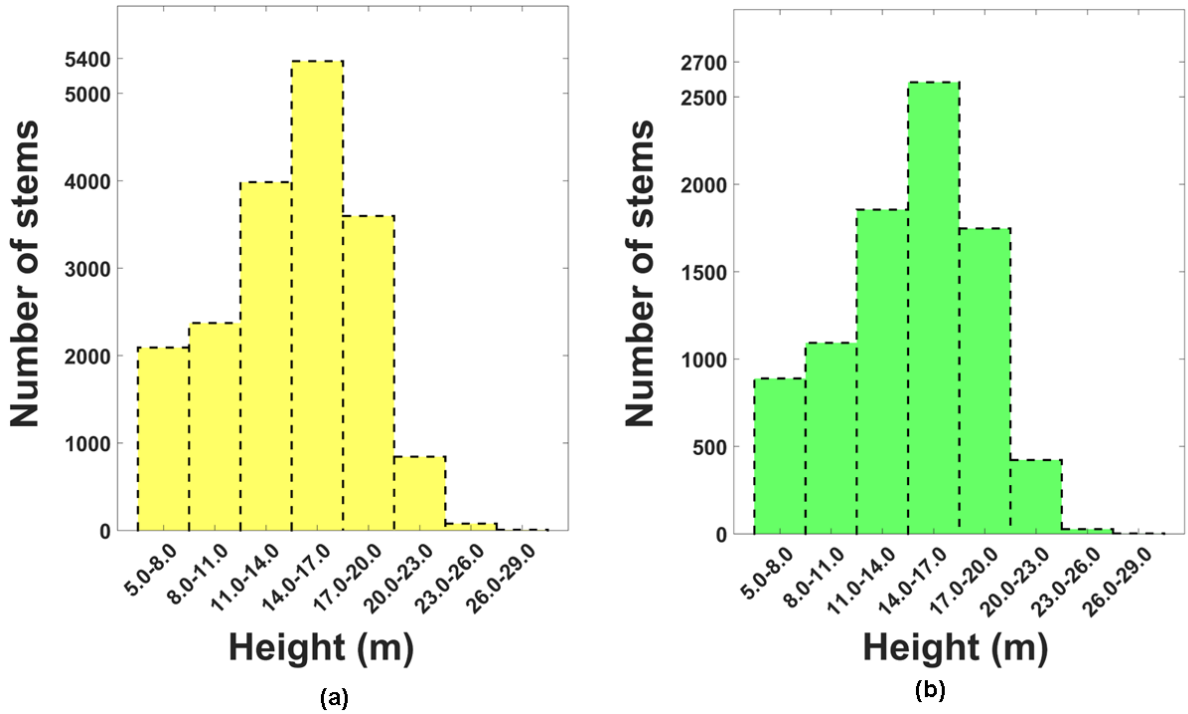

Figure 4.8 Histograms of LiDAR-derived height of (a) Balsam fir and (b) Black spruce.

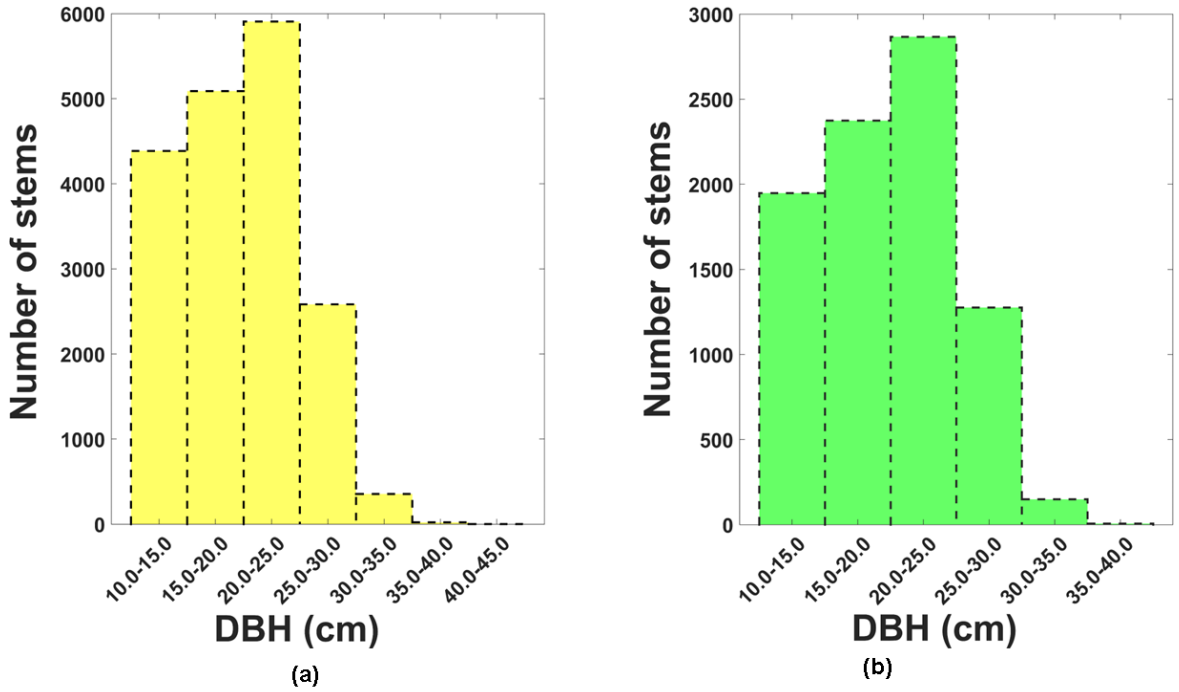

Figure 4.9 Histograms of estimated DBH (a) Balsam fir and (b) Black spruce

Maximum and minimum heights of balsam fir trees derived from LiDAR data are 5.004 m and 29.9490 m, respectively. Estimated DBH for balsam fir by the allometric equation ranges from 10.3730 cm to 45.6221 cm. Similarly, for black spruce, the DBH ranges from 10.3728 cm to 38.1824 cm, while their heights range from 8.0018 m to 28.3802 m. As maximum value of estimated DBH and LiDAR captured height (H) of the Acadian Forest species are less than those specified in forest inventory data (from DNR), developed allometric equations and biomass carbon model are expected to underestimate both DBH and calculated aboveground biomass values. Histogram distributions indicate more than 45% of trees heights are less or equal to 14m, confirming participation of young to mature species of Balsam fir and Black spruce in EDM simulation. EDM with modified PFT parameters simulated above ground biomass for mentioned tree species of Northern pine for maximum of 75years. Next subsections explains reliability and accuracy of simulated values and biomass (AGB and BGB) variations.

4.4.2 EDM outputs verification

Dashti et al. (2021) reported that monthly EDM GPP values when compared with Eddy covariance data had an uncertainty of 0.39 $kg.C/m^2$. On the other hand, Wu et al. (2010) reported that MODIS and Eddy covariance has a RMSE of 18.464 $g.C/m^2/8\ day$. Thus, to validate results, GPP values obtained by EDM, are compared with MODIS data for years 2021 and 2023 as eddy covariance data of the study site is not available. Comparison of simulated

values by EDM and MODIS data was not possible for year 2022 as GPP values by MODIS are not available. Validation was performed for 15 months (last seven months of year 2021 and first eight months of year 2023) for which MODIS data are available. Table 4.6 shows the monthly variations of the simulated GPP by EDM and GPP values by MODIS for years 2021 and 2023.

Table 4.6 Comparison of monthly simulated GPP by EDM and MODIS GPP of the Northern pines

EDM GPP ($kg.\frac{C}{m^2}/month$)	**MODIS GPP** ($kg.\frac{C}{m^2}/month$)	**Month of Year**
0.132936	0.065549	June 2021
0.138208	0.076084	July 2021
0.126246	0.070404	August 2021
0.109841	0.069219	September 2021
0.100596	0.083207	October 2021
0.026468	0.021658	November 2021
0	-0.00053	December 2021
2.6E-08	-0.0003	January 2023
0	-0.00019	February 2023
0	-0.00227	March 2023
9E-08	-0.01606	April 2023
0.010981	-0.02708	May 2023
0.015813	-0.03249	June 2023
0.017982	-0.04852	July 2023
0.018759	-0.03967	August 2023

$RMSE$ calculated using 15 months data with MODIS GPP as a reference was equal to 4.75066 $\times 10^{-3} kg.C/m^2$. In addition, notably, for the year 2021, simulated values superseded reference values. Whereas for the year 2023, simulated values were less than the reference values. This variation could stem from methodological disparities - MODIS calculates GPP using a fraction of photo synthetically active radiation and land cover classification, which may result in overestimation or underestimation due to potential errors in these datasets. Additionally, parameters such as maximum light utilization efficiency employed in EDM might not align with actual field values (Gelybó et al. 2013; Oliphant et al. 2011; Pandit et al. 2021; Verma et

al. 2015; Wang et al. 2017). Moreover, the simulation by EDM did not incorporate disturbances like wildfires.

Figure 4.10 below depicts the EDM simulated GPP and NPP values for the study site drawn for 55 years. Although random fluctuations in GPP and NPP are discernible in the simulation results up to year 2025, discrepancies converge subsequently for random fluctuations in GPP and NPP are discernible in the simulation results up to year 2025, discrepancies converge subsequently for the remaining years. These early oscillations may result from changes in vegetation composition and climate variations (temperature, precipitation, sunlight availability, etc.), significantly affecting photosynthesis, and consequently, GPP and NPP values are also modified (Gelybó et al. 2013; Thomas et al. 2009). Modifications made to the PFT parameters could also contribute to these fluctuations. Consistency in variation after year 2025 suggests that the forest ecosystem has attained equilibrium with stable rates of respiration and photosynthesis. This stabilization could be attributed to the vegetation age or specific climatic conditions (Pandit et al., 2021).

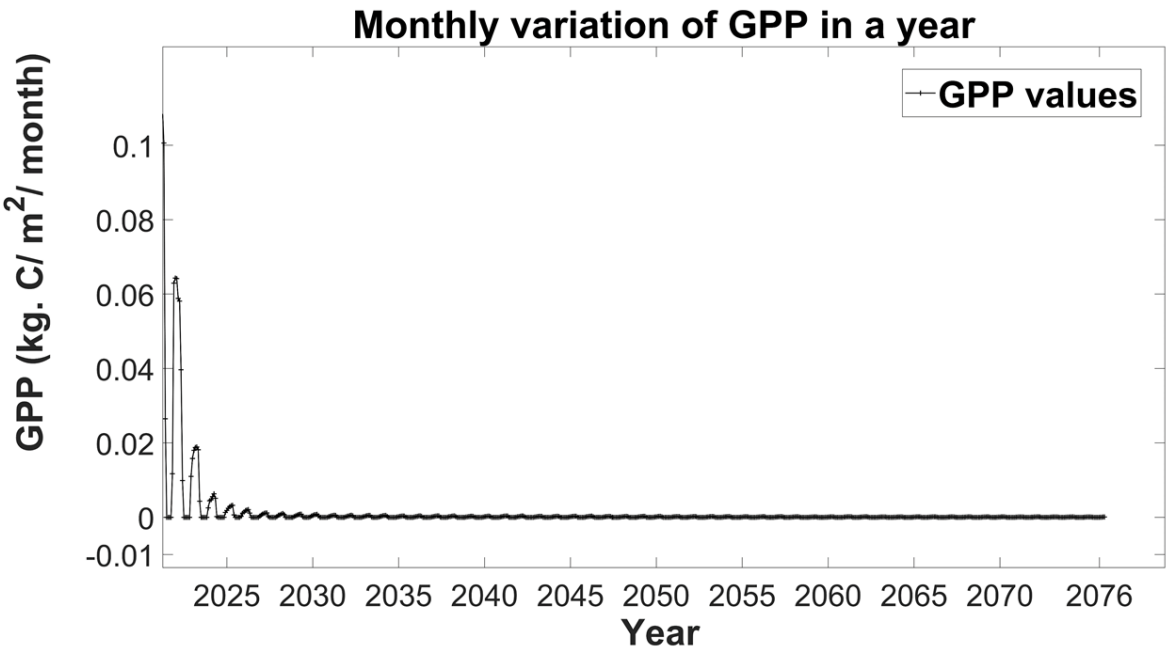

(a)

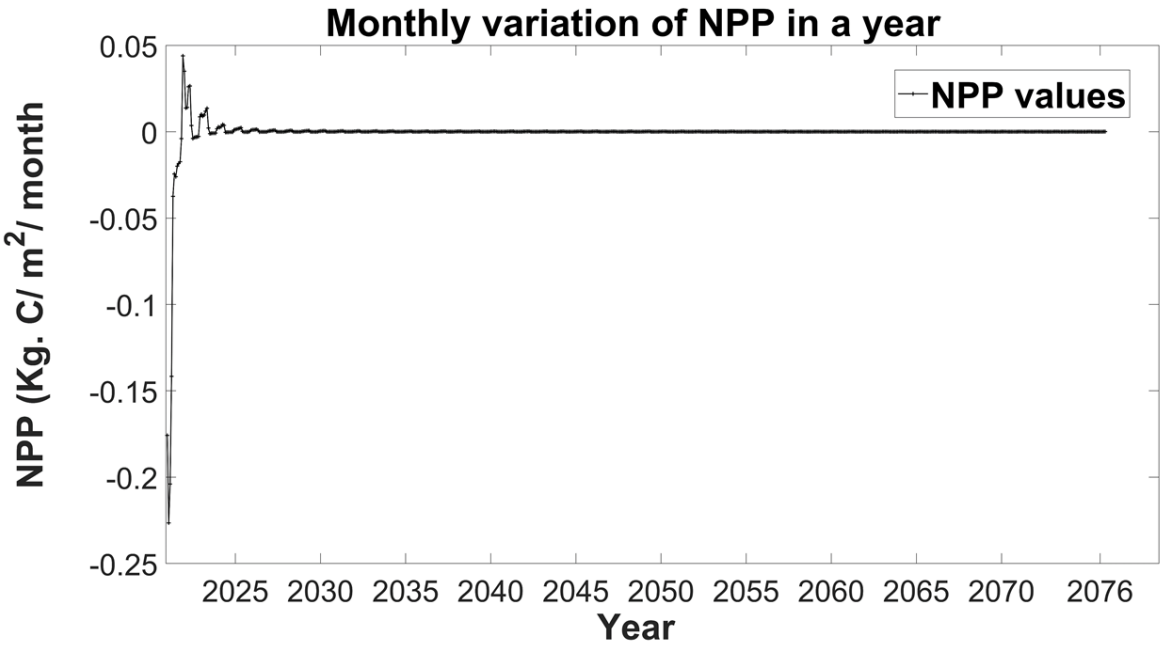

(b)

Figure 4.10 Yearly variations of EDM simulated (a) GPP and (b) NPP values for 55 years (from years 2021 to 2076)

4.4.3 AGB and BGB dynamics

Figure 4.10 below illustrates the annual variation of simulated aboveground biomass (AGB) using the EDM from the current year (2021) to August 2076 for 27,119 numbers of cohorts (AGB distribution for the year 2021 for the whole LiDAR polygon area is given in figure 4.5 above. A decline in AGB for the study area was observed, which aligns with findings of Dimitrov et al. (2014) of diminished carbon capture over time in ecotone regions. Variations

in AGB remained minimal until year 2048, after which a significant decrease was observed. This trend corresponds with the stable temperature and precipitation patterns projected by representative concentration pathways (RPC) models up to year 2048 (Taylor et al., 2017). RPC Projections indicate a 4-6°C increase in mean annual temperature across New Brunswick by years 2071-2100. This will be accompanied by a 39-77% rise in growing degree-days and a 48-79 mm decrease in summer atmospheric water balance. These shifts may stress vegetation, hinder tree growth, and diminish soil moisture and nutrient availability, consequently reducing AGB (Albert et al., 2023; Xiao et al., 2023). Contrarily belowground biomass (BGB) has shown decline in year 2048 (Fig. 4.11 below). Moreover, according to Ma et al. (2022), EDM estimates of AGB are in close agreement with filed data.

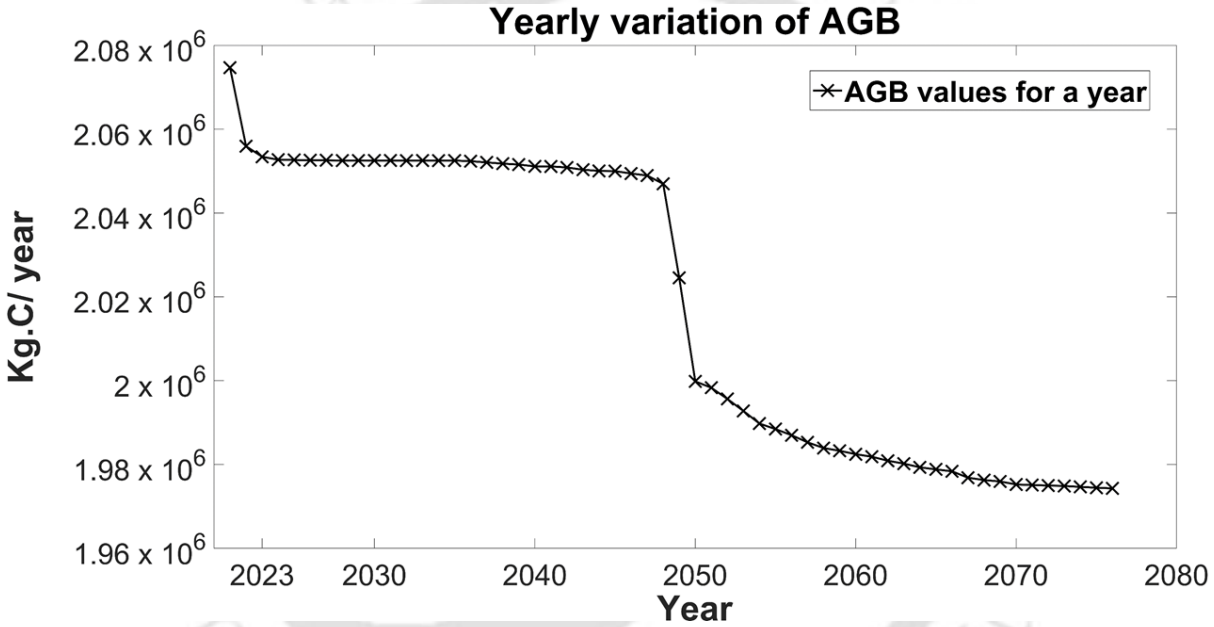

Figure 4.11 Yearly variation of simulated AGB values by EDM for years 2021 to 2076 for study site

Additionally, EDM outputs confirm a steady fall in evapotranspiration and LAI from year 2021 to year 2029, indicating probable water stress and loss in photosynthetic capability, both of which contributed to the AGB decline during the 9 years. From years 2029 to 2045, no major changes in stored biomass are observed due to stable values of evapotranspiration, and LAI. Stable behavior of forest biomass can be attributed to reaching maturity by most of the cohorts. However, increase in temperature and decrease in precipitation caused decrease in structural soil carbon from year 2045 onwards. This negatively affected plant production and soil health, aggravating the AGB reduction in the Acadia Forest. This dramatic drop in AGB, which originally commenced in year 2045 is observed in year 2048.

4.4.4 Carbon sequestration model

Simulation error in GPP, indicated by RMSE of 4.75066 × 10^{-3} $kg.C/m^2$ is acceptable (Gelybó et al., 2013; Oliphant et al., 2011; Verma et al., 2015). Also, trend of the simulated values of biomass are consistent with prior research by Bashir et al. (2019) , who reported a decrease in carbon sequestration pools consisting of Balsam fir and Black spruce.

Dynamically varying AGB values obtained by EDM for a year (as shown in figure 4.11 above) for trees are used for calculating above ground biomass carbon for that particular year. Thus, C_{AGB_t} for the current year (2021) is calculated as average carbon over all trees (27119 cohorts) used for simulation for the year 2021 and extrapolated for the area of the Acadian Forest (90 km^2). Next, C_{AGB_t} is used as one component in equation 4 for calculating the carbon sequestered (C_{s_t}) by the study site in current year (2021). Moreover, EDM calculates BGB values based on the root to shoot ratio of a plant species. Using the simulated below ground biomass authors calculated C_{BGB_t} in a reference year and extrapolated for the entire Acadian Forest. Figure 4.12 shows the BGB dynamics.

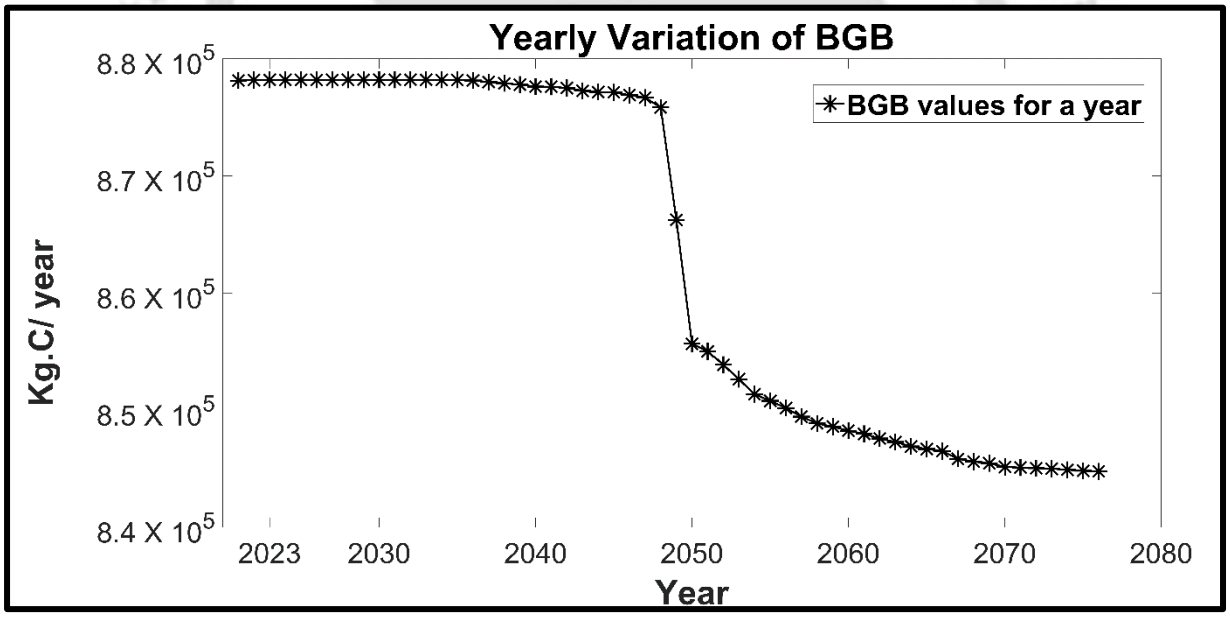

Figure 4.12 Below ground biomass variation for the whole LiDAR polygon area from 2021 to 2076.

Remaining three components in equation 3.11 and 3.12 are soil organic carbon, greenhouse emissions over New Brunswick, and wood harvesting in the Acadian Forest, which are calculated as follows:

(i) **Carbon from soil organic carbon (C_{SOC_t}):** C_{SOC_t} for the year 2021 is calculated from the repository created by Sothe et al. (2022). For this, first mean value of the soil organic carbon for the LiDAR polygon is extracted. The extracted mean, minimum and maximum values of soil organic carbon for year 2021 for the LiDAR polygon are 12.13, 7.43 and 24.51 $kg.C/m^2$, respectively. Using the mean value, authors extrapolated the SOC for the Acadian Forest for year 2021. For the remaining years i.e., from 2022 to 2076, equation 5 has been used, in which λ_1 is assumed as 1.2% and we assumed that 100% of the forest cover change is converted to AGB. Authors obtained forest cover change from the Global Forest Watch (*Global Forest Watch*, 2021). Moreover, λ_2 value is assumed as same as λ_1. In addition d value is taken as 0.02 as the study site soil texture is sandy clay loom (Wang et al., 2019). The extracted soil organic carbon for the LiDAR polygon area and trends are shown in Figure 4.13 and 4.14 below.

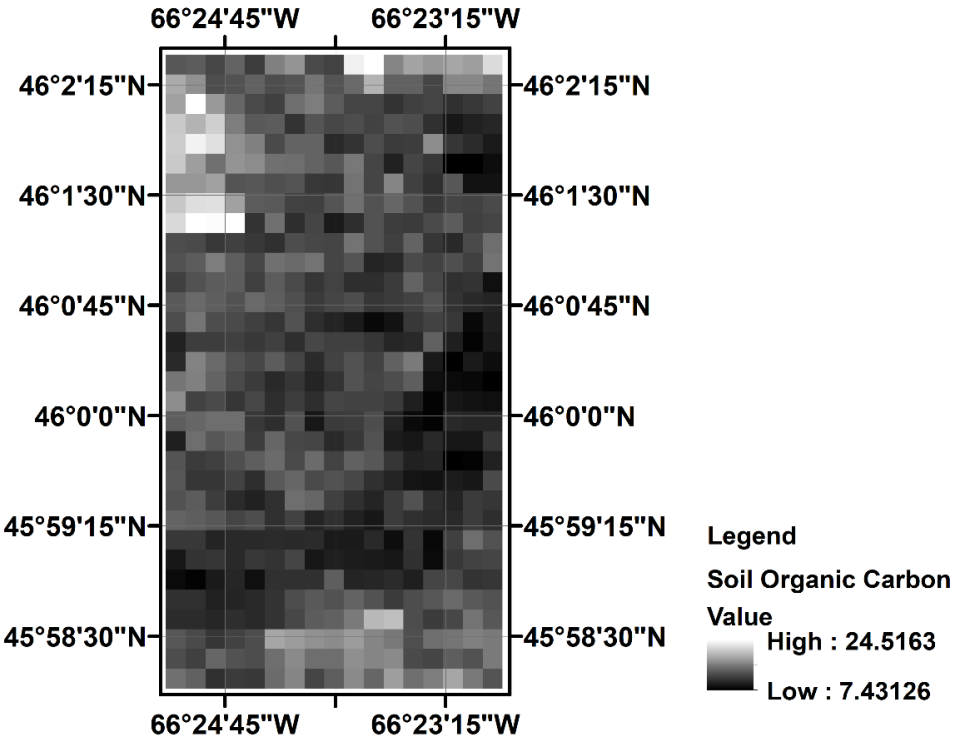

Figure 4.13 Soil organic carbon variation for the whole LiDAR polygon area for year 2021.

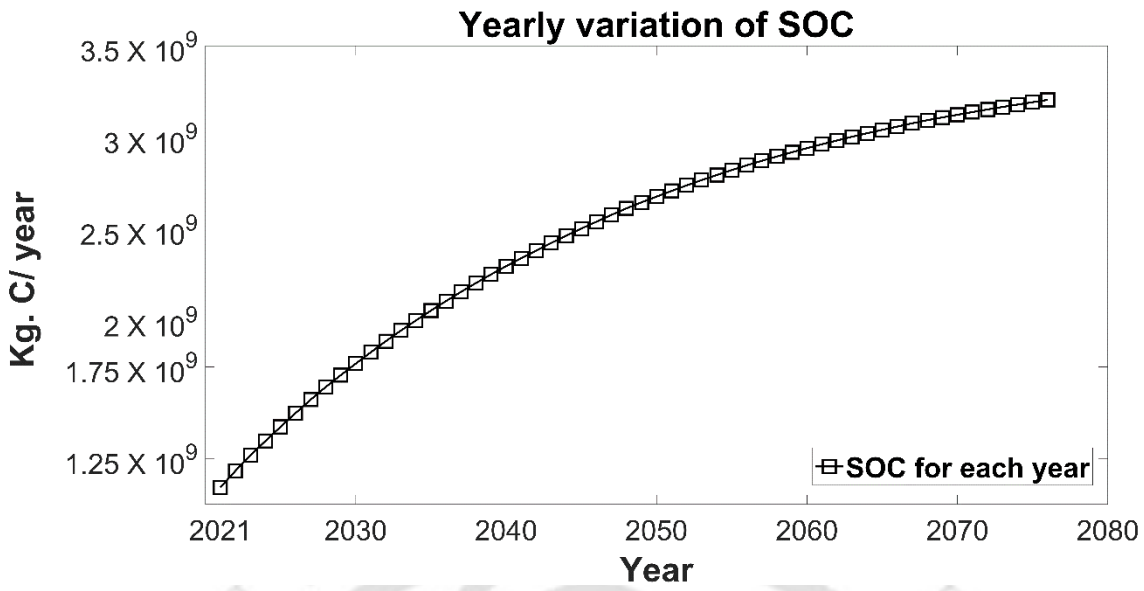

Figure 4.14 Soil organic carbon variation for the whole LiDAR polygon area from 2021 to 2076.

(ii) **Carbon from greenhouse gas emission (C_{GHG_t}):** As the Acadian Forest are surrounded by New Brunswick, Nova Scotia and Prince Edward Island of Canada, emissions from the three neighbouring provinces or the regions impact carbon sequestered in the Acadian Forest. Currently, carbon emission in New Brunswick (NB), Nova Scotia (NS) and Prince Edward Island (PEI) is equivalent to 12.4, 14.8 and 1.610 MT of carbon dioxide, respectively (National Resource Canada, NRC, 2021). Applying a carbon conversion factor of 0.27, to carbon dioxide values, calculates carbon from gas emission as $3.382 \times 10^9\ kg.C$, $4.038 \times 10^9\ kg.C$ and $0.439 \times 10^9\ kg.C$ (kilograms of carbon) for NB, NS and PEI provinces, respectively. From these values, we have generated uniformly distributed random samples in the three regions. Initially a total number of 30 samples are selected for the three provinces. Numbers of samples in each of the three areas are selected according of the size of the area. Therefore, 17, 12, and 1 samples are collected from NB, NS, PEI provinces, respectively, and corresponding gas emission values are assigned. Increasing number of samples for the three regions did not alter the Kriging performance and interpolated values. Figure 4.15 shows, interpolated values of gas emissions for the three provinces and Acadian Forest.

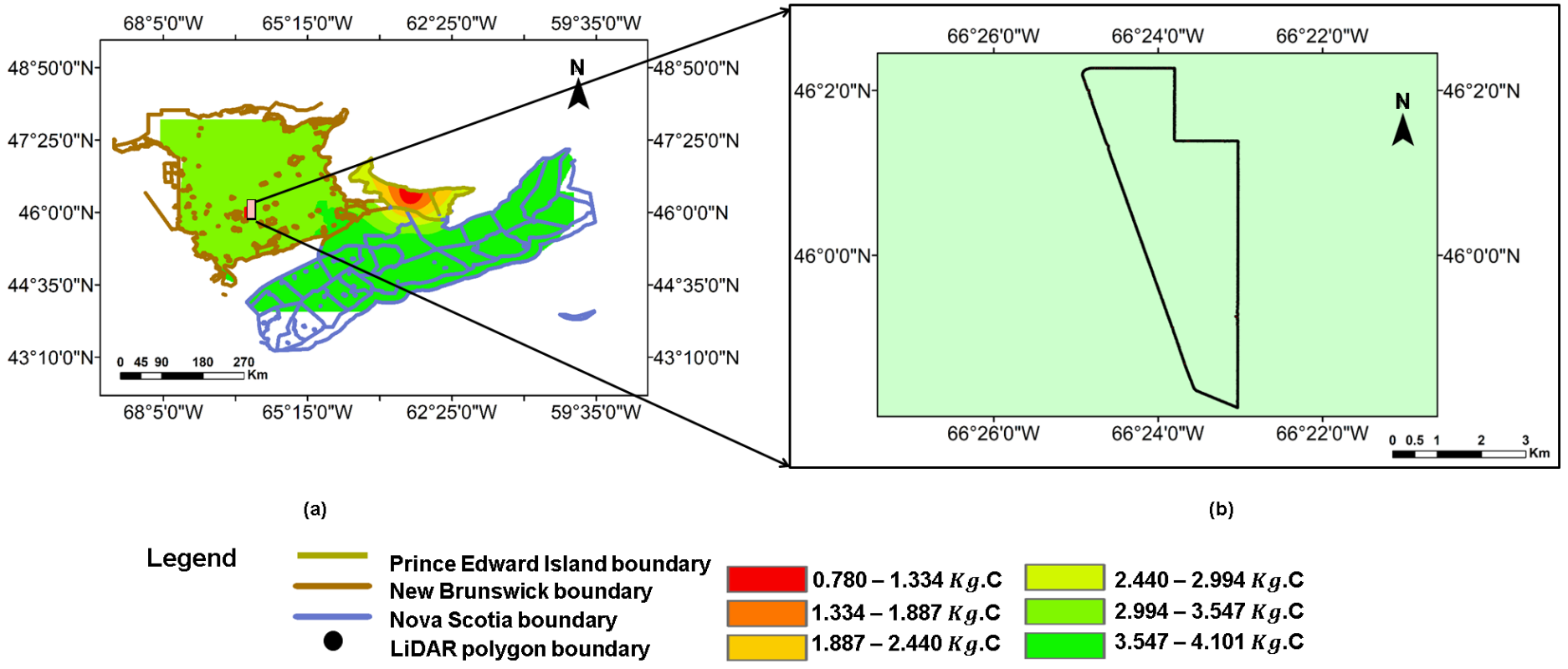

Figure 4.15 (a) Kriging process for the NB, NS and PEI provinces and (b) estimated carbon values for the Area of Interest (LiDAR polygon).

Figure 4.15 indicates that the Acadian Forest show same values of carbon gas emission as that of NB region. However, as NS and PEI regions are very far from the Acadian Forest and thus the carbon emissions from the two regions influence the forest minimal. Thus, authors adopted the carbon emission values of NB site for the AOI of the study site (LiDAR polygon). Further, authors also adopted 1.2% reduction of greenhouse gas emission each year as recommended by the greenhouse gas projections (NRC) and Government of New Brunswick province.

(iii) **Wood harvesting (C_h):** In New Brunswick, volume of woodcut is $9{,}341{,}187\ m^3$ (NRC, 2021). Multiplying this quantity with average wood density of 0.5 g/cm^3 and carbon conversion factor of 0.5 (Pingoud et al., 2006) provides C_h as 2335296750 $kg.C$. This value is assumed constant for each year because the volume of woodcut has not change since 2019 (NRC, 2021) (Table 4.7).

Year	Wood Volume	Population
1990	8,824,139	739547
1991	8,642,707	744717
1992	9,204,727	747418
1993	8,958,814	748620
1994	9,268,820	749965
1995	10,054,901	750907
1996	10,902,048	752062
1997	11,252,750	752385
1998	11,534,357	751457
1999	11,293,764	750362
2000	11,872,453	750525
2001	10,185,695	749656
2002	9,989,404	749203
2003	10,788,255	749356
2004	11,004,084	749301
2005	9,968,491	748359
2006	10,450,510	745949
2007	8,943,599	745337
2008	8,930,707	746864
2009	7,939,664	749641
2010	9,218,941	752656
2011	9,231,392	755354
2012	9,437,285	757468
2013	9,901,514	758130
2014	10,167,917	758783
2015	9,362,789	759262
2016	9,345,246	762785
2017	9,347,159	776049
2018	9,362,714	770036
2019	9,341,187	776408

2020	9,341,187	782703
2021	9,341,187	789622

Table 4.7 Harvested wood volume and population of the New Brunswick province from 1990 to 2021 (Source National Resource Canada).

Figure 4.16 illustrates the yearly variation of simulated biomass (AGB+ BGB) and the carbon sequestered (C_{s_t}) over 55 years for the Acadian Forest.

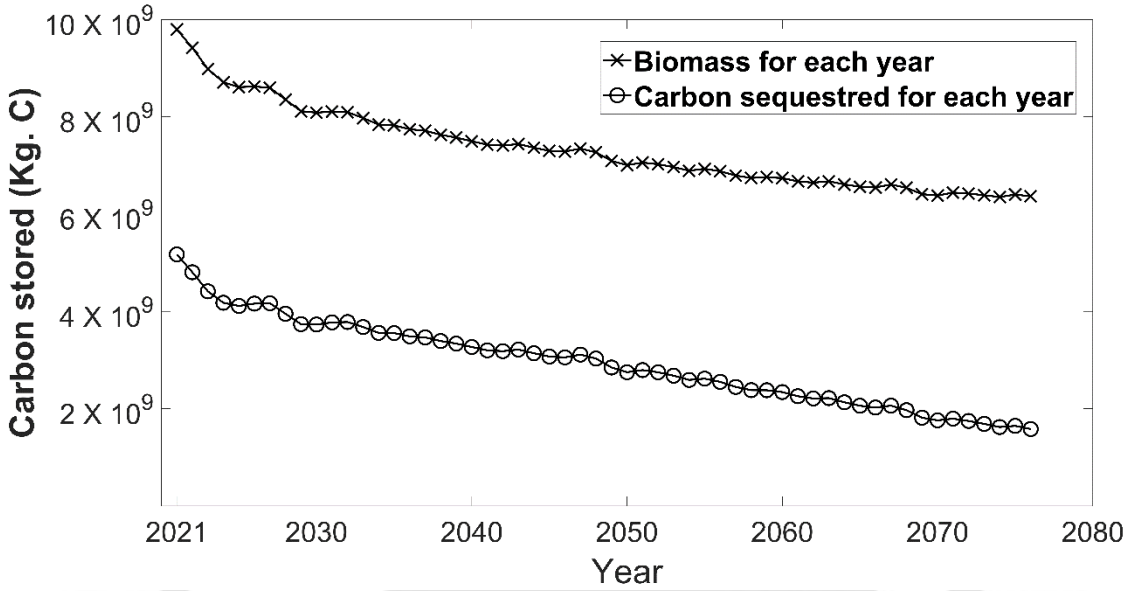

Figure 4.16 Yearly variation of biomass values and carbon sequestered from years 2021 to 2076.

Next chapter describes analysis of results of proposed biomass estimation method for individual tree and forest from terrestrial and airborne LiDAR data. Moreover, it also provides limitations of each method and uncertainties of the proposed carbon sequestration model.

CHAPTER 5 DISCUSSION

5.1 Biomass estimation from terrestrial LiDAR data

As evident in Table 4.1, all errors are negative, i.e. the proposed method always underestimates the values of stem volume, crown volume and total volume. Errors in volume estimates are contributed by various sources including LiDAR data as well as limitations of the proposed method. As the LiDAR data is acquired by TLS, data with lower point density (or sparse data) are obtained for higher heights of tree stem. Similarly, branches at lower elevations obscured line of sight of TLS for branches at higher elevations and near the canopy surface. This leads to sparse data for branches at the higher elevations. As a result, for some branches located near canopy surface, a single line of point data is also observed. For such branches, the proposed method could not fit a 3D cylinder as estimated radius for the fitted cylinder was infinity. Consequently, the error in stem volume increases with stem height. Similarly, the error in the crown volume is proportional to the crown height. Therefore, if the stem height is higher than the other trees in a region, the error in the crown volume of the same tree is also higher. Furthermore, in addition to higher stem height, if crown height is also higher, errors in crown volume are not only higher but also error in total volume is compounded by the two errors. Apart from that, the proposed method could not model thin branches i.e. branches with less than 3 cm diameter. Moreover, the method segments a branch joint of two or more branches into one cluster or branch, if three-dimensional angle and distance between the two branches is 2.5° or 4 cm, respectively. In addition, if two branches belonging to different joints, yet if distance between the branches is less than 4 cm, the two branches are classified in one data cluster. In addition to errors in the cylindrically shaped branches and stems, shape modelling by alpha shapes for portion of a stem located near buttress also contributes to the error and lower stem volumes.

In the Peruvian site for trees M02, M08, and M05, errors in estimated stem volumes increased with the heights of the stems. Similarly, trees I08, I03 in the Indonesia site and trees G01, G04, and G09 in the Guyana site are increasing with tree heights. However, some deviations are also observed for remaining trees. For M09, M06 and M07 trees in the Peruvian region, the shape of tree stems are vertically straight and close to the cylinder, leading to accurate estimates of the stem volume. Similarly, for I04 and I07 trees in the Indonesia and G02, G03, G06 and G07 in the Guyana region, shape of stems are close to cylindrical. On the

other hand, stem data for M03, G05, and I02 trees contains segments of length more than minimum bin interval for which stem data are not available. In these cases, the cylinder cannot be fitted, resulting in higher errors in stem volume estimates. However, for M01, I01, and G08, tree stems are of irregular and non-linear shapes. As a result, stems deviate from the cylindrical shape, and variations of LiDAR data in the horizontal direction are more than 10 cm. Due to these two characteristics of stem and data for a slice, shape fitting by RANSAC rejects the points showing variations more than the threshold of linear deviation (1.5 cm). This provides less estimates of cylinder volume of a slice. In the Guyana site, error in estimated crown volume for trees G04, G09, and G07 increases with their crown height. Similarly, for tress I02, I03, I04, I07 and I08 in Indonesia, tress M03, M02, M07, M06 and M01, crown volume errors increase with crown heights of the trees. Following the same pattern, for tree G06, insufficient point data for branches that are either thin in thickness or situated at higher heights or obscured by other lower branches, the proposed method could not segment the branches. This led to higher error estimates in crown volume. However, the proposed method provided better estimates of crown volumes for trees despite having higher heights. For instance, trees G01, G02, G07, G05, G08, and G03 have less number of branches with larger canopy voids compared to other trees in the region. However, for I01, M08 and M09 trees, despite having lower heights, the accuracy of crown volumes are inferior as multiple branches showing less angular deviation are classified as a single cluster by the algorithm. As a result, angular deviation between any two branches is less than 2.5° and linear deviation is less than 4cm, making complex canopy. Due to the complexity, the proposed method could not segregate two branches resulting to errors in crown volumes.

5.1.1 Limitations

Comparing errors in stem volumes and crown volumes in Table 4.1 reveals that the stem volumes are estimated more accurately than crown volumes in the Peruvian and the Guyana regions. In the Peruvian region, vertically straight, thick and longer stems in comparison to thin branches in crown cause less errors. For the latter region, crown heights are larger than the stem heights, causing sparse line-type data near canopy surface and thus more errors in crown volumes are obtained. However, though stem heights are smaller than crown heights for the Indonesia region, stems are of irregular and non-linear shapes. In addition, larger voids in canopy resulted in smaller errors in crown volumes. Figure 10 shows cases of data gap in stem data for more than 38 cm, horizontal variation of 10 cm in stem data and, distance of 4 cm between two branches near canopy surface.

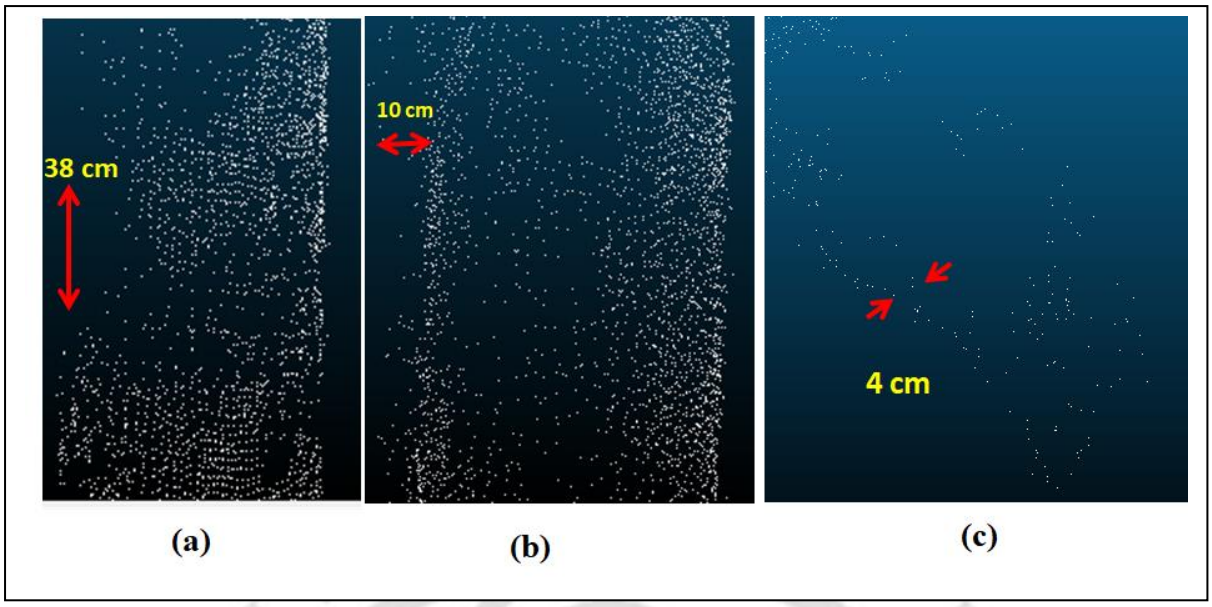

Figure 5.1 (a) Data gap in stem point cloud data, (b) horizontal variation of LiDAR points on stem surface and (c) distance between two branches.

Table 4.2 shows species-wise accuracy statistics of the proposed method for the three regions. The accuracy is not correlated with any geometric parameters of trees. Moreover, irrespective of number of trees in a species, stem volume accuracies are more than crown volume accuracies except for Korokororo species and Tetramerista Glabra species in the Guyana and Indonesia regions, respectively. For the species in the three regions, trees geometric structures show vertically straight cylindrical stems compared to curvilinear crown branches. Also, stem heights are higher compared to crown heights.

For the Korokororo species in the Guyana region, due to higher height of stem (24.2 m) compared to that of crown (5.56 m), LiDAR data for stem are sparse or less dense near *BCL* leading to lower accuracies in stem volume than crown volume accuracy. On the other hand, for two trees of the Tetramerista glabra species in the Indonesia region, horizontal variation in the stems are larger and thus the algorithm rejected many points for cylinder fitting.

Apart from the error analysis and species wise accuracy analysis, the performance of the algorithm is different for three sites. The method achieved less errors and higher accuracy for both stem volume and crown volume in the Indonesia region. The Indonesia region comprises of trees having smaller heights of stems and crowns, (tree heights range from 23.15 m to 27.32 m, except for tree I07). Whereas, heights of the trees of other two regions are in range 22 m to 44 m. Due to smaller stem and crown heights in the former region, TLS captures denser 3D data resulting in better estimates of both stem and crown volumes.

Authors realized some limitations of the proposed method and the developed algorithm. The algorithm is highly sensitive to straight cylindrical shape and thickness of stems and branches i.e. data points belonging to curvilinear stems and branches not conforming to cylindrical shape are rejected in multiple stages of branch and stem extractions. Also, thin branches of less than 3 cm cannot be modelled. On the other hand, the algorithm is also sensitive to tree height, which is function of tree age. For immature trees having smaller heights with non-linear branches and stems, number of data points are less. As the algorithm systematically removes data not conforming to cylindrical shape for both stem and branches, the extraction process and subsequent volume calculations led to higher errors and lower accuracy for both stem and crown volumes (e.g. tree I04 in the Indonesian region).

5.2 Biomass estimation from Airborne LiDAR data

5.2.1 Limitations

The method provided is an approximate approach that does not overestimate biomass values. The calculated biomass for balsam fir and black spruce is compared with the findings of Ter-Mikaelian and Korzukhin (1997), which indicate that for no tree, the calculated carbon exceeds 500 kg C. This benchmark serves as a critical reference point for validating the accuracy of biomass estimates. While LiDAR data is a powerful tool for forest analysis, it is important to note that the retrieval of tree species is not exact. The accuracy of species identification is influenced by the structural characteristics of the forest, which can lead to misclassification. This limitation is particularly relevant in mixed-species stands where overlapping canopies and varying growth forms complicate species differentiation. The use of Diameter at Breast Height (DBH) derived from LiDAR-based CHM (canopy height models) introduces additional uncertainties in biomass calculations. However, as the Acadian Forest contains sparse canopy, therefore we could assume very less certainties in tree species retrieval and classification.

DBH is a critical parameter in estimating biomass, as it is used in allometric equations that relate tree size to biomass. Any inaccuracies in DBH measurements can significantly affect the resulting biomass estimates. For instance, if the DBH is underestimated due to limitations in LiDAR resolution or data processing, the biomass calculations will also be lower than the actual values. Conversely, overestimating DBH can lead to inflated biomass figures. Therefore, it is essential to consider these uncertainties when interpreting biomass data derived from LiDAR and to complement these findings with ground-truthing methods whenever possible.

5.3 Biomass estimation from Satellite data

Results of parametric model for estimating biomass without ground truth data, which has traditionally been used in most of the previous studies (Francini et al., 2022; Mohite et al., 2024; Musthafa and Singh, 2022; Ni et al., 2021; Tamiminia et al., 2024). By achieving comparable levels of accuracy by R^2 across two geographically and ecologically distinct boreal forest sites, this study demonstrates potential, robustness, and applicability of the developed parametric model for biomass estimation. Without the use of ground truth data, simplified model appears to be more feasible and cost-effective for the first hand analysis, particularly for remote or inaccessible forested areas. The robustness of the model was validated by performing the same set of experiments in both the Acadia Forest in Canada and the Taiga Forest in Russia, achieving consistent and similar levels of accuracies. The Random Forest model yielded better results than KNN with superior RMSE and R^2 values at both study sites demonstrating more acceptability of the former algorithm as regression technique. This methodology advances biomass mapping and environmental monitoring by demonstrating the efficiency of integrating remote sensing data for AGBD estimation. Also, it highlights importance of combining spectral, spatial, and terrain information to enhance our understanding of biomass mapping for ecosystem dynamics and support sustainable resource management practices.

5.4 Carbon sequestration dynamics from airborne LiDAR data

From year 2021, trend in values of carbon sequestered of the Acadian Forest in New Brunswick starts to decrease. The trends are similar to the biomass that indicates that biomass is the major contributing factor to the carbon sequestration of the Acadian Forest. Moreover, rate of carbon sequestration (equation 3.13) from year 2029 starts oscillating between positive and negative values due to multiple factors affecting the balance between carbon storage and loss. As forests mature, their growth slows, reducing the rate of carbon uptake, while natural disturbances such as extreme weather events—exacerbated by climate change—can further diminish sequestration capacity. Rising temperatures and water stress may also increase tree respiration and soil carbon decomposition, leading to higher carbon emissions. These combined factors create a dynamic environment where the rate of carbon sequestration varies, leading to oscillations between positive and negative rates after 2029. In other words, the current state of the forest or its species composition may not effectively sequester carbon after the year 2029. Moreover, it also reveals that species like Black spruce and Balsam fir though adapt to environmental changes, compared to temperate species (Maple and Birch), former are

more susceptible to variations in temperature and precipitation as observed by Albert et al. (2023) and Taylor et al. (2017). This highlights the potential necessity for temperate species, which are more stable against temperature and precipitation changes, and thus enhance stability of the Acadian Forest ecosystem by carbon degradation in the forest at slower rate. Increment in greenhouse gas emissions and wood harvesting because of population increment may further reduce the carbon sequestration of the forest. Furthermore, use of species such as Spruce, which is widely used in Canada, especially for paper production and as a source of softwood lumber, will be the cause of major land-use changes, deforestation, and increased wood harvesting in the Acadian Forest. These factors collectively can reduce biomass further and soil organic carbon storage. Further, economic and policy shifts possibly influence the forest management and its conservation efforts, and increased greenhouse gas emissions from industrial and transportation sectors.

This thesis highlights the potential of Ecological demography model (EDM) in assessing carbon sequestration potential of the Acadian Forest. The carbon sequestration model proposed can be used for any forest especially to ascertain the current forest policies and management practices. Moreover, the allometric model modified for species can be used to estimate its biomass for the nearby provinces Nova Scotia and Prince Edward Island.

5.4.1 Model Uncertainties

Simulations of configured EDM for the study area may potentially underestimate biomass due to several factors. For instance, disturbances such as the spruce webworm disease, which is prevalent in the Acadian Forests, were not considered in this study, which effect the soil carbon and in turn on the growth of roots and branch biomass. Default parameters adapted for EDM including allometric biomass progression, leaf phenology, water tilting points, and soil saturation levels may introduce uncertainties in AGB results. While our species classification is not entirely precise, it may not significantly impact uncertainties in EDM results because Balsam fir and Black spruce belong to the same plant functional type. Furthermore, authors provided uniform soil depth for the entire forest due to the limitation of EDM.

For the carbon sequestration model, we employed an average value of AGB and BGB. So, biomass estimates (AGB+BGB) are not entirely precise, yet it offers valuable insight into forest carbon dynamics. Moreover, for soil organic carbon, we have used simple linear model, for which constant proportion of biomass carbon loss from tree fall has been adapted. Modelled values may not be exact yet reliable and also authors did not incorporate dead organic matter for carbon sequestration model as the information is not available. Moreover, it contributes to

less than 2% of the forest storage (Haseeb et al., 2024). Furthermore, the proposed method could be improved by modelling λ_1 and λ_2 factors and decomposition factor d for soil organic carbon. In addition, in conjunction with field soil samples, one can improve the simulation of biomass by improving inputs to the EDM such as calculating actual fast (soil carbon from litter), structural (soil carbon from wood twigs or fallen wooden branches) and slow soil carbon (decomposed soil carbon). Moreover developing crown allometric model using Tong et al. (2021), and Tong and Zhang (2025) can improve the reliability of EDM simulations of AGB and BGB.

5.4.2 Impact of tree structural parameters on EDM simulations

While TLS provides high-resolution data that can accurately capture tree dimensions, it has limitations when applied over extensive areas, where technologies like ALS, GEDI, and satellite imagery are more efficient. Structural details—such as tree height, DBH, canopy density, and species composition—materially affect carbon estimates in predictive models. By integrating data from multiple sources, hybrid models can be developed for structural details that leverage the precision of TLS in localized studies while capitalizing on the broader coverage offered by ALS and satellite data. This integrated approach can enhance our understanding of forest dynamics and improve the accuracy of carbon stock assessments, ultimately guiding management practices and conservation efforts more effectively. Exploring these relationships can also inform future research directions, particularly in delineating the interactions between forest structure and ecosystem functioning at scale.Next chapter presents conclusion and future scope of the thesis work.

CONCLUSION

The aim of the thesis entitled *"**A Pipeline of Methods for Evaluating Carbon Sequestration Potential of Forest using LiDAR Data and Abiotic Factors**"* is incorporating LiDAR remote sensing, analytical analysis, bio-geophysical models and anthropogenic emissions to investigate carbon pools of the Acadian Forests, which are in ecotone regions amidst climate driven shifts and human interventions. Major conclusions of the thesis are summarised as follows:

- A modified method for crown structure modelling, branch collar detection and branch structure modelling from terrestrial LiDAR data has been presented. Automated branch collar level and crown based height has been given with a precision level of 5cm in vertical accuracy, where these two can be used for automated stem detection and crown detection for extensive forest data. Angular and linear constraints are presented to extract curvilinear branch and stem segments and shape model into small straight cylindrical segments. These two constraints can be used for assessing the data density required for accurate branch segment modelling.
- Errors in stem volumes are in range from 0.03 – 0.87 m^3 for estimated stem volumes in 1.1 – 17.68 m^3. Similarly, errors in crown volume are in range from 0.013 – 2.33 m^3 for estimated crown volumes in range of 0.105 – 25.95 m^3. Irrespective of type of species, errors in each of the stem volume, crown volume, and total volume increase with shape, size, and height of stem, crown, and tree, respectively. Stems and branches deviating from straight and cylindrical shapes contribute more errors. Higher errors in stem further increase the errors in crown volumes. However, for crown volume calculations, errors are mainly contributed by complex crown structure, thinner and curvilinear branches, and sparse data for branches owing to occlusions.
- An approximate method of biomass estimation from Airborne LiDAR Data has been given especially for the Acadian Forests that considers individual species canopy structure, and their growth characteristics (allometrics). The method can be used where limited or no field samples are available. Furthermore, the method replicates shadow fraction method. Therefore, the method can be applied to boreal forests in United Kingdom and other parts of CANADA, where the climate is harsh and collecting field data is cumbersome.

- A carbon sequestration model is given for the Acadian Forests, where it considers varied biomass storage, soil organic storage. Moreover, the model accounts for abiotic factors that are essential for sustainable human survival. The presented soil organic carbon model can be further refined with real time field core soil samples. Moreover, utilization of soil water characteristic curve of a soil, which describes the relationship between soil suction and the water content or degree of saturation of an unsaturated soil. This helps to determine how much water a soil can hold at different suction levels, which is vital for predicting soil strength, permeability, and volume change. The output can be used for improving inputs to simulation, such as water saturation, soil depth etc. These results are inputs for root growth dynamics of a tree and thus enhance the belowground biomass predictions.
- Aboveground biomass dynamics of the Acadian Forests revealed a decrease of forest carbon storage approximately 60,000 $kg.C$ at year 2048 compared to that of year 2021. This amount of carbon corresponds to approximately one lakh m^2 area assuming a tree occupies 30m crown width upon its maturity and a maximum carbon storage of 500 $Kg.C$. Biotic and abiotic factors collectively resulting to carbon sequestered in the Acadian Forests suggest that the current state of the Acadian Forests can remain stable up to year 2029. Afterwards, negative and positive trend of rate of carbon sequestration would commence, mainly contributed by biomass, greenhouse gas emissions and wood harvesting up to year 2076.
- Results indicate that while Black Spruce and Balsam Fir are less adaptive to environmental changes as they are more sensitive to temperature and precipitation. Therefore, introducing temperate species (e.g., Maple and Birch), which are more stable under on-going environmental changes, may enhance biomass production to stabilize the Acadian ecosystem for longer period. These results can be used for sustainable development goals especially for forest inventory, management and for organisations like IPCC and REDD to make policies where human and forest both survive. And also it will help for country growth in terms of Greenhouses regulation by reducing carbon tax so that economy of a country can growth, which will help for growth of humanity

In future, the presented method of biomass estimation in this thesis can be improved for varied tree species and stand structures. Further, attempting tree species classification with synergy of airborne LiDAR data and hyperspectral remote sensing will enhance the accuracy of satellite-based and airborne LiDAR data based biomass methods. A detailed study on forest carbon which includes the ground lithology, geomorphology and ground water table will involve more variables of forest ecosystem and can be used for long-term study for new tree plantations for assessing ecological balance of a forest. Following are the two specific directions for future development:

- Expansion of carbon sequestration to various forests with use of economic resources like satellite remote sensing data and nuanced generative AI methods.
- Development of sustainable management plans for forestry in collaboration with humanity and governments.

References

Abas, N., Khan, N., 2014. Carbon conundrum, climate change, CO_2 capture and consumptions. J. CO_2 Util. 8, 39–48. https://doi.org/10.1016/J.JCOU.2014.06.005

Ai, M., Yao, Y., Hu, Q., Wang, Y., Wang, W., 2020. An automatic tree skeleton extraction approach based on multi-view slicing using terrestrial lidar scans data. Remote Sens. 12, 1–19. https://doi.org/10.3390/rs12223824

Albert, C., Taylor, A.R., Logan, T., D'Orangeville, L., 2023. The Acadian Forest of New Brunswick in the 21st century: what shifting heat and water balance imply for future stand dynamics and management. Environ. Rev. 31, 690–707. https://doi.org/10.1139/er-2022-0122

Alexander, C., 2009. Delineating tree crowns from airborne laser scanning point cloud data using Delaunay triangulation. Int. J. Remote Sens. 30, 3843–3848.

Amuyou, U.A., Wang, Y., Ebuta, B.F., Iheaturu, C.J., Antonarakis, A.S., 2022. Quantification of Above-Ground Biomass over the Cross-River State, Nigeria, Using Sentinel-2 Data. Remote Sens. 14. https://doi.org/10.3390/rs14225741

Askar, Nuthammachot, N., Phairuang, W., Wicaksono, P., Sayektiningsih, T., 2018. Estimating Aboveground Biomass on Private Forest Using Sentinel-2 Imagery. J. Sensors 2018, 6745629. https://doi.org/10.1155/2018/6745629

Asner, G.P., Mascaro, J., 2014. Mapping tropical forest carbon: Calibrating plot estimates to a simple LiDAR metric. Remote Sens. Environ. 140, 614–624. https://doi.org/10.1016/j.rse.2013.09.023

Asner, G.P., Mascaro, J., Muller-Landau, H.C., Vieilledent, G., Vaudry, R., Rasamoelina, M., Hall, J.S., van Breugel, M., 2012. A universal airborne LiDAR approach for tropical forest carbon mapping. Oecologia 168, 1147–1160. https://doi.org/10.1007/s00442-011-2165-z

Bailey, B.N., Ochoa, M.H., 2018. Semi-direct tree reconstruction using terrestrial LiDAR point cloud data. Remote Sens. Environ. 208, 133–144. https://doi.org/10.1016/J.RSE.2018.02.013

Bashir, A., MacLean, D.A., Hennigar, C.R., 2019. Growth-mortality attributes and species composition determine carbon sequestration and dynamics of old stand types in the Acadian Forest of New Brunswick, Canada. Ann. For. Sci. 76. https://doi.org/10.1007/s13595-019-0821-3

Beer, C., Reichstein, M., Tomelleri, E., Ciais, P., Jung, M., Carvalhais, N., Rödenbeck, C., Arain, M.A., Baldocchi, D., Bonan, G.B., Bondeau, A., Cescatti, A., Lasslop, G., Lindroth, A., Lomas, M., Luyssaert, S., Margolis, H., Oleson, K.W., Roupsard, O., Veenendaal, E., Viovy, N., Williams, C., Woodward, F.I., Papale, D., 2010. Terrestrial gross carbon dioxide uptake: Global distribution and covariation with climate. Science (80-.). 329, 834–838. https://doi.org/10.1126/SCIENCE.1184984/SUPPL_FILE/BEER_SOM.PDF

Bennemann, C., Labelle, E.R., Lussier, J.M., 2023. Influence of Tree, Stand, and Site Attributes on Hardwood Product Yield: Insights into the Acadian Forests. Forests 14. https://doi.org/10.3390/f14020182

Bill, K.E., Dieleman, C.M., Baltzer, J.L., Degré-Timmons, G., Mack, M.C., Day, N.J., Cumming, S.G., Walker, X.J., Turetsky, M.R., 2023. Post-fire Recovery of Soil Organic Layer Carbon in Canadian Boreal Forests. Ecosystems 26, 1623–1639. https://doi.org/10.1007/s10021-023-00854-0

Blanco, J.A., Lo, Y.H., 2023. Latest Trends in Modelling Forest Ecosystems: New Approaches or Just New Methods? Curr. For. Reports 9, 219–229. https://doi.org/10.1007/s40725-023-00189-y

Bonan, G.B., 2008. Forests and climate change: Forcings, feedbacks, and the climate benefits of forests. Science (80-.). 320, 1444–1449. https://doi.org/10.1126/SCIENCE.1155121/SUPPL_FILE/BONAN_SOM.PDF

Bouchard, M., Aquilué, N., Périé, C., Lambert, M.C., 2019. Tree species persistence under warming conditions: A key driver of forest response to climate change. For. Ecol. Manage. 442, 96–104. https://doi.org/10.1016/J.FORECO.2019.03.040

Boulanger, Y., Pascual, J., Bouchard, M., D'Orangeville, L., Périé, C., Girardin, M.P., 2022. Multi-model projections of tree species performance in Quebec, Canada under future climate change. Glob. Chang. Biol. 28, 1884–1902. https://doi.org/10.1111/gcb.16014

Bouman, O.T., Mazzocca, M.A., Bennett, E.E., Oakes, K.D., 2020. Water quality benefits of Acer rubrum and Betula alleghaniensis in the boreal-temperate ecotone on Eastern Cape Breton Island, Canada. For. Ecol. Manage. 460, 117869. https://doi.org/10.1016/j.foreco.2020.117869

Brecka, A.F.J., Boulanger, Y., Searle, E.B., Taylor, A.R., Price, D.T., Zhu, Y., Shahi, C., Chen, H.Y.H., 2020. Sustainability of Canada's forestry sector may be compromised by impending climate change. For. Ecol. Manage. 474, 118352. https://doi.org/10.1016/J.FORECO.2020.118352

Brede, B., Calders, K., Lau, A., Raumonen, P., Bartholomeus, H.M., Herold, M., Kooistra, L., 2019. Non-destructive tree volume estimation through quantitative structure modelling: Comparing UAV laser scanning with terrestrial LIDAR. Remote Sens. Environ. 233, 111355. https://doi.org/10.1016/J.RSE.2019.111355

Bremer, M., Rutzinger, M., Wichmann, V., 2013. Derivation of tree skeletons and error assessment using LiDAR point cloud data of varying quality. ISPRS J. Photogramm. Remote Sens. 80, 39–50. https://doi.org/10.1016/J.ISPRSJPRS.2013.03.003

Bruening, J., May, P., Armston, J., Dubayah, R., 2023. Precise and unbiased biomass estimation from GEDI data and the US Forest Inventory. Front. For. Glob. Chang. 6. https://doi.org/10.3389/ffgc.2023.1149153

Bucksch, A., Appel Van Wageningen, H., 2006. Skeletonization and segmentation of point clouds using octrees and graph theory. Int. Arch. Photogramm. Remote Sens. Spat. Inf. Sci. - ISPRS Arch. 36. https://doi.org/10.13140/RG.2.1.3705.9922

Bucksch, A., Lindenbergh, R., 2008. CAMPINO — A skeletonization method for point cloud processing. ISPRS J. Photogramm. Remote Sens. 63, 115–127. https://doi.org/10.1016/J.ISPRSJPRS.2007.10.004

Bucksch, A., Lindenbergh, R., Menenti, M., 2010. Robust skeleton extraction from imperfect point clouds. Vis. Comput. 26, 1283–1300. https://doi.org/10.1007/s00371-010-0520-4

Bucksch, A., Lindenbergh, R.C., Menenti, M., 2009. SkelTre - Fast skeletonisation for

imperfect point cloud data of botanic trees. Eurographics Work. 3D Object Retrieval, EG 3DOR 13–20. https://doi.org/10.2312/3DOR/3DOR09/013-020

Calders, K., Newnham, G., Burt, A., Murphy, S., Raumonen, P., Herold, M., Culvenor, D., Avitabile, V., Disney, M., Armston, J., Kaasalainen, M., 2015. Nondestructive estimates of above-ground biomass using terrestrial laser scanning. Methods Ecol. Evol. 6, 198–208. https://doi.org/10.1111/2041-210X.12301

Cao, L., Coops, N.C., Innes, J.L., Sheppard, S.R.J., Fu, L., Ruan, H., She, G., 2016. Estimation of forest biomass dynamics in subtropical forests using multi-temporal airborne LiDAR data. Remote Sens. Environ. 178, 158–171. https://doi.org/10.1016/j.rse.2016.03.012

Cao, L., Coops, N.C., Sun, Y., Ruan, H., Wang, G., Dai, J., She, G., 2019. Estimating canopy structure and biomass in bamboo forests using airborne LiDAR data. ISPRS J. Photogramm. Remote Sens. 148, 114–129. https://doi.org/10.1016/j.isprsjprs.2018.12.006

Cárdenas, J.L., López, A., Ogayar, C.J., Feito, F.R., Jurado, J.M., 2022. Reconstruction of tree branching structures from UAV-LiDAR data. Front. Environ. Sci. 10, 1–15. https://doi.org/10.3389/fenvs.2022.960083

Chave, J., Condit, R., Aguilar, S., Hernandez, A., Lao, S., Perez, R., Chust, G., Condit, R., Aguilar, S., Hernandez, A., Lao, S., Perez, R., 2007. Error propagation and scaling for tropical forest biomass estimates. Trop. For. Glob. Atmos. Chang. 359, 409–420. https://doi.org/10.1093/acprof:oso/9780198567066.003.0013

Chen, J.M., Pavlic, G., Brown, L., Cihlar, J., Leblanc, S.G., White, H.P., Hall, R.J., Peddle, D.R., King, D.J., Trofymow, J.A., Swift, E., Van Der Sanden, J., Pellikka, P.K.E., 2002. Derivation and validation of Canada-wide coarse-resolution leaf area index maps using high-resolution satellite imagery and ground measurements. Remote Sens. Environ. 80, 165–184. https://doi.org/10.1016/S0034-4257(01)00300-5

Cho, M.A., Skidmore, A., Corsi, F., van Wieren, S.E., Sobhan, I., 2007. Estimation of green grass/herb biomass from airborne hyperspectral imagery using spectral indices and partial least squares regression. Int. J. Appl. Earth Obs. Geoinf. 9, 414–424. https://doi.org/10.1016/j.jag.2007.02.001

Cho, M.A., Skidmore, A.K., 2009. Hyperspectral predictors for monitoring biomass production in Mediterranean mountain grasslands: Majella National Park, Italy. Int. J. Remote Sens. 30, 499–515. https://doi.org/10.1080/01431160802392596

Chu, X., Man, R., Dang, Q.L., 2023. Spring phenology, phenological response, and growing season length. Front. For. Glob. Chang. 6. https://doi.org/10.3389/ffgc.2023.1041369

Collins, J.N., Hutley, L.B., Williams, R.J., Boggs, G., Bell, D., Bartolo, R., 2009. Estimating landscape-scale vegetation carbon stocks using airborne multi-frequency polarimetric synthetic aperture radar (SAR) in the savannahs of north Australia. Int. J. Remote Sens. 30, 1141–1159. https://doi.org/10.1080/01431160802448935

Coomes, D.A., Dalponte, M., Jucker, T., Asner, G.P., Banin, L.F., Burslem, D.F.R.P., Lewis, S.L., Nilus, R., Phillips, O.L., Phua, M.H., Qie, L., 2017. Area-based vs tree-centric approaches to mapping forest carbon in Southeast Asian forests from airborne laser scanning data. Remote Sens. Environ. 194, 77–88. https://doi.org/10.1016/j.rse.2017.03.017

Côté, G., Bouchard, M., Pothier, D., Gauthier, S., 2010. Linking stand attributes to cartographic information for ecosystem management purposes in the boreal forest of eastern Québec. For. Chron. 86, 511–519. https://doi.org/10.5558/tfc86511-4

Cox, E., Beckley, T.M., de Graaf, M., 2023. Carbon sequestration and storage implications of three forest management regimes in the Wabanaki-Acadian Forest: A review of the evidence. https://doi.org/10.1139/er-2022-0097 32, 1–15. https://doi.org/10.1139/ER-2022-0097

Croci, M., Impollonia, G., Marcone, A., Antonucci, G., Letterio, T., Colauzzi, M., Vignudelli, M., Ventura, F., Anconelli, S., Amaducci, S., 2022. RTM Inversion through Predictive Equations for Multi-Crop LAI Retrieval Using Sentinel-2 Images. Agronomy 12. https://doi.org/10.3390/agronomy12112835

Culas, R.J., 2009. The Causes and Consequences of Tropical Deforestation: A Review 1.

Curran, J.C., Curran, S.A., 2025. Natural sequestration of carbon dioxide is in decline: climate change will accelerate. Weather 80, 85–87. https://doi.org/10.1002/WEA.7668

D'Orangeville, L., Maxwell, J., Kneeshaw, D., Pederson, N., Duchesne, L., Logan, T., Houle, D., Arseneault, D., Beier, C.M., Bishop, D.A., Druckenbrod, D., Fraver, S., Girard, F., Halman, J., Hansen, C., Hart, J.L., Hartmann, H., Kaye, M., Leblanc, D., Manzoni, S., Ouimet, R., Rayback, S., Rollinson, C.R., Phillips, R.P., 2018. Drought timing and local climate determine the sensitivity of eastern temperate forests to drought. Glob. Chang. Biol. 24, 2339–2351. https://doi.org/10.1111/gcb.14096

Dalponte, M., Jucker, T., Liu, S., Frizzera, L., Gianelle, D., 2019. Characterizing forest carbon dynamics using multi-temporal lidar data. Remote Sens. Environ. 224, 412–420. https://doi.org/10.1016/j.rse.2019.02.018

Dashti, H., Pandit, K., Glenn, N.F., Shinneman, D.J., Flerchinger, G.N., Hudak, A.T., de Graaf, M.A., Flores, A., Ustin, S., Ilangakoon, N., Fellows, A.W., 2021. Performance of the ecosystem demography model (EDv2.2) in simulating gross primary production capacity and activity in a dryland study area. Agric. For. Meteorol. 297, 108270. https://doi.org/10.1016/j.agrformet.2020.108270

Descals, A., Gaveau, D.L.A., Wich, S., Szantoi, Z., Meijaard, E., 2024. Global mapping of oil palm planting year from 1990 to 2021 11034131, 1–24. https://doi.org/10.5281/zenodo.11034131

Dimitrov, D.D., Bhatti, J.S., Grant, R.F., 2014. The transition zones (ecotone) between boreal forests and peatlands: Ecological controls on ecosystem productivity along a transition zone between upland black spruce forest and a poor forested fen in central Saskatchewan. Ecol. Modell. 291, 96–108. https://doi.org/10.1016/j.ecolmodel.2014.07.020

Dong, P., 2010. Sensitivity of LiDAR-derived three-dimensional shape signatures for individual tree crowns: a simulation study. Remote Sens. Lett. 1, 159–167. https://doi.org/10.1080/01431161003631550

Dong, P., 2009. Characterization of individual tree crowns using three-dimensional shape signatures derived from LiDAR data. Int. J. Remote Sens. 30, 6621–6628. https://doi.org/10.1080/01431160903140761

Du, H., Zhou, G., Ge, H., Fan, W.W., Xu, X., Fan, W.W., Shi, Y., 2012. Satellite-based carbon stock estimation for bamboo forest with a non-linear partial least square regression

technique. Int. J. Remote Sens. 33, 1917–1933. https://doi.org/10.1080/01431161.2011.603379

Dumais, D., Prévost, M., Thomas, S., 2014. Physiology and growth of advance Picea rubens and Abies balsamea regeneration following different canopy openings. Tree Physiol. 34, 194–204. https://doi.org/10.1093/TREEPHYS/TPT114

Duncanson, L., Armston, J., Disney, M., Avitabile, V., Barbier, N., Calders, K., Carter, S., Chave, J., Herold, M., MacBean, N., McRoberts, R., Minor, D., Paul, K., Réjou-Méchain, M., Roxburgh, S., Williams, M., Albinet, C., Baker, T., Bartholomeus, H., Bastin, J.F., Coomes, D., Crowther, T., Davies, S., de Bruin, S., De Kauwe, M., Domke, G., Dubayah, R., Falkowski, M., Fatoyinbo, L., Goetz, S., Jantz, P., Jonckheere, I., Jucker, T., Kay, H., Kellner, J., Labriere, N., Lucas, R., Mitchard, E., Morsdorf, F., Naesset, E., Park, T., Phillips, O.L., Ploton, P., Quegan, S., Saatchi, S., Schaaf, C., Schepaschenko, D., Scipal, K., Stovall, A., Thiel, C., Wulder, M.A., Camacho, F., Nickeson, J., Román, M., Margolis, H., 2021. Aboveground Woody Biomass Product Validation Good Practices Protocol. Version 1.0. Good Pract. Satell. Deriv. L. Prod. Valid.

Duncanson, L.I., Niemann, K.O., Wulder, M.A., 2010. Integration of GLAS and Landsat TM data for aboveground biomass estimation. Can. J. Remote Sens. 36, 129–141. https://doi.org/10.5589/m10-037

Eckert, S., 2012. Improved forest biomass and carbon estimations using texture measures from worldView-2 satellite data. Remote Sens. 4, 810–829. https://doi.org/10.3390/rs4040810

Eto, S., Masuda, H., Hiraoka, Y., Matsushita, M., Takahashi, M., 2020. Precise calculation of cross sections and volume for tree stem using point clouds. Int. Arch. Photogramm. Remote Sens. Spat. Inf. Sci. XLIII-B2-2020, 205–210. https://doi.org/10.5194/ISPRS-ARCHIVES-XLIII-B2-2020-205-2020

Filonchyk, M., Peterson, M.P., Zhang, L., Hurynovich, V., He, Y., 2024. Greenhouse gases emissions and global climate change: Examining the influence of CO2, CH4, and N2O. Sci. Total Environ. 935. https://doi.org/10.1016/j.scitotenv.2024.173359

Fischler, M.A., Bolles, R.C., 1981. Random sample consensus. Commun. ACM 24, 381–395. https://doi.org/10.1145/358669.358692

Foody, G.M., Boyd, D.S., Cutler, M.E.J., 2003. Predictive relations of tropical forest biomass from Landsat TM data and their transferability between regions. Remote Sens. Environ. 85, 463–474. https://doi.org/10.1016/S0034-4257(03)00039-7

Forest Monitoring, Land Use & Deforestation Trends | Global Forest Watch [WWW Document], n.d. URL https://www.globalforestwatch.org/ (accessed 7.24.24).

Francini, S., D'Amico, G., Vangi, E., Borghi, C., Chirici, G., 2022. Integrating GEDI and Landsat: Spaceborne Lidar and Four Decades of Optical Imagery for the Analysis of Forest Disturbances and Biomass Changes in Italy. Sensors 22. https://doi.org/10.3390/s22052015

Frazier, R.J., Coops, N.C., Wulder, M.A., 2015. Boreal Shield forest disturbance and recovery trends using Landsat time series. Remote Sens. Environ. 170, 317–327. https://doi.org/10.1016/j.rse.2015.09.015

Fu, L., Liu, J., Zhou, J., Zhang, M., Lin, Y., 2020. Tree Skeletonization for Raw Point Cloud Exploiting Cylindrical Shape Prior. IEEE Access 8, 27327–27341.

https://doi.org/10.1109/ACCESS.2020.2971549

Gao, T., Xu, B., Yang, X., Jin, Y., Ma, H., Li, J., Yu, H., 2013. Using MODIS time series data to estimate aboveground biomass and its spatio-temporal variation in Inner Mongolia's grassland between 2001 and 2011. Int. J. Remote Sens. 34, 7796–7810. https://doi.org/10.1080/01431161.2013.823000

García, M., Riaño, D., Chuvieco, E., Danson, F.M., 2010. Estimating biomass carbon stocks for a Mediterranean forest in central Spain using LiDAR height and intensity data. Remote Sens. Environ. 114, 816–830. https://doi.org/10.1016/j.rse.2009.11.021

Gelybó, G., Barcza, Z., Kern, A., Kljun, N., 2013. Effect of spatial heterogeneity on the validation of remote sensing based GPP estimations. Agric. For. Meteorol. 174–175, 43–53. https://doi.org/10.1016/J.AGRFORMET.2013.02.003

Ghosh, S.M., Behera, M.D., 2018. Aboveground biomass estimation using multi-sensor data synergy and machine learning algorithms in a dense tropical forest. Appl. Geogr. 96, 29–40. https://doi.org/10.1016/j.apgeog.2018.05.011

Goldbergs, G., Levick, S.R., Lawes, M., Edwards, A., 2018. Hierarchical integration of individual tree and area-based approaches for savanna biomass uncertainty estimation from airborne LiDAR. Remote Sens. Environ. 205, 141–150. https://doi.org/10.1016/j.rse.2017.11.010

Gong, B., Im, J., Jensen, J., Coleman, M., Rhee, J., Nelson, E., 2012. Characterization of forest crops with a range of nutrient and water treatments using AISA hyperspectral imagery. GIScience Remote Sens. 49, 463–491. https://doi.org/10.2747/1548-1603.49.4.463

Gonzalez de Tanago, J., Lau, A., Bartholomeus, H., Herold, M., Avitabile, V., Raumonen, P., Martius, C., Goodman, R.C., Disney, M., Manuri, S., Burt, A., Calders, K., 2018. Estimation of above-ground biomass of large tropical trees with terrestrial LiDAR. Methods Ecol. Evol. 9, 223–234. https://doi.org/10.1111/2041-210X.12904

Graves, S.J., Caughlin, T.T., Asner, G.P., Bohlman, S.A., 2018. A tree-based approach to biomass estimation from remote sensing data in a tropical agricultural landscape. Remote Sens. Environ. 218, 32–43. https://doi.org/10.1016/j.rse.2018.09.009

Greenberg, J.A., Dobrowski, S.Z., Ustin, S.L., 2005. Shadow allometry: Estimating tree structural parameters using hyperspatial image analysis. Remote Sens. Environ. 97, 15–25. https://doi.org/10.1016/j.rse.2005.02.015

Guo, B., Menon, J., Willette, B., 1997. Surface Reconstruction Using Alpha Shapes. Comput. Graph. Forum 16, 177–190. https://doi.org/10.1111/1467-8659.00178

Hackenberg, J., Morhart, C., Sheppard, J., Spiecker, H., Disney, M., 2014. Highly Accurate Tree Models Derived from Terrestrial Laser Scan Data: A Method Description. For. 2014, Vol. 5, Pages 1069-1105 5, 1069–1105. https://doi.org/10.3390/F5051069

Hadas, E., Borkowski, A., Estornell, J., Tymkow, P., 2017. Automatic estimation of olive tree dendrometric parameters based on airborne laser scanning data using alpha-shape and principal component analysis. GIScience Remote Sens. 54, 898–917. https://doi.org/10.1080/15481603.2017.1351148

Haseeb, M., Tahir, Z., Mehmood, S.A., Gill, S.A., Farooq, N., Butt, H., Iftikhar, A., Maqsood, A., Abdullah-Al-Wadud, M., Tariq, A., 2024. Enhancing Carbon Sequestration through Afforestation: Evaluating the Impact of Land Use and Cover Changes on Carbon Storage

Dynamics. Earth Syst. Environ. 1563–1582. https://doi.org/10.1007/s41748-024-00414-z

Holmgren, J., Persson, Å., Söderman, U., Persson{, A.˚, So¨derman, U., So¨derman, S., 2008. Species identification of individual trees by combining high resolution LiDAR data with multi-spectral images. Int. J. Remote Sens. 29, 1537–1552. https://doi.org/10.1080/01431160701736471

Hu, Y., Xu, X., Wu, F., Sun, Z., Xia, H., Meng, Q., Huang, W., Zhou, H., Gao, J., Li, W., Peng, D., Xiao, X., 2020. Estimating forest stock volume in Hunan Province, China, by integrating in situ plot data, Sentinel-2 images, and linear and machine learning regression models. Remote Sens. 12. https://doi.org/10.3390/RS12010186

Hufkens, K., Scheunders, P., Ceulemans, R., 2009. Ecotones in vegetation ecology: Methodologies and definitions revisited. Ecol. Res. 24, 977–986. https://doi.org/10.1007/s11284-009-0584-7

Hui, Z., Cheng, P., Yang, B., Zhou, G., 2022. Multi-level self-adaptive individual tree detection for coniferous forest using airborne LiDAR. Int. J. Appl. Earth Obs. Geoinf. 114, 103028. https://doi.org/10.1016/J.JAG.2022.103028

Hurtt, G.C., Dubayah, R., Drake, J., Moorcroft, P.R., Stephen, W., Blair, J.B., Fearon, M.G., 2004. Beyond Potential Vegetation : Combining Lidar Data and a Height-Structured Model for Carbon Studies Published by : Wiley on behalf of the Ecological Society of America Stable URL : https://www.jstor.org/stable/4493586 REFERENCES Linked references are avai. Ecol. Appl. 14, 873–883.

Ismaili Alaoui, H., Chemchaoui, A., El Asri, B., Ghazi, S., Brhadda, N., Ziri, R., 2023. Modeling predictive changes of carbon storage using invest model in the Beht watershed (Morocco). Model. Earth Syst. Environ. 9, 4313–4322. https://doi.org/10.1007/S40808-023-01697-3/TABLES/3

Jayakrishnan, K.U., Bala, G., Cao, L., Caldeira, K., 2022. Contrasting climate and carbon-cycle consequences of fossil-fuel use versus deforestation disturbance. Environ. Res. Lett. 17, 064020. https://doi.org/10.1088/1748-9326/AC69FD

Jucker, T., Asner, G.P., Dalponte, M., Brodrick, P.G., Philipson, C.D., Vaughn, N.R., Arn Teh, Y., Brelsford, C., Burslem, D.F.R.P., Deere, N.J., Ewers, R.M., Kvasnica, J., Lewis, S.L., Malhi, Y., Milne, S., Nilus, R., Pfeifer, M., Phillips, O.L., Qie, L., Renneboog, N., Reynolds, G., Riutta, T., Struebig, M.J., Svátek, M., Turner, E.C., Coomes, D.A., 2018. Estimating aboveground carbon density and its uncertainty in Borneo's structurally complex tropical forests using airborne laser scanning. Biogeosciences 15, 3811–3830. https://doi.org/10.5194/bg-15-3811-2018

Jucker, T., Fischer, F.J., Chave, J., Coomes, D.A., Caspersen, J., Ali, A., Loubota Panzou, G.J., Feldpausch, T.R., Falster, D., Usoltsev, V.A., Adu-Bredu, S., Alves, L.F., Aminpour, M., Angoboy, I.B., Anten, N.P.R., Antin, C., Askari, Y., Muñoz, R., Ayyappan, N., Balvanera, P., Banin, L., Barbier, N., Battles, J.J., Beeckman, H., Bocko, Y.E., Bond-Lamberty, B., Bongers, F., Bowers, S., Brade, T., van Breugel, M., Chantrain, A., Chaudhary, R., Dai, J., Dalponte, M., Dimobe, K., Domec, J.C., Doucet, J.L., Duursma, R.A., Enríquez, M., van Ewijk, K.Y., Farfán-Rios, W., Fayolle, A., Forni, E., Forrester, D.I., Gilani, H., Godlee, J.L., Gourlet-Fleury, S., Haeni, M., Hall, J.S., He, J.K., Hemp, A., Hernández-Stefanoni, J.L., Higgins, S.I., Holdaway, R.J., Hussain, K., Hutley, L.B., Ichie, T., Iida, Y., Jiang, H. sheng, Joshi, P.R., Kaboli, H., Larsary, M.K., Kenzo, T., Kloeppel, B.D., Kohyama, T., Kunwar, S., Kuyah, S., Kvasnica, J., Lin, S., Lines, E.R., Liu, H., Lorimer,

C., Loumeto, J.J., Malhi, Y., Marshall, P.L., Mattsson, E., Matula, R., Meave, J.A., Mensah, S., Mi, X., Momo, S., Moncrieff, G.R., Mora, F., Nissanka, S.P., O'Hara, K.L., Pearce, S., Pelissier, R., Peri, P.L., Ploton, P., Poorter, L., Pour, M.J., Pourbabaei, H., Dupuy-Rada, J.M., Ribeiro, S.C., Ryan, C., Sanaei, A., Sanger, J., Schlund, M., Sellan, G., Shenkin, A., Sonké, B., Sterck, F.J., Svátek, M., Takagi, K., Trugman, A.T., Ullah, F., Vadeboncoeur, M.A., Valipour, A., Vanderwel, M.C., Vovides, A.G., Wang, W., Wang, L.Q., Wirth, C., Woods, M., Xiang, W., Ximenes, F. de A., Xu, Y., Yamada, T., Zavala, M.A., 2022. Tallo: A global tree allometry and crown architecture database. Glob. Chang. Biol. 28, 5254–5268. https://doi.org/10.1111/GCB.16302

Kanmegne Tamga, D., Latifi, H., Ullmann, T., Baumhauer, R., Bayala, J., Thiel, M., 2023. Estimation of Aboveground Biomass in Agroforestry Systems over Three Climatic Regions in West Africa Using Sentinel-1, Sentinel-2, ALOS, and GEDI Data. Sensors 23. https://doi.org/10.3390/s23010349

Kark, S., 2012. Encyclopedia of Sustainability Science and Technology. Encycl. Sustain. Sci. Technol. 147–160. https://doi.org/10.1007/978-1-4419-0851-3

Keenan, R.J., Reams, G.A., Achard, F., de Freitas, J. V., Grainger, A., Lindquist, E., 2015. Dynamics of global forest area: Results from the FAO Global Forest Resources Assessment 2015. For. Ecol. Manage. 352, 9–20. https://doi.org/10.1016/J.FORECO.2015.06.014

Kindermann, G., Obersteiner, M., Sohngen, B., Sathaye, J., Andrasko, K., Rametsteiner, E., Schlamadinger, B., Wunder, S., Beach, R., 2008. Global cost estimates of reducing carbon emissions through avoided deforestation. Proc. Natl. Acad. Sci. 105, 10302–10307.

Kwak, D.A., Lee, W.K., Cho, H.K., Lee, S.H., Son, Y., Kafatos, M., Kim, S.R., 2010. Estimating stem volume and biomass of Pinus koraiensis using LiDAR data. J. Plant Res. 123, 421–432. https://doi.org/10.1007/s10265-010-0310-0

Leboeuf, A., Beaudoin, A., Fournier, R.A., Guindon, L., Luther, J.E., Lambert, M.C., 2007. A shadow fraction method for mapping biomass of northern boreal black spruce forests using QuickBird imagery. Remote Sens. Environ. 110, 488–500. https://doi.org/10.1016/j.rse.2006.05.025

Lee, S.J., Kim, J.R., Choi, Y.S., 2013. The extraction of forest CO2 storage capacity using high-resolution airborne lidar data. GIScience Remote Sens. 50, 154–171. https://doi.org/10.1080/15481603.2013.786957

Lefsky, M.A., Harding, D., Cohen, W.B., Parker, G., Shugart, H.H., 1999. Surface lidar remote sensing of basal area and biomass in deciduous forests of eastern Maryland, USA. Remote Sens. Environ. 67, 83–98.

Li, F., Zeng, Y., Luo, J., Ma, R., Wu, B., 2016. Modeling grassland aboveground biomass using a pure vegetation index. Ecol. Indic. 62, 279–288. https://doi.org/10.1016/j.ecolind.2015.11.005

Li, Q., Wong, F.K.K., Fung, T., 2021. Mapping multi-layered mangroves from multispectral, hyperspectral, and LiDAR data. Remote Sens. Environ. 258, 112403. https://doi.org/10.1016/j.rse.2021.112403

Li, Y., Brando, P.M., Morton, D.C., Lawrence, D.M., Yang, H., Randerson, J.T., 2022. Deforestation-induced climate change reduces carbon storage in remaining tropical forests. Nat. Commun. 2022 131 13, 1–13. https://doi.org/10.1038/s41467-022-29601-0

Lillesand, T., Kiefer, R.W., Chipman, J., 2015. Remote sensing and image interpretation. John Wiley \& Sons.

Lindberg, E., Eysn, L., Hollaus, M., Holmgren, J., Pfeifer, N., 2014. Delineation of tree crowns and tree species classification from full-waveform airborne laser scanning data using 3-d ellipsoidal clustering. IEEE J. Sel. Top. Appl. Earth Obs. Remote Sens. 7, 3174–3181. https://doi.org/10.1109/JSTARS.2014.2331276

Lindenbergh, R., Anders, K., Campos, M., Czerwonka-Schröder, D., Höfle, B., Kuschnerus, M., Puttonen, E., Prinz, R., Rutzinger, M., Voordendag, A., Vos, S., 2025. Permanent terrestrial laser scanning for near-continuous environmental observations: Systems, methods, challenges and applications. ISPRS Open J. Photogramm. Remote Sens. 17, 100094. https://doi.org/10.1016/j.ophoto.2025.100094

Liu, H., Wu, C., 2019. Developing a Scene-Based Triangulated Irregular Network (TIN) Technique for Individual Tree Crown Reconstruction with LiDAR Data. For. 2020, Vol. 11, Page 28 11, 28. https://doi.org/10.3390/F11010028

Liu, J., Miller, J.R., Pattey, E., Haboudane, D., Strachan, I.B., Hinther, M., 2004. Monitoring crop biomass accumulation using multi-temporal hyperspectral remote sensing data. Int. Geosci. Remote Sens. Symp. 3, 1637–1640. https://doi.org/10.1109/IGARSS.2004.1370643

Longo, M., Knox, R.G., Medvigy, D.M., Levine, N.M., Dietze, M.C., Kim, Y., Swann, A.L.S., Zhang, K., Rollinson, C.R., Bras, R.L., Wofsy, S.C., Moorcroft, P.R., 2019. The biophysics, ecology, and biogeochemistry of functionally diverse, vertically and horizontally heterogeneous ecosystems: The Ecosystem Demography model, version 2.2-Part 1: Model description. Geosci. Model Dev. 12, 4309–4346. https://doi.org/10.5194/gmd-12-4309-2019

Luo, S., Wang, C., Xi, X., Pan, F., Peng, D., Zou, J., Nie, S., Qin, H., 2017. Fusion of airborne LiDAR data and hyperspectral imagery for aboveground and belowground forest biomass estimation. Ecol. Indic. 73, 378–387. https://doi.org/10.1016/j.ecolind.2016.10.001

Ma, L., Hurtt, G., Ott, L., Sahajpal, R., Fisk, J., Lamb, R., Tang, H., Flanagan, S., Chini, L., Chatterjee, A., Sullivan, J., 2022. Global evaluation of the Ecosystem Demography model (ED v3.0). Geosci. Model Dev. 15, 1971–1994. https://doi.org/10.5194/gmd-15-1971-2022

Ma, T., Hu, Y., Wang, J., Beckline, M., Pang, D., Chen, L., Ni, X., Li, X., 2023. A Novel Vegetation Index Approach Using Sentinel-2 Data and Random Forest Algorithm for Estimating Forest Stock Volume in the Helan Mountains, Ningxia, China. Remote Sens. 15. https://doi.org/10.3390/rs15071853

Mahendrappa, M.K., Foster, N.W., Weetman, G.F., Krause, H.H., 1986. Nutrient cycling and availability in forest soils. Can. J. Soil Sci. 66, 547–572. https://doi.org/10.4141/cjss86-056

Malhi, Y., Meir, P., Brown, S., 2002. Forests, carbon and global climate. Philos. Trans. R. Soc. A Math. Phys. Eng. Sci. 360, 1567–1591. https://doi.org/10.1098/RSTA.2002.1020;PAGEGROUP:STRING:PUBLICATION

Mansuy, N., Thiffault, E., Paré, D., Bernier, P., Guindon, L., Villemaire, P., Poirier, V., Beaudoin, A., 2014. Digital mapping of soil properties in Canadian managed forests at 250m of resolution using the k-nearest neighbor method. Geoderma 235–236, 59–73.

https://doi.org/10.1016/j.geoderma.2014.06.032

Marchand, W., Girardin, M.P., Gauthier, S., Hartmann, H., Bouriaud, O., Babst, F., Bergeron, Y., 2018. Untangling methodological and scale considerations in growth and productivity trend estimates of Canada's forests. Environ. Res. Lett. 13, 093001. https://doi.org/10.1088/1748-9326/AAD82A

Matthew E. Akalusi, 2021. MORPHOLOGICAL AND PHYSIOLOGICAL RESPONSES OF BALSAM FIR PROVENANCES IN EASTERN CANADA TO CLIMATIC VARIATION.

Medvigy, D., Wofsy, S.C., Munger, J.W., Hollinger, D.Y., Moorcroft, P.R., 2009. Mechanistic scaling of ecosystem function and dynamics in space and time: Ecosystem Demography model version 2. J. Geophys. Res. Biogeosciences 114. https://doi.org/10.1029/2008JG000812

Menéndez-Miguélez, M., Madrigal, G., Sixto, H., Oliveira, N., Calama, R., 2023. Terrestrial Laser Scanning for Non-Destructive Estimation of Aboveground Biomass in Short-Rotation Poplar Coppices. Remote Sens. 15. https://doi.org/10.3390/rs15071942

Meng, Q., Cieszewski, C.J., Madden, M., Borders, B., 2007. A linear mixed-effects model of biomass and volume of trees using Landsat ETM+ images. For. Ecol. Manage. 244, 93–101. https://doi.org/10.1016/j.foreco.2007.03.056

Meunier, F., Krishna Moorthy, S.M., Peaucelle, M., Calders, K., Terryn, L., Verbruggen, W., Liu, C., Saarinen, N., Origo, N., Nightingale, J., Disney, M., Malhi, Y., Verbeeck, H., 2022. Using terrestrial laser scanning to constrain forest ecosystem structure and functions in the Ecosystem Demography model (ED2.2). Geosci. Model Dev. 15, 4783–4803. https://doi.org/10.5194/gmd-15-4783-2022

Milburn, P., Rees, H., Fahmy, S., Gartley, C., 1989. Soil depth groups for agricultural land development planning in New Brunswick. Can. Agric. Eng. 31, 1–5.

Mohite, J., Sawant, S., Pandit, A., Sakkan, M., Pappula, S., Parmar, A., 2024. Forest aboveground biomass estimation by GEDI and multi-source EO data fusion over Indian forest. Int. J. Remote Sens. 45, 1304–1338. https://doi.org/10.1080/01431161.2024.2307944

Moorcroft, P.R., Hurtt, G.C., Pacala, S.W., 2001. A method for scaling vegetation dynamics: The ecosystem demography model (ED). Ecol. Monogr. 71, 557–586. https://doi.org/10.1890/0012-9615(2001)071[0557:AMFSVD]2.0.CO;2

Morin, D., Planells, M., Baghdadi, N., Bouvet, A., Fayad, I., Le Toan, T., Mermoz, S., Villard, L., 2022. Improving Heterogeneous Forest Height Maps by Integrating GEDI-Based Forest Height Information in a Multi-Sensor Mapping Process. Remote Sens. 14. https://doi.org/10.3390/rs14092079

Musthafa, M., Singh, G., 2022. Forest above-ground woody biomass estimation using multi-temporal space-borne LiDAR data in a managed forest at Haldwani, India. Adv. Sp. Res. 69, 3245–3257. https://doi.org/10.1016/j.asr.2022.02.002

Mutanga, O., Masenyama, A., Sibanda, M., 2023. Spectral saturation in the remote sensing of high-density vegetation traits: A systematic review of progress, challenges, and prospects. ISPRS J. Photogramm. Remote Sens. 198, 297–309. https://doi.org/10.1016/j.isprsjprs.2023.03.010

Muukkonen, P., Heiskanen, J., 2007. Biomass estimation over a large area based on standwise forest inventory data and ASTER and MODIS satellite data: A possibility to verify carbon inventories. Remote Sens. Environ. 107, 617–624. https://doi.org/10.1016/j.rse.2006.10.011

Muukkonen, P., Heiskanen, J., 2005. Estimating biomass for boreal forests using ASTER satellite data combined with standwise forest inventory data. Remote Sens. Environ. 99, 434–447. https://doi.org/10.1016/j.rse.2005.09.011

Næsset, E., Bollandsås, O.M., Gobakken, T., Gregoire, T.G., Ståhl, G., 2013. Model-assisted estimation of change in forest biomass over an 11year period in a sample survey supported by airborne LiDAR: A case study with post-stratification to provide "activity data." Remote Sens. Environ. 128, 299–314. https://doi.org/10.1016/j.rse.2012.10.008

NOAA, National Ocean and Atmospheric Administration, USA

Natural Resources and Energy Development - New Brunswick [WWW Document], n.d. URL https://www2.gnb.ca/content/gnb/en/departments/erd.html (accessed 6.15.24).

Neilson, E.T., Maclean, D.A., Meng, F.-R.R., Arp, P.A., 2007. Spatial distribution of carbon in natural and managed stands in an industrial forest in New Brunswick, Canada. For. Ecol. Manage. 253, 148–160.

Nguyen, T.D., Kappas, M., 2020. Estimating the aboveground biomass of an evergreen broadleaf forest in Xuan Lien Nature Reserve, Thanh Hoa, Vietnam, using SPOT-6 data and the random forest algorithm. Int. J. For. Res. 2020. https://doi.org/10.1155/2020/4216160

Ni, W., Zhang, Z., Sun, G., 2021. Assessment of Slope-Adaptive Metrics of GEDI Waveforms for Estimations of Forest Aboveground Biomass over Mountainous Areas. J. Remote Sens. (United States) 2021. https://doi.org/10.34133/2021/9805364

Nilsson, M., 1996. Estimation of tree heights and stand volume using an airborne lidar system. Remote Sens. Environ. 56, 1–7. https://doi.org/10.1016/0034-4257(95)00224-3

Nurunnabi, A., Sadahiro, Y., Lindenbergh, R., 2017. Robust cylinder fitting in three-dimensional point cloud data. Int. Arch. Photogramm. Remote Sens. Spat. Inf. Sci. 42, 63–70. https://doi.org/10.5194/ISPRS-ARCHIVES-XLII-1-W1-63-2017

Nuthammachot, N., Askar, A., Stratoulias, D., Wicaksono, P., 2022. Combined use of Sentinel-1 and Sentinel-2 data for improving above-ground biomass estimation. Geocarto Int. 37, 366–376. https://doi.org/10.1080/10106049.2020.1726507

Oddou-Muratorio, S., Davi, H., Lefèvre, F., 2020. Integrating evolutionary, demographic and ecophysiological processes to predict the adaptive dynamics of forest tree populations under global change. Tree Genet. Genomes 16. https://doi.org/10.1007/s11295-020-01451-1

Oliphant, A.J., Dragoni, D., Deng, B., Grimmond, C.S.B., Schmid, H.P., Scott, S.L., 2011. The role of sky conditions on gross primary production in a mixed deciduous forest. Agric. For. Meteorol. 151, 781–791. https://doi.org/10.1016/J.AGRFORMET.2011.01.005

Pan, Y., Birdsey, R.A., Fang, J., Houghton, R., Kauppi, P.E., Kurz, W.A., Phillips, O.L., Shvidenko, A., Lewis, S.L., Canadell, J.G., Ciais, P., Jackson, R.B., Pacala, S.W., McGuire, A.D., Piao, S., Rautiainen, A., Sitch, S., Hayes, D., 2011. A large and persistent carbon sink in the world's forests. Science (80-.). 333, 988–993.

https://doi.org/10.1126/SCIENCE.1201609

Pandey, P.C., Anand, A., Srivastava, P.K., 2019. Spatial distribution of mangrove forest species and biomass assessment using field inventory and earth observation hyperspectral data. Biodivers. Conserv. 28, 2143–2162. https://doi.org/10.1007/s10531-019-01698-8

Pandit, K., Dashti, H., Hudak, A.T., Glenn, N.F., Flores, A.N., Shinneman, D.J., 2021. Understanding the effect of fire on vegetation composition and gross primary production in a semi-arid shrubland ecosystem using the Ecosystem Demography (EDv2.2) model. Biogeosciences 18, 2027–2045. https://doi.org/10.5194/bg-18-2027-2021

Patenaude, G., Hill, R.A., Milne, R., Gaveau, D.L.A., Briggs, B.B.J., Dawson, T.P., 2004. Quantifying forest above ground carbon content using LiDAR remote sensing. Remote Sens. Environ. 93, 368–380. https://doi.org/10.1016/j.rse.2004.07.016

Pearson, E., D'Orangeville, L., 2022. Relating the Growth Phenology and Biomass Allocation in Seedlings of 13 Acadian Tree Species With Their Drought Tolerance. Front. For. Glob. Chang. 5. https://doi.org/10.3389/ffgc.2022.784382

Pereira Coltri, P., Zullo, J., Ribeiro Do Valle Goncalves, R., Romani, L.A.S., Pinto, H.S., 2013. Coffee crop's biomass and carbon stock estimation with usage of high resolution satellites images. IEEE J. Sel. Top. Appl. Earth Obs. Remote Sens. 6, 1786–1795. https://doi.org/10.1109/JSTARS.2013.2262767

Pham, T.D., Ha, N.T., Saintilan, N., Skidmore, A., Phan, D.C., Le, N.N., Viet, H.L., Takeuchi, W., Friess, D.A., 2023. Advances in Earth observation and machine learning for quantifying blue carbon. Earth-Science Rev. 243, 104501. https://doi.org/10.1016/j.earscirev.2023.104501

Pingoud, K., Skog, K.E., Martino, D.L., Tonosaki, M., Xiaoquan, Z., 2006. Agriculture, Forestry and Other Land Use 12 4.

Potapov, P., Li, X., Hernandez-Serna, A., Tyukavina, A., Hansen, M.C., Kommareddy, A., Pickens, A., Turubanova, S., Tang, H., Silva, C.E., Armston, J., Dubayah, R., Blair, J.B., Hofton, M., 2021. Mapping global forest canopy height through integration of GEDI and Landsat data. Remote Sens. Environ. 253, 112165. https://doi.org/10.1016/j.rse.2020.112165

Powell, S.L., Cohen, W.B., Healey, S.P., Kennedy, R.E., Moisen, G.G., Pierce, K.B., Ohmann, J.L., 2010. Quantification of live aboveground forest biomass dynamics with Landsat time-series and field inventory data: A comparison of empirical modeling approaches. Remote Sens. Environ. 114, 1053–1068. https://doi.org/10.1016/j.rse.2009.12.018

Psomas, A., Kneubühler, M., Huber, S., Itten, K., Zimmermann, N.E., 2011. Hyperspectral remote sensing for estimating aboveground biomass and for exploring species richness patterns of grassland habitats. Int. J. Remote Sens. 32, 9007–9031. https://doi.org/10.1080/01431161.2010.532172

Pugh, T.A.M., Lindeskog, M., Smith, B., Poulter, B., Arneth, A., Haverd, V., Calle, L., 2019. Role of forest regrowth in global carbon sink dynamics. Proc. Natl. Acad. Sci. U. S. A. 116, 4382–4387. https://doi.org/10.1073/PNAS.1810512116/SUPPL_FILE/PNAS.1810512116.SD02.TXT

Qin, Q., Xu, D., Hou, L., Shen, B., Xin, X., 2021. Comparing vegetation indices from Sentinel-

2 and Landsat 8 under different vegetation gradients based on a controlled grazing experiment. Ecol. Indic. 133. https://doi.org/10.1016/j.ecolind.2021.108363

Rahman, M.M., Csaplovics, E., Koch, B., 2008. Satellite estimation of forest carbon using regression models. Int. J. Remote Sens. 29, 6917–6936. https://doi.org/10.1080/01431160802144187

Räsänen, A., Rusanen, A., Kuitunen, M., Lensu, A., 2013. What makes segmentation good? A case study in boreal forest habitat mapping. Int. J. Remote Sens. 34, 8603–8627. https://doi.org/10.1080/01431161.2013.845318

Raumonen, P., Casella, E., Calders, K., Murphy, S., Åkerblom, M., Kaasalainen, M., 2015. Massive-scale tree modelling from tls data. ISPRS Ann. Photogramm. Remote Sens. Spat. Inf. Sci. II-3-W4, 189–196. https://doi.org/10.5194/ISPRSANNALS-II-3-W4-189-2015

Raumonen, P., Kaasalainen, M., Markku, Å., Kaasalainen, S., Kaartinen, H., Vastaranta, M., Holopainen, M., Disney, M., Lewis, P., 2013. Fast Automatic Precision Tree Models from Terrestrial Laser Scanner Data. Remote Sens. 2013, Vol. 5, Pages 491-520 5, 491–520. https://doi.org/10.3390/RS5020491

Rosenqvist, Å., Milne, A., Lucas, R., Imhoff, M., Dobson, C., 2003. A review of remote sensing technology in support of the Kyoto Protocol. Environ. Sci. Policy 6, 441–455. https://doi.org/10.1016/S1462-9011(03)00070-4

Rosillo-Calle, F., Hall, D.O., 1992. Biomass energy, forests and global warming. Energy Policy 20, 124–136. https://doi.org/10.1016/0301-4215(92)90106-C

Rusu, R.B., Marton, Z.C., Blodow, N., Dolha, M., Beetz, M., 2008. Towards 3D Point cloud based object maps for household environments. Rob. Auton. Syst. 56, 927–941. https://doi.org/10.1016/J.ROBOT.2008.08.005

Safari, A., Sohrabi, H., Powell, S., Shataee, S., 2017. A comparative assessment of multi-temporal Landsat 8 and machine learning algorithms for estimating aboveground carbon stock in coppice oak forests. Int. J. Remote Sens. 38, 6407–6432. https://doi.org/10.1080/01431161.2017.1356488

Schlamadinger, B., Apps, M., Bohlin, F., Gustavsson, L., Jungmeier, G., Marland, G., Pingoud, K., Savolainen, I., 1997. Towards a standard methodology for Greenhouse Gas Balances of Bioenergy Systems in comparison with fossil energy systems. Biomass and Bioenergy 13, 359–375. https://doi.org/10.1016/S0961-9534(97)10032-0

Schlamadinger, B., Marland, G., 1996. The role of forest and bioenergy strategies in the global carbon cycle, in: Biomass and Bioenergy. Pergamon, pp. 275–300. https://doi.org/10.1016/0961-9534(95)00113-1

Shongming Huang, Titus, S.J., Wiens, D.P., 2011. Comparison of nonlinear height–diameter functions for major Alberta tree species. https://doi.org/10.1139/x92-172 22, 1297–1304. https://doi.org/10.1139/X92-172

Silleos, N.G., Alexandridis, T.K., Gitas, I.Z., Perakis, K., 2006. Vegetation indices: Advances made in biomass estimation and vegetation monitoring in the last 30 years. Geocarto Int. 21, 21–28. https://doi.org/10.1080/10106040608542399

Sloan, S., Sayer, J.A., 2015. Forest Resources Assessment of 2015 shows positive global trends but forest loss and degradation persist in poor tropical countries. For. Ecol. Manage. 352, 134–145. https://doi.org/10.1016/J.FORECO.2015.06.013

Song, C., Dickinson, M.B., 2008. Extracting forest canopy structure from spatial information of high resolution optical imagery: tree crown size versus leaf area index. Int. J. Remote Sens. 29, 5605–5622. https://doi.org/10.1080/01431160802060904

Sothe, C., Gonsamo, A., Arabian, J., Kurz, W.A., Finkelstein, S.A., Snider, J., 2022a. Large Soil Carbon Storage in Terrestrial Ecosystems of Canada. Global Biogeochem. Cycles 36, e2021GB007213. https://doi.org/10.1029/2021GB007213

Sothe, C., Gonsamo, A., Lourenço, R.B., Kurz, W.A., Snider, J., 2022b. Spatially Continuous Mapping of Forest Canopy Height in Canada by Combining GEDI and ICESat-2 with PALSAR and Sentinel. Remote Sens. 14. https://doi.org/10.3390/rs14205158

Srivastava, A.K., Mboh, C.M., Gaiser, T., Ewert, F., 2017. Impact of climatic variables on the spatial and temporal variability of crop yield and biomass gap in Sub-Saharan Africa- a case study in Central Ghana. F. Crop. Res. 203, 33–46. https://doi.org/10.1016/J.FCR.2016.11.010

Staben, G., Lucieer, A., Scarth, P., 2018. Modelling LiDAR derived tree canopy height from Landsat TM, ETM+ and OLI satellite imagery—A machine learning approach. Int. J. Appl. Earth Obs. Geoinf. 73, 666–681. https://doi.org/10.1016/j.jag.2018.08.013

Stephens, P.R., Watt, P.J., Loubser, D., Haywood, A., Kimberley, M.O., 2007. Estimation of carbon stocks in new zealand planted forests using airborne scanning LiDAR. Int. Arch. Photogramm. Remote Sens. Spat. Inf. Sci. - ISPRS Arch. 7.

Su, Z., Li, S., Liu, H., Liu, Y., 2019. Extracting Wood Point Cloud of Individual Trees Based on Geometric Features. IEEE Geosci. Remote Sens. Lett. 16, 1294–1298. https://doi.org/10.1109/LGRS.2019.2896613

Tamiminia, H., Salehi, B., Mahdianpari, M., Goulden, T., 2024. State-wide forest canopy height and aboveground biomass map for New York with 10 m resolution, integrating GEDI, Sentinel-1, and Sentinel-2 data. Ecol. Inform. 79, 102404. https://doi.org/10.1016/j.ecoinf.2023.102404

Taylor, A.R., Boulanger, Y., Price, D.T., Cyr, D., McGarrigle, E., Rammer, W., Kershaw, J.A., 2017. Rapid 21st century climate change projected to shift composition and growth of Canada's Acadian Forest Region. For. Ecol. Manage. 405, 284–294. https://doi.org/10.1016/j.foreco.2017.07.033

Taylor, A.R., Seedre, M., Brassard, B.W., Chen, H.Y.H., 2014. Decline in Net Ecosystem Productivity Following Canopy Transition to Late-Succession Forests. Ecosystems 17, 778–791. https://doi.org/10.1007/s10021-014-9759-3

Ter-Mikaelian, M.T., Korzukhin, M.D., 1997. Biomass equations for sixty-five North American tree species. For. Ecol. Manage. 97, 1–24. https://doi.org/10.1016/S0378-1127(97)00019-4

Thapa, R.B., Watanabe, M., Motohka, T., Shiraishi, T., Shimada, M., 2015. Calibration of aboveground forest carbon stock models for major tropical forests in central sumatra using airborne lidar and field measurement data. IEEE J. Sel. Top. Appl. Earth Obs. Remote Sens. 8, 661–673. https://doi.org/10.1109/JSTARS.2014.2328656

Thapa, R.B., Watanabe, M., Shimada, M., Motohka, T., 2016. Examining High-Resolution PiSAR-L2 Textures for Estimating Tropical Forest Carbon Stocks. IEEE J. Sel. Top. Appl. Earth Obs. Remote Sens. 9, 3202–3209.

https://doi.org/10.1109/JSTARS.2016.2528262

Thenkabail, P.S., Stucky, N., Griscom, B.W., Ashton, M.S., Diels, J., Van der Meer, B., Enclona, E., 2004. Biomass estimations and carbon stock calculations in the oil palm plantations of African derived savannas using IKONOS data. Int. J. Remote Sens. 25, 5447–5472. https://doi.org/10.1080/01431160412331291279

Thomas, R.Q., Hurtt, G.C., Dubayah, R., Schilz, M.H., 2008. Using lidar data and a height-structured ecosystem model to estimate forest carbon stocks and fluxes over mountainous terrain. Can. J. Remote Sens. 34, S351–S363. https://doi.org/10.5589/m08-036

Thomas, V., McCaughey, J.H., Treitz, P., Finch, D.A., Noland, T., Rich, L., 2009. Spatial modelling of photosynthesis for a boreal mixedwood forest by integrating micrometeorological, lidar and hyperspectral remote sensing data. Agric. For. Meteorol. 149, 639–654. https://doi.org/10.1016/J.AGRFORMET.2008.10.016

Tong, F., Tong, H., Mishra, R., Zhang, Y., 2021. Delineation of Individual Tree Crowns Using High Spatial Resolution Multispectral WorldView-3 Satellite Imagery. IEEE J. Sel. Top. Appl. Earth Obs. Remote Sens. 14, 7751–7761. https://doi.org/10.1109/JSTARS.2021.3100748

Tong, F., Zhang, Y., 2025. Individual tree crown delineation in high resolution aerial RGB imagery using StarDist-based model. Remote Sens. Environ. 319, 114618. https://doi.org/10.1016/j.rse.2025.114618

Vauhkonen, J., Tokola, T., Maltamo, M., Packalén, P., 2008. Effects of pulse density on predicting characteristics of individual trees of Scandinavian commercial species using alpha shape metrics based on airborne laser scanning data. Can. J. Remote Sens. 34, S441–S459. https://doi.org/10.5589/M08-052

Vauhkonen, J., Tokola, T., Packalén, P., Maltamo, M., 2009. Identification of Scandinavian Commercial Species of Individual Trees from Airborne Laser Scanning Data Using Alpha Shape Metrics. For. Sci. 55, 37–47. https://doi.org/10.1093/FORESTSCIENCE/55.1.37

Verbeeck, H., Bauters, M., Jackson, T., Shenkin, A., Disney, M., Calders, K., 2019. Time for a Plant Structural Economics Spectrum. Front. For. Glob. Chang. 2, 467434. https://doi.org/10.3389/FFGC.2019.00043/BIBTEX

Verma, M., Friedl, M.A., Law, B.E., Bonal, D., Kiely, G., Black, T.A., Wohlfahrt, G., Moors, E.J., Montagnani, L., Marcolla, B., Toscano, P., Varlagin, A., Roupsard, O., Cescatti, A., Arain, M.A., D'Odorico, P., 2015. Improving the performance of remote sensing models for capturing intra- and inter-annual variations in daily GPP: An analysis using global FLUXNET tower data. Agric. For. Meteorol. 214–215, 416–429. https://doi.org/10.1016/J.AGRFORMET.2015.09.005

Wang, C., Zhang, W., Ji, Y., Marino, A., Li, C., Wang, L., Zhao, H., Wang, M., 2024. Estimation of Aboveground Biomass for Different Forest Types Using Data from Sentinel-1, Sentinel-2, ALOS PALSAR-2, and GEDI. Forests 15. https://doi.org/10.3390/f15010215

Wang, L., Zhu, H., Lin, A., Zou, L., Qin, W., Du, Q., 2017. Evaluation of the latest MODIS GPP products across multiple biomes using global eddy covariance flux data. Remote Sens. 9. https://doi.org/10.3390/rs9050418

Wang, Q., Zhao, X., Chen, L., Yang, Q., Chen, S., Zhang, W., 2019. Global synthesis of

temperature sensitivity of soil organic carbon decomposition: Latitudinal patterns and mechanisms. Funct. Ecol. 33, 514–523. https://doi.org/10.1111/1365-2435.13256

Wang, V., Gao, J., 2019. Importance of structural and spectral parameters in modelling the aboveground carbon stock of urban vegetation. Int. J. Appl. Earth Obs. Geoinf. 78, 93–101. https://doi.org/10.1016/j.jag.2019.01.017

Wei, Y., Liu, S., Huntzinger, D.N., Michalak, A.M., Viovy, N., Post, W.M., Schwalm, C.R., Schaefer, K., Jacobson, A.R., Lu, C., Tian, H., Ricciuto, D.M., Cook, R.B., Mao, J., Shi, X., 2014. The north american carbon program multi-scale synthesis and terrestrial model intercomparison project - Part 2: Environmental driver data. Geosci. Model Dev. 7, 2875–2893. https://doi.org/10.5194/GMD-7-2875-2014,

Wicaksono, P., Danoedoro, P., Hartono, Nehren, U., 2016. Mangrove biomass carbon stock mapping of the Karimunjawa Islands using multispectral remote sensing. Int. J. Remote Sens. 37, 26–52. https://doi.org/10.1080/01431161.2015.1117679

Wu, C., Munger, J.W., Niu, Z., Kuang, D., 2010. Comparison of multiple models for estimating gross primary production using MODIS and eddy covariance data in Harvard Forest. Remote Sens. Environ. 114, 2925–2939. https://doi.org/10.1016/j.rse.2010.07.012

Xiao, J., Yakimowski, S., Brown, M., Heartz, S., Parachnowitsch, A.L., Edge, C.B., 2023. Changes to the understory vegetation community of the Acadian Forest a decade after herbicide use. For. An Int. J. For. Res. 1–10. https://doi.org/10.1093/forestry/cpad052

Xiao, X., Boles, S., Frolking, S., Li, C., Babu, J.Y., Salas, W., Moore, B., 2006. Mapping paddy rice agriculture in South and Southeast Asia using multi-temporal MODIS images. Remote Sens. Environ. 100, 95–113. https://doi.org/10.1016/j.rse.2005.10.004

Xiao, X., Boles, S., Liu, J., Zhuang, D., Frolking, S., Li, C., Salas, W., Moore, B., 2005. Mapping paddy rice agriculture in southern China using multi-temporal MODIS images. Remote Sens. Environ. 95, 480–492. https://doi.org/10.1016/j.rse.2004.12.009

Yang, J., Kang, Z., Cheng, S., Yang, Z., Akwensi, P.H., 2020. An individual tree segmentation method based on watershed algorithm and three-dimensional spatial distribution analysis from airborne LiDAR point clouds. IEEE J. Sel. Top. Appl. Earth Obs. Remote Sens. 13, 1055–1067.

Zhang, X., Shen, H., Huang, T., Wu, Y., Guo, B., Liu, Z., Luo, H., Tang, J., Zhou, H., Wang, L., Xu, W., Ou, G., 2024. Improved random forest algorithms for increasing the accuracy of forest aboveground biomass estimation using Sentinel-2 imagery. Ecol. Indic. 159, 111752. https://doi.org/10.1016/j.ecolind.2024.111752

Zhao, K., Suarez, J.C., Garcia, M., Hu, T., Wang, C., Londo, A., 2018. Utility of multitemporal lidar for forest and carbon monitoring: Tree growth, biomass dynamics, and carbon flux. Remote Sens. Environ. 204, 883–897. https://doi.org/10.1016/j.rse.2017.09.007

Zheng, D., Rademacher, J., Chen, J., Crow, T., Bresee, M., Le Moine, J., Ryu, S.R., 2004. Estimating aboveground biomass using Landsat 7 ETM+ data across a managed landscape in northern Wisconsin, USA. Remote Sens. Environ. 93, 402–411. https://doi.org/10.1016/j.rse.2004.08.008